DEVELOPMENT OF ALKYNE-CONTAINING ISOPRENOID ANALOGUES TO STUDY PROTEIN PRENYLATION IN *IN VIVO* AND *IN VITRO* MODELS OF ALZHEIMER'S DISEASE AND LEUKEMIA

A DISSERTATION SUBMITTED TO THE FACULTY OF THE

UNIVERSITY OF MINNESOTA

BY

MIHAI ALEXANDRU PETRE

IN PARTIAL FULFILLMENT OF THE REQUIREMENTS

FOR THE DEGREE OF

DOCTOR OF PHILOSOPHY

ADVISOR: PROF. MARK D. DISTEFANO

MAY 2024

Acknowledgements

Pursuing my PhD degree has been a non-negotiable goal in my mind for a period of time that is too long for me to remember exactly when it all started. One thing I definitely do remember though is all the people that have been an integral part of this journey and whom I would like to thank herein. I am grateful to the Fulbright foundation to have received the scholarship that allowed me to be here and achieve my dream.

First and foremost, I would like to thank my advisor, Dr. Mark D. Distefano, for being not only an advisor, but a true mentor and role model for me. His fascination with science made me look up to him and always kept my curiosity to learn new things at an all time high, even though this may one day turn me into a “talking encyclopedia”, as he jokingly refers to himself at times. I highly appreciate the trust he’s had in me from the very first moment I asked him if I could join his research group to every time I would start a new collaboration. From him, I learned how to work with people and how to be a team player, how to think under pressure and efficiently manage large workloads, always pushing the boundaries of my comfort zone for a huge return in biological knowledge, of which I hadn’t had much when joining his lab. And outside of science, there were many fields I became interested in, simply from hearing him passionately talk about some of his favorite activities, such as hunting or diving in the ocean with the seals. He made me a better scientist, and a better person, just like a true mentor would.

I am also grateful to Dr. Ling Li who, even though I was never co-advised by her, made me feel like I was. She has also been incredibly supportive of my work and me from the very beginning of our collaboration right after I joined the Distefano Lab. She has always been there for me, offering her guidance and compassionate suggestions, even when I would knock on her office door unannounced. Her biology point of view on the science we have worked on together has always been fascinating to me and made me want to learn more and more about topics I never thought I would be so curious about. Studying Alzheimer's disease has been the primary focus of our work together, which had a deep personal impact on me, having seen the debilitating effects of this condition take away my grandfather when I was only in middle school.

As I am writing this on Mother's Day, I could never even begin to imagine myself being a scientist without the passion for chemistry that my mother, Elena, has instilled in me from a very young age. As the principal scientist of the first ISO 9000 certified laboratory in Romania in the late 1990's, saying that she was a busy person would be an understatement. And yet she always made time to answer my questions about science and chemistry in a very scientifically accurate but easy to understand manner (I was probably 4-5 years old back then). She would always show me some cool reaction she performed or new exotic chemical they got in the lab, which only stimulated my curiosity and yielded more and more new questions from me that she would eagerly explain. Thank you, mom, I wouldn't be here without you.

I would also like to thank my math and science high school teachers for allowing that curious child to grow into an even more curious teenager, that never stopped trying to explain and understand how everything surrounding us works. They definitely helped steer me into pursuing a career in science.

Getting my bachelor's degree in chemistry was no easy feat for me, but my undergrad advisor, Dr. Stéphane Baudron, made it seem easy. The time spent doing research in his lab at the University of Strasbourg, France, gave me the first impression for how pursuing a graduate career would feel and cemented my desire to obtain my PhD degree. Thank you, Stéphane, for teaching me so much so early on, for being so patient even when I would be blanking on a certain word in French and for being so inclusive.

Last but not least, I would like to thank the past and present Distefano lab members for sharing so much of their knowledge and time, especially early on when I was so new to chemical biology. You made the lab a great place to work and learn, and I will always appreciate that.

Dedication

To my dad, Dr. Doru

To my mom, Elena

To my sister, Andreea

Thank you for always being there for me and with me, even 6000 miles apart.

I love you the most.

Contribution of Co-Authors

In chapter 2, the kinetic analysis assays were done by Andrea Sprague-Getsy in Dr. James Hougland's lab at Syracuse University as part of her graduate work.

In chapters 2 and 4, the animal injections, dissections and subsequent tissue collections and homogenization were done by Josslen Thieshafer in Dr. Ling Li's lab at the University of Minnesota as part of her post-baccalaureate work.

In chapter 3, the proteomic experiments and data collection for the L363 cell line were performed by Dr. Nyema Harmon in our lab as part of his postdoctoral work. The proteomic experiments and data collection for the OPM-2 cell line were performed by Kiall Suazo in our lab as part of his graduate work.

In chapter 4, the ProAlaC15AlkOPP and BisC15AlkOPP synthesis and was performed by Dr. Nyema Harmon in our lab as part of his postdoctoral work. He also performed the metabolic labeling experiments comparing the metabolic labeling with ProAlaC15AlkOPP and BisC15AlkOPP versus C15AlkOPP via in-gel fluorescence in OPM-2 cells (Fig. 2) and the ones comparing of metabolic labeling with C15AlkOPP and BisC15AlkOPP versus FPP via in-gel fluorescence in 7 distinct cell lines (Fig. 3).

Abstract

Prenylation is a ubiquitous process in eukaryotes consisting of the post-translational modification of an array of proteins through the attachment of a lipophilic isoprenoid moiety. Prenyltransferase enzymes catalyze this process: farnesyltransferase appends the C_{15} isoprenoid from farnesyl diphosphate (FPP), and geranylgeranyltransferase type I, II and III append one or two C_{20} isoprenoids from geranylgeranyl diphosphate (GGPP). This modification allows proteins to fulfill their essential roles in cellular processes such as signal transduction or mediating protein-protein interactions. It has been reported that prenylation affects approximately 2% of the mammalian proteome. Due to the impact prenylation has on cellular biology, its presence and/or dysregulation has been linked to numerous diseases, including Alzheimer's disease and multiple types of cancer.

To study prenylated proteins as potential drug targets, several alkyne-modified chemical probes have been synthesized: a shorter C15AlkOPP designed to label both farnesylated and geranylgeranylated proteins, a longer C15PentOPP, designed to be specific for geranylgeranylated proteins, and a BisC15AlkOPP probe that uses a prodrug approach to increase the bioavailability of the C15AlkOPP probe when delivered *in vivo*. Proteomic experiments in different cell lines revealed the selectivity of C15PentOPP towards geranylgeranylated proteins (up to 93% of total prenylated proteins identified) and confirmed the C15AlkOPP and BisC15AlkOPP as probes for both farnesylation and geranylgeranylation. The latter 2 probes were used in *in vivo* and *in vitro* experiments using models for Alzheimer's disease and leukemia to identify proteins whose extent of prenylation is altered, with the ultimate goal of discovering new potential drug targets.

Table of Contents

List of Tables

List of Figures

List of Abbreviations

AD	Alzheimer's disease
AML	Acute Myeloid Leukemia
APOE	Apolipoprotein E
CuAAC	Copper-catalyzed alkyne-azide cycloaddition
DMSO	Dimethylsulfoxide
equiv.	Equivalent(s)
EtOAc	Ethyl Acetate
EtOH	Ethanol
FPP	Farnesyl Diphosphate
FTase	Farnesyltransferase
FTI	Farnesyltransferase Inhibitor
GGPP	Geranylgeranyl diphosphate
GGTase	Geranylgeranyltransferase
GGTI	Geranylgeranyltransferase inhibitor
UPLC	Ultra-High Performance Liquid Chromatography
IC_{50}	Half maximal inhibitory concentration
K_M	Michaelis constant
M	Molar concentration
MeOH	Methanol
MS	Mass Spectrometry
^{1}H NMR	Proton nuclear magnetic resonance
^{13}C NMR	Carbon nuclear magnetic resonance
^{31}P NMR	Phosphorous nuclear magnetic resonance
PPTS	Pyridinium p-toluenesulfonate
TAMRA-N_3	5-Carboxytetramethylrhodamine-azide

TEAB	Triethylammonium bicarbonate
TBHP	*t*-Butyl hydroperoxide
THP	Tetrahydropyran
TMT	Tandem Mass Tag
MS	Mass Spectrometry

Chapter 1. Introduction

1. 1. Protein Prenylation

Protein prenylation is a post-translational irreversible modification of proteins, taking place ubiquitously in eukaryotic cells and is named after the polyisoprenyl lipid chains it attaches to proteins. Since its discovery in fungi in the late 1970s and then later in mammalian cells in the 1980s,[1,2] this type of modification has gained attention due to its instrumental role controlling subcellular localization of certain proteins. Prenylation involves the enzyme-catalyzed attachment of an isoprenoid moiety, derived from farnesyl diphosphate (FPP) or geranylgeranyl diphosphate (GGPP), to proteins via a thioether bond, along with loss of diphosphate ion (Fig. 1).[3]

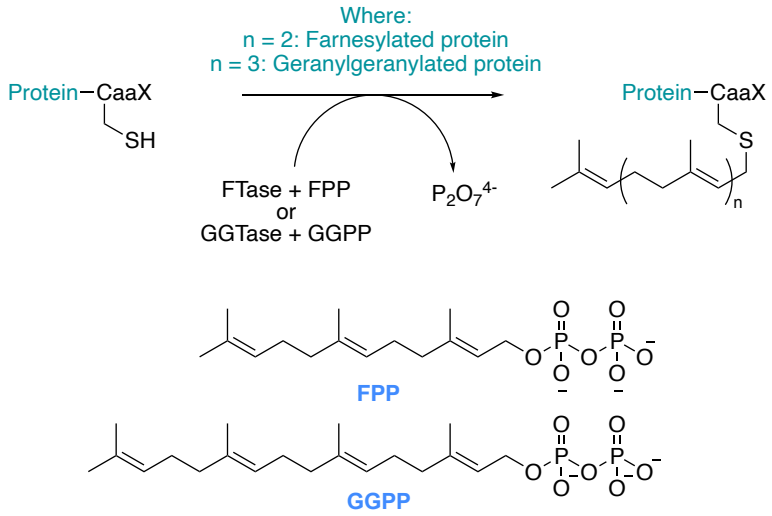

Figure 1. Prenylation mechanism and the 2 endogenous substrates.

In eukaryotic cells, isoprenoids are primarily biosynthesized through the mevalonate-isoprenoid-cholesterol pathway, initially in the form of 5-carbon atom diphosphate building blocks, that are later extended into higher carbon number

isoprenoids.[4] The discovery of the incorporation of these mevalonate-derived isoprenoids into proteins in 1984 by Schmidt and co-workers[5] led to the quest of identifying the enzymes responsible for this transformation, in order to better understand the implications of prenylation in biological systems.

There are 4 enzymes that catalyze this modification reaction: farnesyltransferase (FTase) attaches the 15-carbon isoprenoid from FPP, geranylgeranyltransferase type-I (GGTase type-I) attaches a 20-carbon isoprenoid from GGPP, and geranylgeranyltransferase type-II and type-III (GGTase type-II/type-III) append two geranylgeranyl units from GGPP that are specific to Rab proteins and ubiquitin ligases.[6,7] The prenyltransferase enzymes transfer the isoprenoid moiety from the diphosphate forms to a sulfur atom of a cysteine residue located in the C-terminal region of a protein, usually referred to as a CaaX box. In that motif, “C” represents cysteine, the “a” residues are commonly aliphatic amino acids, and the “X” residue controls whether the protein is farnesylated or geranylgeranylated.[8] The generally accepted prenylation mechanism starts with the enzyme interacting with the isoprenoid diphosphate followed by binding of the CaaX box-containing protein and subsequent thioether bond formation. At this point, binding of another isoprenoid diphosphate molecule occurs, followed by association of another protein substrate and release of the prenylated product.[9,10]

For many proteins, the identity of the prenyl group (farnesyl or geranylgeranyl) is dictated by the “X” position (FTase if X = serine, glutamine, alanine, methionine; GGTase I if X = phenylalanine, leucine, isoleucine). For other proteins, such as K-Ras4B, alternative prenylation can occur, typically resulting in the transfer of a geranylgeranyl

group instead of a farnesyl isoprenoid.[11] This is particularly important as it leads to resistance to prenyltransferase inhibitors.

Protein prenylation affects approximately 2% of the mammalian proteome, allowing proteins to fulfill their essential roles in cellular processes such as membrane localization, signal transduction or mediating protein-protein interactions.[12] Owing to its vital importance on cell physiology, protein prenylation has been linked to a variety of diseases, including ALS, progeria, different types of cancers and Alzheimer's disease (AD). [13,14] In order to study protein prenylation in different diseases, several probes modified with an alkyne moiety have been developed, having different lengths and mechanisms of action, taking advantage of the promiscuity of the prenyltransferase enzymes to incorporate them into the prenylation machinery.

1. 2. Prenylation's Implication in Alzheimer's disease and the APOE Alleles

AD is a debilitating neurodegenerative disease that affects the elderly, leading to dementia and ultimately death. According to the Alzheimer's Association, there is a new AD patient diagnosed every 66 seconds in the United States, with 6.2 million people currently living with this condition across the country, a figure expected to increase to almost 14 million by 2050.[15] Protein prenylation has been implicated in AD pathogenesis and development, but it has not been sufficiently explored to date. It is known that there is a direct link between apolipoprotein E (APOE) isoforms and their impact on AD onset.[16] There are three APOE isoforms, with APOE2 (E2) having a functional effect that reduces the risk of AD, APOE3 (E3) bearing a non-significant influence on AD pathogenesis and APOE4 (E4) having a deleterious effect, increasing the risk of developing AD.[17] The

presence of one APOE4 gene increases the risk of developing AD 4-fold, while the presence of 2 APOE4 isoforms increases the risk up to 33-fold.[18,19] With APOE being synthesized in the brain and in higher quantities in the liver, the importance of studying protein prenylation in animal models with varying APOE genotypes could reveal changes in the levels of expression of different proteins, indicating their involvement or association with AD pathogenesis.[20,21] Studies addressing protein prenylation in transgenic mice containing APOE3 and APOE4 alleles are reported in this thesis.

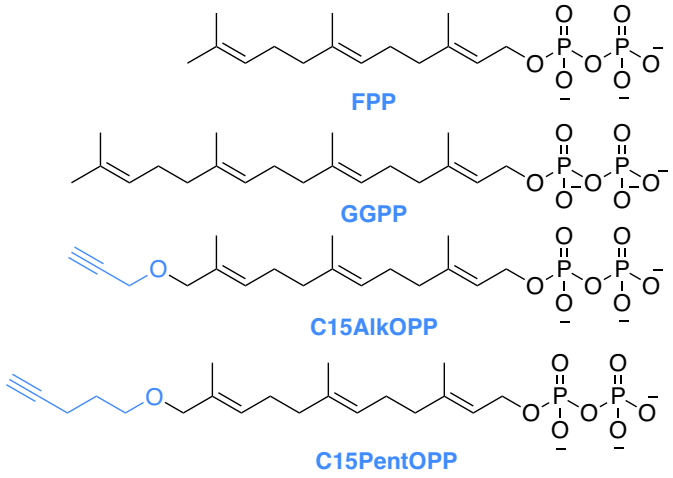

Figure 2. Structures of the C15AlkOPP and C15PentOPP probes used in studying prenylated proteins and the two endogenous prenylation substrates.

1. 3. Prenylation's Implication in leukemia

Leukemia is another disease that has been linked to prenylation, but the mechanism that is involved in this process is yet to be elucidated. Given that studies involving inhibition of GGTase type-I led to cancer cell apoptosis,[22] identifying which geranylgeranylated proteins are involved in leukemia and targeting them in different therapies may be the key to developing a successful anti-cancer therapy.

One of the drugs used in treating leukemia and lymphoma is the BCL2 inhibitor venetoclax. Several studies that led to clinical trials included the successful use of this drug in combination with other inhibitors to drive the apoptosis of some acute myeloid leukemia-derived cell lines (AML).[23,24] Statins are cholesterol lowering drugs that act as potent inhibitors early in the mevalonate pathway and have previously been linked to lowering the risk of AD.[25] When used in biological systems, statins lead to suppression of the production of the endogenous substrates for prenylation, FPP and GGPP. Notably, the Fruman group observed a synergistic effect when combining venetoclax and a statin. They followed up those initial results with studies using different prenyltransferase inhibitors in combination with venetoclax and they observed that only the inhibition of geranylgeranylation type-I upregulated AML-cells apoptosis.[22] When administering a combination of venetoclax and geranylgeranyltransferase type-I inhibitors (GGTI 298 and GGTI 2133), the Fruman group observed an enhanced cytotoxic effect with the GGTI 298 compared to GGTI 2133.[22] Identifying which geranylgeranylated type-I proteins are involved in this process is a key requirement for defining the molecular mechanism of how GGTIs act synergistically with venetoclax and could contribute to the development of new approaches for leukemia treatment.

1. 4. Using a Protide Approach to Deliver Alkyne-Modified Isoprenoids *in vivo*

In some *in vivo* experiments, it can be challenging to deliver isoprenoid analogues due to the charged nature of the diphosphate group. While this makes these probes water soluble, it also means they are unable to cross the blood-brain barrier. Hence AD studies on the brain require new methods for delivering probes that go beyond systemic delivery.

To overcome these challenges, a prodrug approach was employed here for systemic administration in animal studies. Prodrugs are molecules that are pharmacologically inactive but, upon cellular internalization, they are metabolized to release the active form of the drug. Using an established chemical scaffold previously developed for the delivery of nucleotide analogues known as protides,[26] neutral molecules were designed to deliver probes for prenylation *in vivo*.[27,28] To this aim, a stable phosphoramidate prodrug form was chosen[27] and linked to the C15AlkOH scaffold to develop 2 new compounds that would be activated *in vivo* by a kinase, HINT1, which is overexpressed in the liver and hydrolyzes phosphoramidates.[29] The ProAlaC15AlkOPP contains one C15AlkOH moiety and the BisC15AlkOPP contains 2 such moieties (Fig. 3).

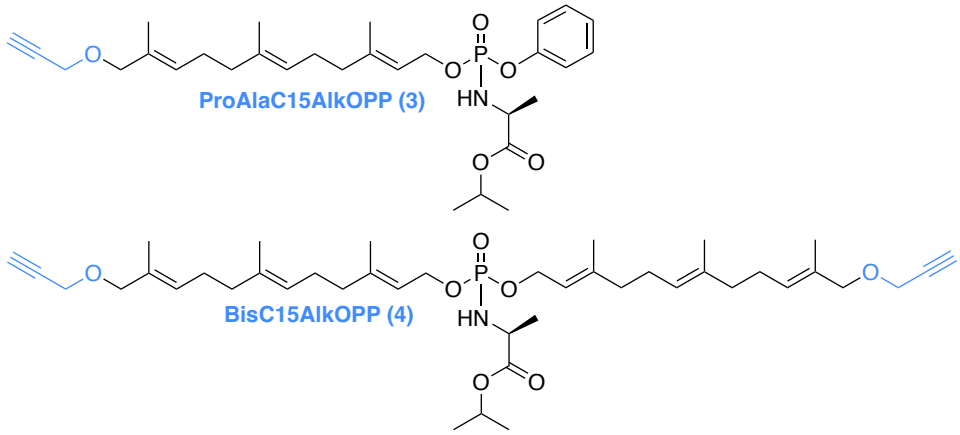

Figure 3. Structures of the two protide probes synthesized to study prenylation *in vivo*.

The proposed activation mechanism for phosphoramidates begins with ester cleavage by a serine protease such as Cathepsin A. The newly formed carboxylate attacks the phosphorous atom and displaces the aryl ether in a cyclization reaction. Upon hydrolysis, the dianion formed is processed by HINT1 which cleaves the phosphoramide bond, revealing the monophosphate form of the probe (Fig. 4). Next, this is then phosphorylated to the diphosphate analogue C15AlkOPP that is subsequently

incorporated by prenyltransferases. Using this approach could result in better labeling in animal tissues, potentially increasing the number of targets for prenylation detected in proteomic profiling and expanding the pool of possible drug targets in different disease models.

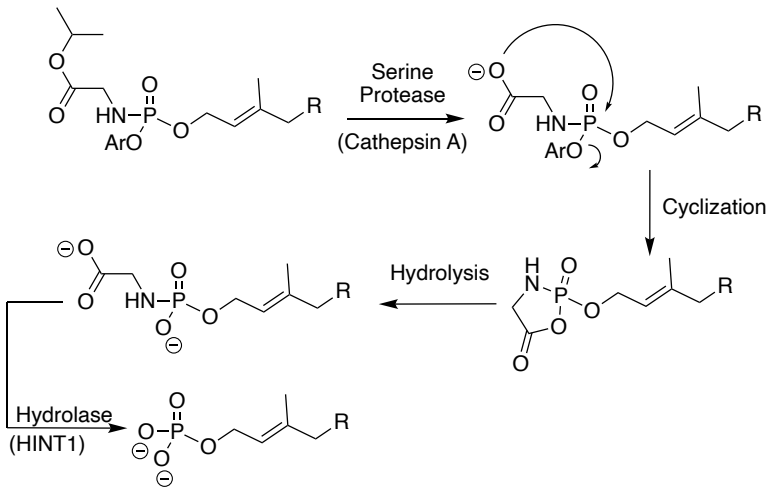

Figure 4. Proposed mechanism for prodrug metabolic activation and prenylation probe delivery *in vivo*.

1.5 Scope of Thesis

Chapter 2 of this dissertation describes the synthesis of the C15PentOPP probe and its use, along with the C15AlkOPP probe, in in-gel fluorescence metabolic labeling experiments and *in vitro* proteomic analyses. Moreover, *in vivo* labeling experiments in Alzheimer's disease model mice and proteomic analyses are described. In Chapter 3, the use of the C15AlkOPP probe in *in vitro* proteomic experiments in combination with two distinct geranylgeranyltransferase type-I inhibitors shows differential depletion some of geranylgeranylation type-I targets, which can be used as drug targets in the context of leukemia. Lastly, in Chapter 4, advances in bioavailability of the C15AlkOPP probe are described via the use of a prodrug-like scaffold, creating the BisC15AlkOPP probe. The

labeling of the BisC15AlkOPP probe is investigated in humanized Alzheimer's disease mice and the proteomic results are compared with those previously described in Chapter 2 with the C15AlkOPP probe. This dissertation highlights the use of proteomic analysis in studying prenylated proteins in different disease models, both *in vitro* and *in vivo*.

Chapter 2. *In Vivo* Metabolic Labeling with an Isoprenoid Probe Reveals APOE Allele-specific Differences in the Prenylome with Applications for Alzheimer's Disease Research.

2. 1. Introduction

Prenylation is a ubiquitous process in eukaryotes consisting of the irreversible post-translational modification of an array of proteins through the attachment of a lipophilic isoprenoid moiety to the C-terminus of the proteins via a thioether bond.[12] There are four prenyltransferase enzymes that catalyze this process: farnesyl transferase (FTase), appends the C_{15} isoprenoid from farnesyl diphosphate (FPP) (Fig. 1), and geranylgeranyl transferase type I, II and III (GGTase type-I, GGTase type-II and GGTase type-III), that append one or two C_{20} isoprenoids from geranylgeranyl diphosphate (GGPP) (Fig. 1).[30,7] It is known that approximately 2 % of the mammalian proteome is prenylated, with this modification allowing proteins to fulfill their essential roles in cellular processes such as membrane localization, signal transduction or mediating protein-protein interactions.[12,6] Due to the important functional role prenylation has on cellular biology,[30] its presence and/or dysregulation has been linked to numerous diseases, including ALS, progeria, different types of cancer and, Alzehimer's Disease (AD). [13,14]

AD is a debilitating neurodegenerative disease that affects the elderly, leading to dementia and ultimately death. Currently, there are over 6 million people living with this condition in the United States, with that number expected to double in the next 30 years.[15]

Protein prenylation has been implicated in AD pathogenesis and development, but it has not been sufficiently explored. It is known that there is a correlation between APOE isoforms and their impact on AD onset.[16] There are three APOE isoforms, with APOE2 (E2) having a functional effect that reduces the risk of AD, APOE3 (E3) bearing a non-significant influence on AD pathogenesis and APOE4 (E4) having a deleterious effect, increasing the risk of developing AD. The presence of one APOE4 gene increases the risk of developing AD 4-fold, while the presence of 2 APOE4 isoforms increases the risk up to 15-fold.[18] With APOE being synthesized in the brain and in higher quantities the liver, the importance of studying protein prenylation in animal models with varying APOE genotypes could reveal changes in the levels of expression of different proteins, indicating their involvement or association with AD pathogenesis.[20,21] Given most of the APOE biosynthesis takes place in the liver and then enters the bloodstream, this tissue played a central role in our studies in the context of AD.

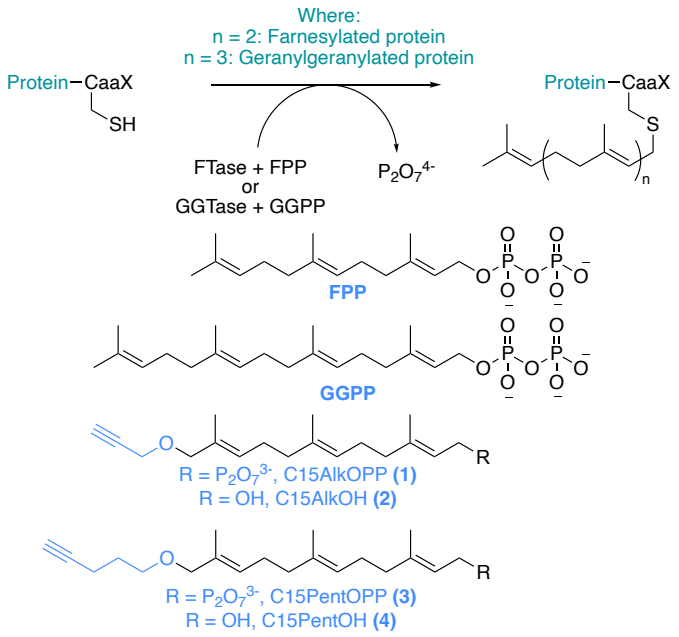

Figure 1. Prenylation mechanism, its natural FPP and GGPP substrates and the alkyne-containing analogs discussed here.

In the work reported here, to identify how levels of prenylated proteins were altered in APOE animal models, two chemical probes have been synthesized: a previously reported C15AlkOPP designed to label both farnesylated (F) and geranylgeranylated (GG) proteins,[3] and a new, longer C15PentOPP probe, designed to label geranylgeranylated proteins selectively (Fig. 1). These probes incorporate an alkyne handle, which can be used for bio-orthogonal copper-catalyzed click reaction with a TAMRA fluorophore for in-gel fluorescence visualization or a biotin moiety for enrichment in proteomic studies.[31] A proteomic experiment confirmed the selectivity of the C15PentOPP probe towards geranylgeranylated proteins. However, the proteins identified there were a subset of the proteins identified using C15AlkOPP; no new geranylgeranylated proteins were identified with the longer probe. Hence subsequent experiments focused on the more general C15AlkOPP analogue. Next, we report a methodology for labeling prenylated proteins *in vivo* via daily subcutaneous injections in transgenic APOE3 and APOE4 mice. This approach is different from a previously reported method from our lab, where the probe was delivered via intracerebroventricular infusion, and allows facile labeling of certain peripheral tissues.[32] The liver samples showed higher labeling in E4 mice compared to E3 mice as determined via in-gel fluorescence analysis and 23 significantly enriched prenylated proteins were detected via proteomic analysis. The E4 samples showed proteins had higher fold changes overall than the E3 samples and statistically significant differences in their fold change values based on proteomic data. Importantly, some of these proteins have links to AD neuropathology.

2. 2. Results and Discussion

2. 2. 1. Synthesis of a Probe Selective for Geranylgeranylated Proteins

To generate a probe selective for geranylgeranylated proteins, a synthesis was designed based on the route previously employed for the preparation of the pan-reactive compound, C15AlkOPP.[3] The synthesis began with THP protection of farnesol that yielded compound **5**, which was then subjected to a catalytic allylic oxidation in the presence of SeO_2 and *t*-Bu-OOH. Two isomeric products (previously characterized)[33] were obtained due to the dual reactive sites identified in **5**, which prompted a necessary chromatographic separation on the way to obtaining compound **6** with high purity. In order to circumnavigate the issue of overoxidation of **6** to the corresponding aldehyde, a $NaBH_4$ reduction was performed after the oxidation reaction in order to increase the yield of desired allylic alcohol. Next, **6** was converted to the corresponding allylic chloride **7** in the presence of NCS and dimethyl sulfide. With **7** obtained, it was subjected to the alkoxide nucleophile resulting from the addition of 4-pentyn-1-ol to a solution of *t*-BuOK to yield the protected ether **8**. It is noteworthy that an approach to synthesize ether **8** in one less step, where the allylic alcohol **6** was used as a nucleophile in the presence of the strong *t*-BuOK base and 5-chloro-1-pentyne as the electrophile did not yield the desired product, the starting materials being found at the end of the reaction, meaning the allylic alkoxide formed was not a strong enough nucleophile. Ether **8** was then deprotected under acidic conditions and the resulting alcohol **4** was converted to the bromide **9** via an Appel reaction involving polymer-supported triphenylphosphine in the presence of CBr_4. Finally, to create a diphosphate probe suitable for metabolic labeling, bromide **9** was subjected to a phosphorylation reaction with $(n\text{-}Bu_4N)_3HP_2O_7$. Purification via ion exchange and

cellulose chromatography afforded the C15PentOPP probe (compound **3**). The overall yield for the entire 7-step linear synthetic sequence was 1.5% (Fig. 2). It should be noted that Tate et al. previously reported the synthesis of a related geranylgeranyl diphosphate analogue containing an alkyne group suitable for metabolic labeling. While that compound has the advantage that it more closely reflects the all carbon composition of a natural isoprenoid, it requires the formation of a C-C bond that makes the synthesis more complex.[34]

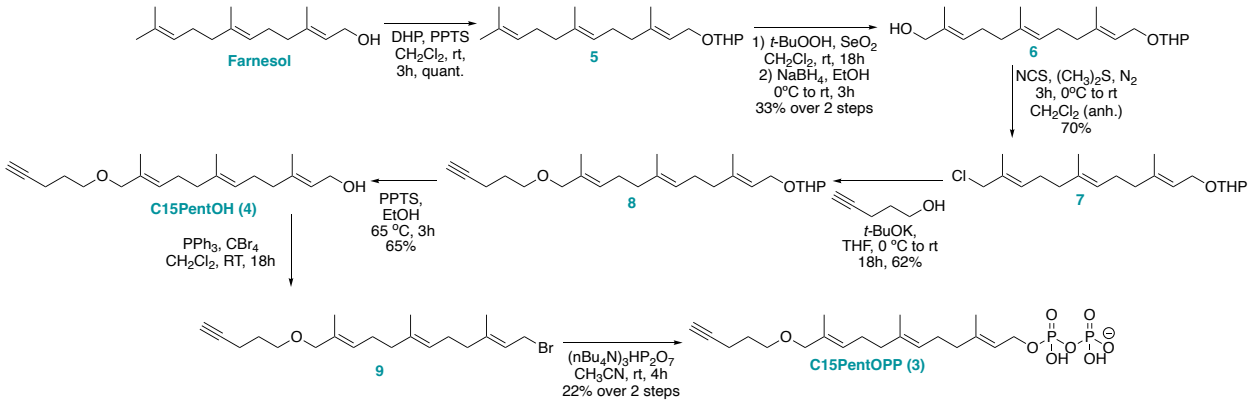

Figure 2. Seven-step synthesis of the C15PentOPP probe starting from 5 g of farnesol.

2. 2. 2. In Vitro Analysis of C15PentOPP as a Prenyltransferase Substrate

In order to evaluate the C15PentOPP as a substrate for GGTase-I rather than FTase, a continuous spectrofluorimetric assay monitoring the time-dependent increase in fluorescence upon prenylation of a dansylated peptide substrate was employed. The well-characterized peptide substrates Dns-GCVLS and Dns-GCVLL were used to evaluate FTase[35] and GGTase-I[36] activity, respectively. Incubation of FTase with C15PentOPP revealed a lower use of the diphosphate to yield the prenylated product, with a relative

catalytic efficiency (k_{cat}/K_M) of 30% of that for FPP (Fig. 5A). In contrast, substantially higher utilization of C15PentOPP by GGTase-I was observed, with a relative catalytic efficiency (k_{cat}/K_M) of 65% of that for GGPP for that enzyme (Fig. 5B). This is consistent with the previously reported isoprenoid length limitations exhibited by FTase and GGTase-I.[37,38] Overall, these results indicate that C15PentOPP is an efficient substrate for GGTase-I and is not an efficient substrate for FTase, suggesting that the longer probe would indeed manifest selectivity in labeling geranylgeranylated proteins over farnesylated proteins.

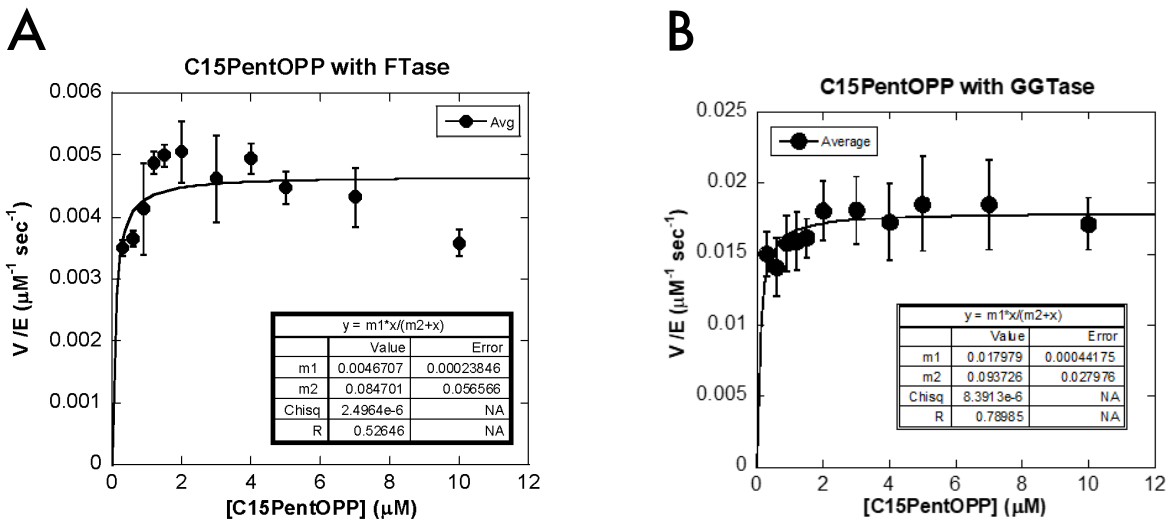

Figure 3. Kinetic analysis of C15PentOPP as a substrate for prenylation reactions of Dns-GCVLS and Dns-GCVLL with rFTase and rGGTase-I using C15PentOPP.
(A) Kinetic analysis of rFTase-catalyzed reaction between C15PentOPP and Dns-GCVLS. **(B)** Kinetic analysis of rGGTase-catalyzed reaction between C15PentOPP and Dns-GCVLL. This data was obtained by Andrea Sprague-Getsy in the laboratory of James Hougland at Syracuse University.

2. 2. 3. Initial Evaluation of Metabolic Labeling

2. 2. 3. 1. The Alcohol Form of the Probe is Less Efficient Compared to the Diphosphate Equivalent

Synthetically, the alcohol form of the C15PentOPP probe is more readily available compared to the diphosphate, which requires two additional synthetic steps and a more complex purification, lowering the overall yield. However, it has previously been shown that the alcohol form of the shorter C15AlkOPP probe (C15AlkOH) is less efficient in cell-based metabolic labeling compared with the diphosphate.[3] To assess if this was the case with the new C15PentOPP probe, metabolic labeling followed by in-gel fluorescence analysis was performed. After cell-based labeling with the probe in different cell lines, the cells were lysed and then subjected to a CuAAC (click) reaction with TAMRA-N_3. The cellular proteins were resolved via SDS-PAGE and the fluorescence of the prenylated proteins was analyzed. Those experiments revealed that the diphosphate yielded superior labeling compared to the alcohol form of the probe in all three cell lines tested including COS-7, HeLa and AML-3 (Fig. 4A, lanes 4 and 5, Fig. 4B lanes 4 and 5). This effect is presumably due to the necessity of having to metabolically activate the alcohol probe to the corresponding diphosphate form, which is the actual substrate of the prenyltransferase. Thus, it appears that the additional steps required for diphosphate synthesis are advantageous since they result in improvement in metabolic labeling efficiency.

2. 2. 3. 2. Statin Pre-treatment Modestly Increases Probe Incorporation

Previous studies have shown that inclusion of a statin (mevalonate pathway inhibitor) to suppress the endogenous production of FPP and GGPP[39] can lead to increased metabolic labeling of prenylated proteins with C15AlkOPP. Choosing an appropriate statin concentration is important to minimize cellular toxicity and perturbation of cellular biological functions. Previously, it has been shown that 10 μM lovastatin can augment probe incorporation with no apparent toxicity.[40] As a result, that concentration was used throughout the experiments reported here with C15PentOPP, pre-incubating the cells with statin for 6 h prior to addition of probe. Indeed, in COS-7 cells, labeling was enhanced, with an apparent enhancement of band intensity in the 20-25 kDa and 37-75 kDa regions in the presence of statin (Fig. 4A, lane 10), compared to in its absence (Fig. 4A, lane 5). A similar effect, although much less pronounced, was observed in HeLa cells in the presence (Fig. 4B, lane 5) versus the absence of statin (Fig. 4B, lane 10) and AML-3 cells in the presence (Fig. 4C, lane 7) versus the absence of statin (Fig. 4C, lane 3). Overall, the use of statin allowed modest increases in the level of metabolic labeling with C15PentOPP.

2. 2. 3. 3. Metabolic Labeling is Cell Line Dependent

To investigate the versatility of the C15PentOPP probe, its use in metabolic labeling was investigated in multiple cell lines. Given that different cell lines display variations in protein levels that are, in part, related to differences in their biological function,[40] the labeling obtained with the C15PentOPP probe was examined in 3 different

mammalian cell lines including 2 adherent cell types (COS-7 and HeLa) and one suspension cell type (AML-3). As a further point of comparison, a parallel set of experiments was performed with the C15AlkOPP analogue. Comparing the adherent cell lines, HeLa cells (Fig. 4B lanes 8 and 10) showed overall lower labeling incorporation with both the C15AlkOPP and C15PentOPP probes relative to that obtained with COS-7 cells (Fig. 4A lanes 8 and 10). In contrast, labeling in the suspension cell line AML-3 (Fig. 4C lanes 6 and 7) was comparable to COS-7 (Fig. 4A lanes 8 and 10). Since maximal detection of the prenylome was one of the main initial goals here, COS-7 and AML-3 were chosen for subsequent proteomic profiling, with COS-7 treatments performed in the presence of statin, since the effect was more potent there, and AML-3 treatments in the absence of statin, since its effects on probe incorporation in this cell line were lower.

2. 2. 3. 4. C15PentOPP Labeling is Localized in the 20-25 kDa Region

In previous studies, it was shown that the C15AlkOPP probe was capable of labeling all classes of prenylated proteins, including farnesylated and geranylgeranylated proteins.[40] To label geranylgeranylated proteins in a selective manner, the C15PentOPP probe was designed to be two carbon atoms longer than the C15AlkOPP (Fig. 1) in order to more closely approximate the length of GGPP. When performing in-gel fluorescence analysis, we noticed that the labeling obtained with the C15PentOPP probe was primarily localized in the 20-25 kDa region (Fig. 4A, lane 10; 4B, lane 10; 4C, lane 7), whereas the labeling observed with the C15AlkOPP probe included additional proteins in the 37-75 kDa region (Fig. 4A, lane 8; 4B, lane 8; 4C, lane 6).

This behavior was consistent across the 3 cell lines tested, albeit at different intensities, depending on the respective cell line. Since the major proteins in the 37-75 kDa region are thought to include nuclear lamin and DNAJ which are farnesylated proteins, their absence in the samples labeled with the C15PentOPP probe provided a preliminary indication that the probe was indeed a selective substrate for geranylgeranylating enzymes.

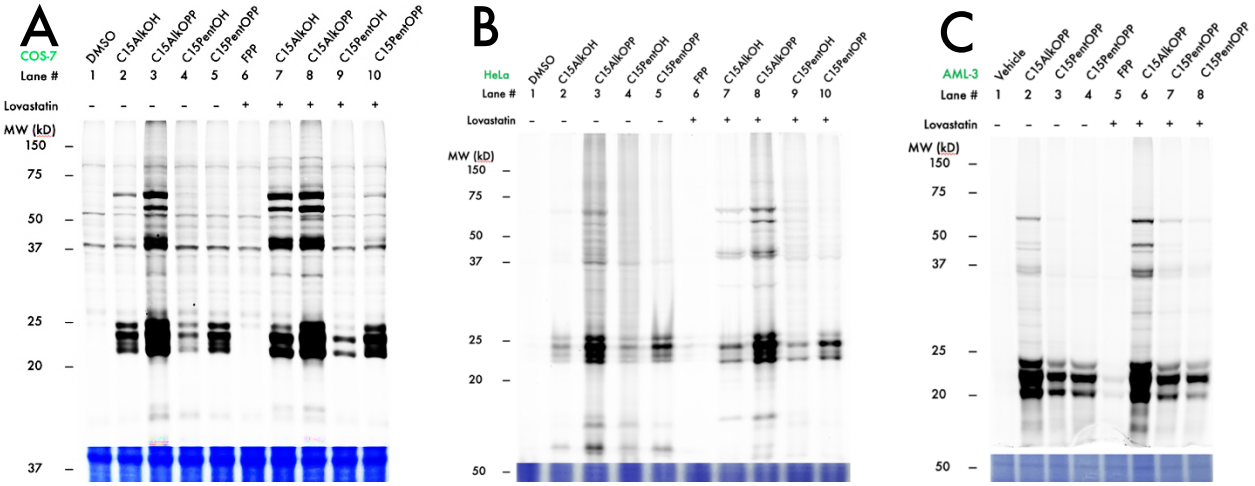

Figure 4. The C15AlkOPP and C15PentOPP probes are compared with their respective alcohol forms via metabolic labeling.
(A) In-gel fluorescence analysis in COS-7 cells **(B)** In-gel fluorescence analysis in HeLa cells. **(C)** In-gel fluorescence analysis in AML-3 cells. All treatments were performed at 10 μM probe final concentration. Labeling is more potent in COS-7 and AML-3 cells compared to HeLa cells. The C15PentOPP labeling appears more specific for geranylgeranylated proteins. All lanes were subjected to click reaction with TAMRA-N_3, followed by electrophoretic separation on 12% SDS-PAGE gels.

2. 2. 4. Cell Culture-based Proteomics for Protein Identification

2. 2. 4. 1. Proteomic Analysis of *in-cellulo* Profiling

To evaluate the selective labeling of geranylgeranylated proteins by the C15PentOPP probe, it was next analyzed in proteomic experiments. Parallel experiments with C15AlkOPP were performed to serve as a point of comparison. For these

experiments, COS-7 cells were pre-treated with lovastatin for 6 h, followed by 24 h of incubation with C15AlkOPP, C15PentOPP or FPP (as a control). The FPP control served to offset any possible deleterious effect that the statin treatment could cause on the cell physiology. As AML-3 cells displayed little statin-dependent changes in labeling in response to lovastatin, they were incubated directly with the corresponding diphosphates, without exposure to statin and using a vehicle control in lieu of FPP. Triplicate samples were lysed and subjected to a biotin-N_3 click reaction for enrichment of prenylated proteins via neutravidin pull-down. Subsequent washes were used to remove non-specifically bound proteins followed by tryptic digestion and collection. After Tandem Mass Tag (TMT) 6-plex labeling, the peptides from 3 replicate samples and 3 control samples were combined and fractionated at high pH under reversed-phase conditions with increasing acetonitrile concentrations. Each fraction was then subjected to UPLC-MS^3 analysis, followed by identification of enriched prenylated proteins by comparison of detected peptides with the human database and statistical analysis.

2. 2. 4. 2. Results in COS-7 in the Presence of Statin and AML-3 in the Absence of Statin

To detect which prenylated proteins could be labeled by the two probes, proteomic profiling was first performed using COS-7 cells incubated with the probe in the presence of 10 μM lovastatin, since those cells showed the best in-gel fluorescence labeling. Using this approach, a total of 78 and 58 prenylated proteins were significantly enriched with the C15AlkOPP probe and C15PentOPP probe, respectively (Fig. 5A and 5B). Out of these, 53 were found in common between the 2 datasets (Fig. 6A).

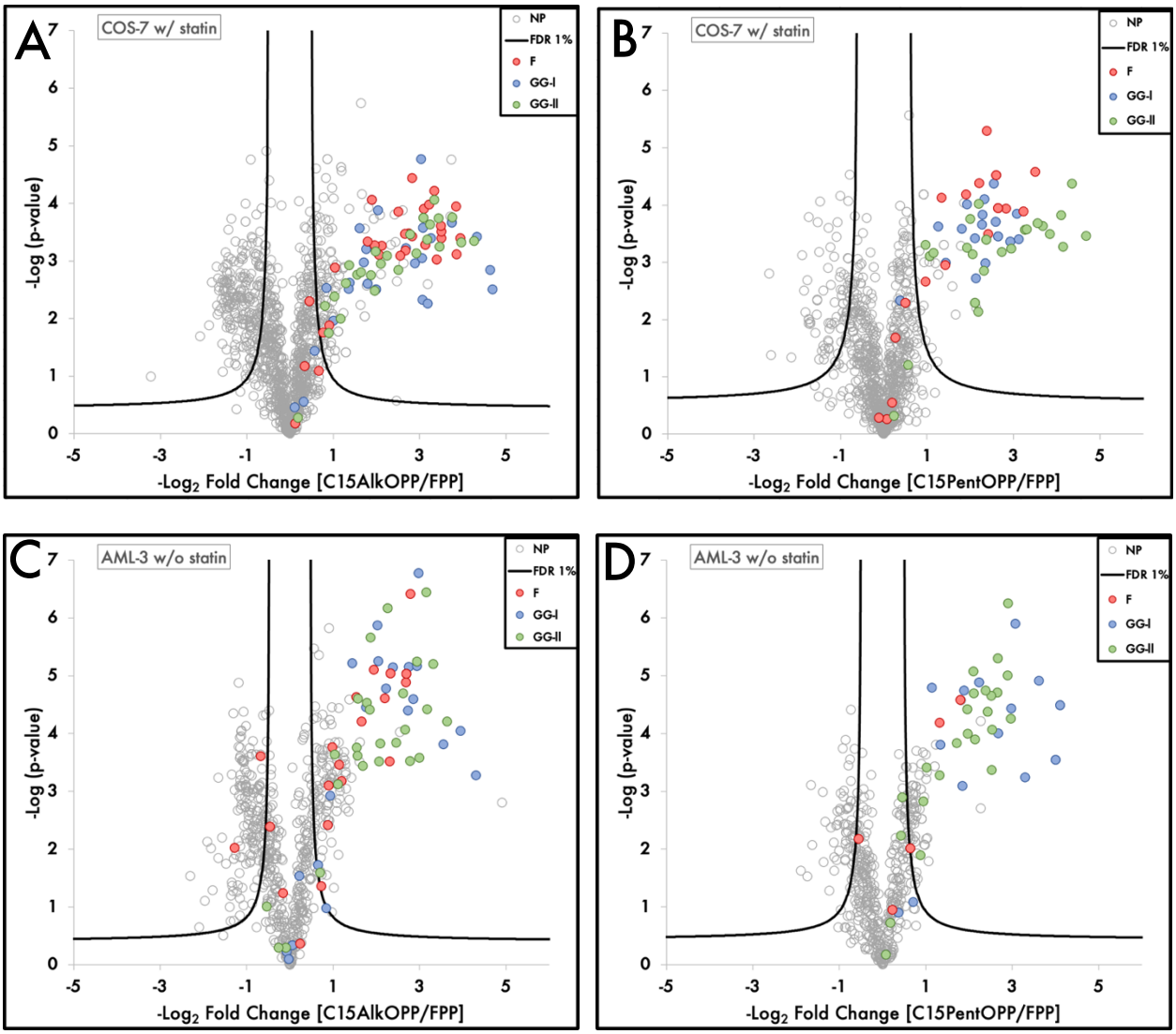

Figure 5. Prenylome profiling with the C15AlkOPP and C15PentOPP probes in 2 different cell lines.
(A) Volcano plot showing prenylated proteins identified with C15AlkOPP in COS-7 cells in the presence of statin. **(B)** Volcano plot showing prenylated proteins identified with C15PentOPP in COS-7 cells in the presence of statin. **(C)** Volcano plot showing prenylated proteins identified with C15AlkOPP in AML-3 cells in the absence of statin. **(D)** Volcano plot showing prenylated proteins identified with C15PentOPP in AML-3 cells in the absence of statin. All treatments were performed at n = 3 and 10 μM probe/statin final concentration. FPP was used as the control comparison in all cases with stringent FDR = 0.01, s0 = 0.5 parameters.

The C15AlkOPP dataset contained 65% GG proteins, whereas the C15PentOPP dataset contained 74% GG proteins, showing more selectivity towards geranylgeranylated proteins. There were 5 proteins found only with the longer probe,

namely HRAS, RAB13, RAB3B, RAB9B and RAB1C, that have been previously reported in our group as prenylated proteins (Fig. 6A).[40]

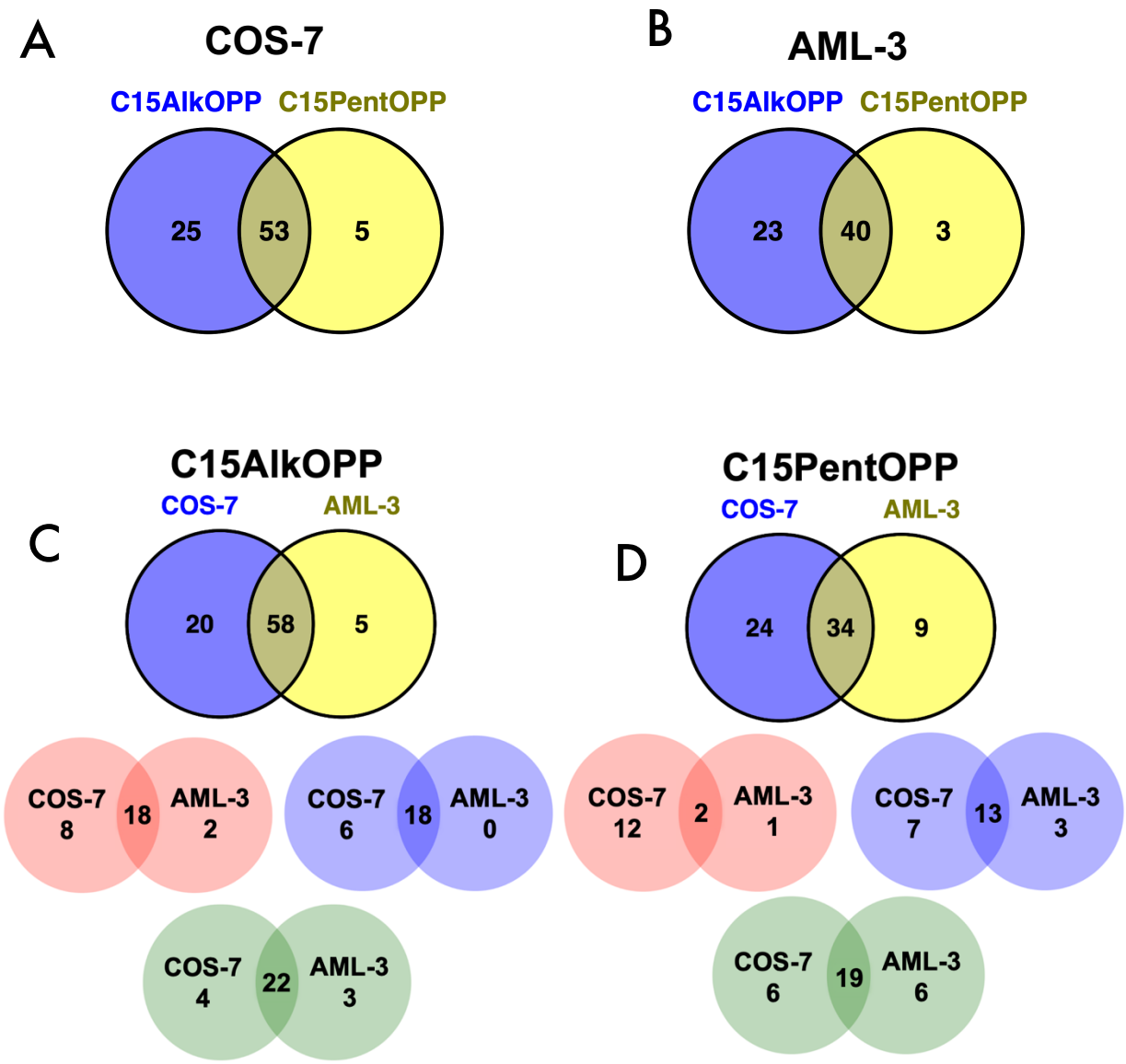

Figure 6. Significantly enriched prenylated proteins found with C15AlkOPP and C15PentOPP COS-7 and AML-3 cell lines.
(A) Venn diagram showing the overlap of proteins identified in COS-7. **(B)** Venn diagram showing the overlap of proteins identified in AML-3. **(C)** Venn diagrams showing the overlap of proteins identified in COS-7 and AML-3 with C15AlkOPP in total and in the 3 classes of prenylation. **(D)** Venn diagrams showing the overlap of proteins identified in COS-7 and AML-3 with C15PentOPP in total and in the 3 classes of prenylation. Protein groups were separated into individual proteins. The types of prenylation were color coded as follows: farnesylation (red), geranylgeranylation type-I (blue), geranylgeranylation type-II (green).

In AML-3, in the absence of statin (Fig. 5C and 5D), the total number of significantly enriched prenylated proteins identified was lower, with 63 identified with the C15AlkOPP probe and 43 with the C15PentOPP probe (Fig. 6B). Overall, the C15PentOPP protein dataset is largely a subset of the C15AlkOPP dataset in both cell lines, with the proteins uniquely identified by C15PentOPP (5 in COS-7 and 3 in AML-3) having been previously identified as prenylated proteins.[3] The C15AlkOPP dataset contained 68% GG proteins, whereas the C15PentOPP dataset comprised of 93% geranylgeranylated proteins, showing almost total selectivity towards geranylgeranylation in the absence of statin. Three proteins that we have previously reported as prenylated (RHOC, RAB8B, RAB2B), were solely found in the C15PentOPP dataset (Fig. 6B).[40] Overall, C15AlkOPP labeled more proteins than C15PentOPP in both cell lines, with a greater number of proteins uniquely found with C15AlkOPP (25 in COS-7 and 23 in AML-3).

2. 2. 4. 3. Comparing Proteins Found in COS-7 vs AML-3

When examining the total number of proteins identified by the C15AlkOPP probe, there were 58 found in common between COS-7 and AML-3, with 5 others found only in the latter cell line, namely ALDH9A1 (F), HRAS (GG-I), RAB27A, RAB7B, RAB1C (GG-II), representing primarily geranylgeranylated proteins (Fig. 6C). With the C15PentOPP probe, 34 proteins were identified in both cell lines, with 9 proteins unique in the AML-3 data set. Of those 9, geranylgeranylated proteins were again the major type, with 8 proteins (RALB, RHOC, RAB3A, RAB27A, RAB2B, RAB24, RAB7B, RAB34) belonging to that class (Fig. 6D).

2. 2. 4. 4. Comparing Proteins Based on Prenylation Type

For geranylgeranylated proteins, there was substantial overlap between the 2 cell types with both probes (Fig. 6C and 6D, blue and green Venn diagrams). For farnesylated proteins, the C15AlkOPP (Fig. 6C) showed good overlap again, but the C15PentOPP, being very selective for geranylgeranylated proteins, especially in the absence of statin, had a lower number of farnesylated proteins to compare in AML-3 versus COS-7 (Fig. 6D). The overall tendency was towards good overlap between the 2 different cell types, with more proteins identified overall in COS-7 than in AML-3. One reason for this is undoubtedly due to the presence of statin in the experiments in COS-7 but not AML-3 (Fig. 6).

2. 2. 4. 5. Comparing Prenylation Types with YnGG and YnF Probes Created by Tate and Coworkers

While the experiments performed by Tate and coworkers had some differences,[34,41] it is still relevant to compare their results with ours. It is worth mentioning that the length of their geranylgeranylation specific probe, YnGG, was one carbon atom shorter than C15PentOPP and that their YnF probe is 2 carbon atoms shorter than C15AlkOPP (Fig. 7C).[34] Also, the Tate group performed metabolic labeling using label-free quantitation and the alcohol form of their probes in their experiments, whereas tandem-mass-tag quantitation and the diphosphate form of the probe were used in our experiments. Finally, our experiments were performed using COS-7 cells pre-incubated

with statin while theirs were carried out in EA.hy926 cells without any statin pre-treatment. Despite those differences, comparison of the data obtained here in COS-7 cells with the Tate data obtained in EA.hy926 cells, indicates that there is significant overlap between the sets of proteins identified with each group of probes (Fig. 5A and 5B).

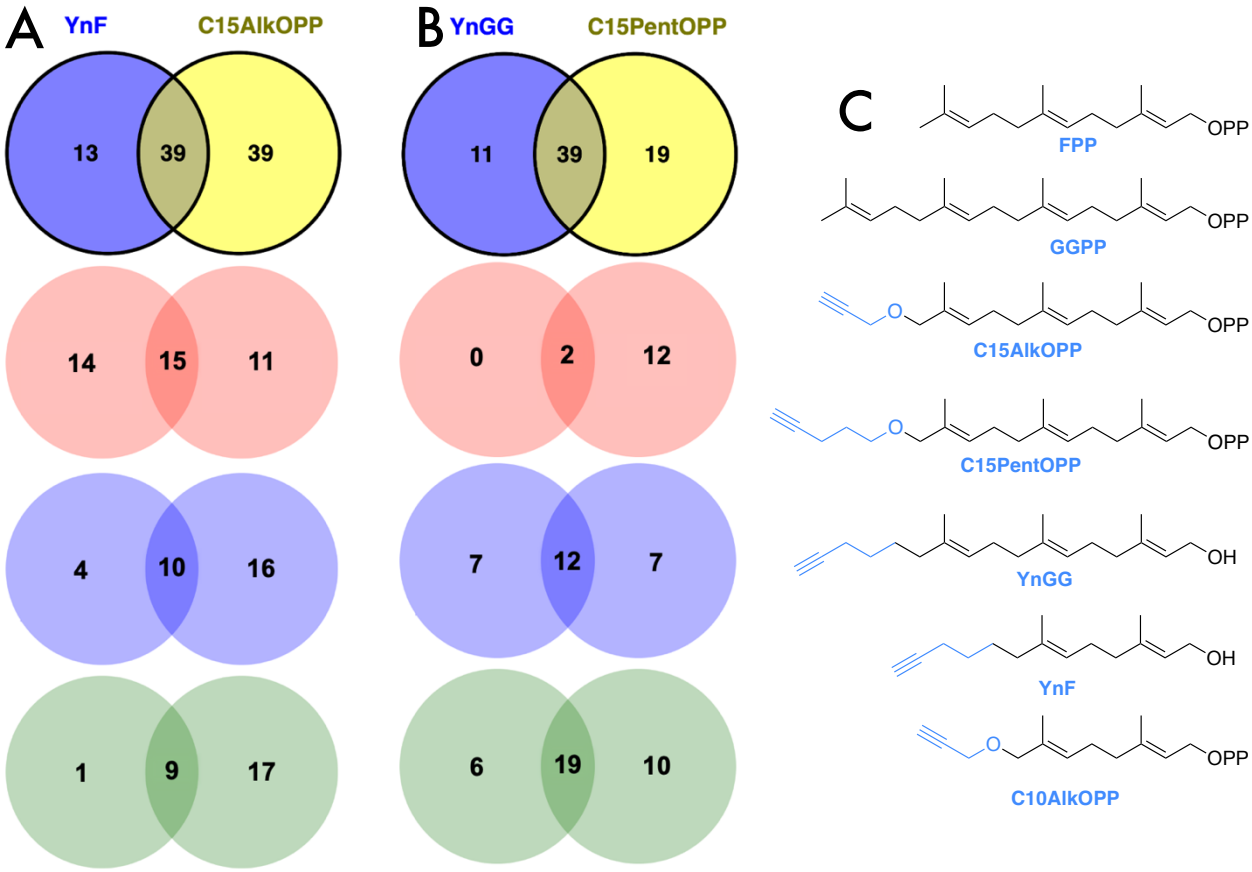

Figure 7. Significantly enriched prenylated proteins found by the Tate group with YnF and YnGG in EA.hy926 cells compared with the COS-7 analysis with C15AlkOPP and C15PentOPP used in this chapter.
(A) YnF compared with C15AlkOPP data. **(B)** YnGG compared with C15PentOPP data. **(C)** Structures of the probes used in our experiments and the 2 probes used by the Tate group. Our C10AlkOPP showed poor labeling results but the structure is included for length comparison with YnF. All prenylation categories contain some overlap. C15AlkOPP and C15PentOPP detected overall more proteins than the YnF and YnGG probes. The types of prenylation were color coded as follows: farnesylated (red), geranylgeranylated type-I (blue), geranylgeranylated type-II (green).

The YnF probe identified more farnesylated proteins (29) than the C15AlkOPP probe (26), but for geranylgeranylation targets, the latter probe identified more (52 total for C15AlkOPP versus 24 for YnF) (Fig. 7A). The C15PentOPP probe labeled more FTase and GGTase-II targets and an equal number of GGTase-I substrates compared with YnGG (Fig. 7B). Overall, the C15AlkOPP and C15PentOPP probes label more proteins than YnF and YnGG (78 and 58 for C15AlkOPP and C15PentOPP respectively, versus 52 for YnF and 50 for YnGG), however our experiments were performed in the presence of statin. Probably the most noteworthy difference between these isoprenoid analogues is that the C15AlkOPP probe labels all classes of prenylated proteins whereas the YnF probe labels predominantly farnesylated proteins. Similarly, the C15PentOPP probe labels a wide variety of prenylated proteins including farnesylated proteins whereas the YnGG probe is considerably more selective for geranylgeranylated proteins compared with C15PentOPP. That latter observation is somewhat surprising since C15PentOPP is one carbon longer than YnGG. However, again, the inclusion of statin in the C15PentOPP experiment likely contributes to this. The aforementioned in-gel fluorescence experiments shown in Figure 4 show enhanced incorporation in the 37-75 kDa region in the presence of statin. Those proteins are likely farnesylated suggesting that the inclusion of statin effectively suppresses endogenous FPP levels allowing the longer but poorer substrate (the probe) to be incorporated.

When combining the 2 datasets of C15AlkOPP and C15PentOPP profiling, there were 83 unique prenylated proteins identified (Table 1, left hand side), whereas combining the Tate's group YnF and YnGG profiling datasets yielded 80 proteins uniquely identified (Table 1, right hand side). Interestingly, despite the differences in experimental conditions

including cell type and methodology, 61 prenylated proteins were identified as common between the 2 combined datasets (Table 1, green), highlighting the similarities obtained with these probes.

Table 1. Protein datasets for the C15AlkOPP and C15PentOPP combined for a total of 83 distinct prenylated proteins are compared with the datasets of the YnF and YnGG probes that have a combined total of 80 distinct prenylated proteins.
In green, 61 proteins are commonly found across the 2 combined datasets.

	C15AlkOPP & C15PentOPP			YnF & YnGG		
No.	C15AlkOPP	C15PentOPP	Combined	Combined	YnF	YnGG
1	BROX	BROX	BROX	BROX	BROX	CDC42
2	CDC42	CDC42	CDC42	CDC42	CDC42	CNP
3	CENPF	CNP	CENPF	CENPF	CENPF	FBXL2
4	CNP	DNAJA1	CNP	CNP	CEP85	GNG10
5	DNAJA1	DNAJA2	DNAJA1	DNAJA1	CNP	GNG12
6	DNAJA2	GNG12	DNAJA2	DNAJA2	DCAF8	GNG5
7	GBP1	GNG5	GBP1	GBP1	DCAF8	MIEN1
8	GBP2	HRAS	GNG10	GNG10	DNAJA1	RAB10
9	GNG10	KRAS	GNG12	GNG12	DNAJA2	RAB11B
10	GNG12	LMNB1	GNG5	GNG5	DPCD	RAB12
11	GNG5	LMNB2	KRAS	KRAS	EHBP1	RAB13
12	GNG7	MRAS	LMNB1	LMNB1	EHBP1L1	RAB14
13	INPP5A	NRAS	LMNB2	LMNB2	GBP1	RAB18
14	KRAS	PTP4A1	MIEN1	MIEN1	GNG12	RAB1A
15	LMNB1	PTP4A2	NAP1L1	NAP1L1	GNG5	RAB1B
16	LMNB2	RAB10	PEX19	PEX19	INF2	RAB21
17	MIEN1	RAB11A	PHKB	PHKB	KRAS	RAB22A
18	MRAS	RAB11B	PTP4A1	PTP4A1	LMNA	RAB23
19	NAP1L1	RAB13	PTP4A2	PTP4A2	LMNB1	RAB27A
20	NRAS	RAB14	RAB10	RAB10	LMNB2	RAB2A
21	PALM	RAB18	RAB11A	RAB11A	LRRFIP1	RAB30
22	PEX19	RAB1A	RAB11B	RAB11B	NAP1L1	RAB31
23	PHKA1	RAB1B	RAB13	RAB13	NAP1L4	RAB32
24	PHKA2	RAB1C	RAB14	RAB14	PEX19	RAB33B
25	PHKB	RAB21	RAB18	RAB18	PHKB	RAB34
26	PTP4A1	RAB22A	RAB1A	RAB1A	PTP4A1	RAB35
27	PTP4A2	RAB23	RAB1B	RAB1B	PTP4A2	RAB3B
28	PTP4A3	RAB2A	RAB21	RAB21	RAB10	RAB3D
29	RAB10	RAB31	RAB22A	RAB22A	RAB11A	RAB4A

30	RAB11A	RAB32	RAB23	RAB23	RAB11B	RAB5A
31	RAB11B	RAB33B	RAB2A	RAB2A	RAB14	RAB5B
32	RAB14	RAB35	RAB31	RAB31	RAB1B	RAB5C
33	RAB18	RAB3B	RAB32	RAB32	RAB21	RAB6A
34	RAB1A	RAB3D	RAB33B	RAB33B	RAB5C	RAB7A
35	RAB1B	RAB4B	RAB34	RAB34	RAB6A	RAB8A
36	RAB21	RAB5A	RAB35	RAB35	RAB7A	RAB8B
37	RAB22A	RAB5B	RAB3B	RAB3B	RAB8A	RAC1
38	RAB23	RAB5C	RAB3D	RAB3D	RAC1	RAC2
39	RAB24	RAB6A	RAB4A	RAB4A	RALB	RALA
40	RAB2A	RAB6B	RAB5A	RAB5A	RAP1B	RALB
41	RAB31	RAB7A	RAB5B	RAB5B	RAP2B	RAP1B
42	RAB32	RAB8A	RAB5C	RAB5C	RAP2C	RAP2B
43	RAB33B	RAB8B	RAB6A	RAB6A	RHEB	RHOA
44	RAB34	RAB9A	RAB7A	RAB7A	RHOA	RHOB
45	RAB35	RAB9B	RAB8A	RAB8A	RHOBTB3	RHOF
46	RAB3A	RAC1	RAB8B	RAB8B	RHOG	RHOG
47	RAB3D	RAC2	RAC1	RAC1	RND3	RHOJ
48	RAB4A	RALA	RAC2	RAC2	RRAS	RRAS
49	RAB4B	RAP1A	RALA	RALA	RRAS2	RRAS2
50	RAB5A	RAP1B	RALB	RALB	SPDL1	YKT6
51	RAB5B	RAP2B	RAP1B	RAP1B	ULK3	
52	RAB5C	RHEB	RAP2B	RAP2B	YKT6	
53	RAB6A	RHOA	RAP2C	RAP2C	ZC3HAV1	
54	RAB6B	RHOB	RHEB	RHEB		
55	RAB7A	RHOG	RHOA	RHOA		
56	RAB8A	RRAS	RHOB	RHOB		
57	RAB8B	RRAS2	RHOG	RHOG		
58	RAB9A	YKT6	RND3	RND3		
59	RAC1		RRAS	RRAS		
60	RAC2		RRAS2	RRAS2		
61	RALA		YKT6	YKT6		
62	RALB		GBP2	CEP85		
63	RAP1A		GNG7	DCAF8		
64	RAP1B		HRAS	DPCD		
65	RAP2A		INPP5A	EHBP1		
66	RAP2B		MRAS	EHBP1L1		
67	RAP2C		NRAS	FBXL2		
68	RHEB		PALM	INF2		
69	RHOA		PHKA1	LMNA		
70	RHOB		PHKA2	LRRFIP1		

71	RHOC		PTP4A3	NAP1L4		
72	RHOG		RAB1C	RAB12		
73	RND3		RAB24	RAB27A		
74	RRAS		RAB3A	RAB30		
75	RRAS2		RAB4B	RHOBTB3		
76	STK11		RAB6B	RHOF		
77	UBL3		RAB9A	RHOJ		
78	YKT6		RAB9B	SPDL1		
79			RAP1A	ULK3		
80			RAP2A	ZC3HAV1		
81			RHOC			
82			STK11			
83			UBL3			

2. 2. 5. Proteomic Analysis of GGTase-I Inhibition Data with C15PentOPP

Given the superior preference for geranylgeranylated proteins of the C15PentOPP probe in the absence of statin (Fig. 5D), an inhibition experiment was carried out to further examine the selectivity of this probe towards geranylgeranylated proteins and the possibility of using this approach to to examine geranylgeranylation inhibition of many proteins simultaneously in a single experiment. Out of the 16 geranylgeranylation type-I proteins identified with C15PentOPP in AML-3, almost half (7) were inhibited by GGTI-298, a GGTase-I inhibitor (RAP2A, RALA, RAP1B, RAP1A, RAP2B, RAP2C, GNG5). That experiment was performed using 10 μM GGTI-298 which has a reported IC_{50} of 5 μM in NIH 3T3 cells.[42] It is worth noting that RAP2A is known to be one of the proteins that is subjected to alternative prenylation allowing it to be prenylated by either FTase or GGTase-I.[34,43] Using a different GGTase-I inhibitor, GGTI-2133, only detected 4 proteins significantly depleted (RALA, RAP1B, RAP1A, MIEN). This experiment was also

performed using 10 μM GGTI-2133 which has a reported IC_{50} of 10 μM in NIH 3T3 cells.[42] When using a less stringent but still statistically significant false discovery rate of 5% (FDR = 0.05), the number of significantly depleted geranylgeranylated type-I proteins grew to 14 for GGTI-298 (Fig. 8A) and 10 for GGTI-2133 (Fig. 8B), which indicates that almost all of the geranylgeranylated type-I proteins discovered during profiling were selectively inhibited by this class of enzyme inhibitors. The diminished inhibition obtained with GGTI-2133 compared with GGTI-298 is consistent with the differences in their published IC_{50} values of 10 μM and 5 μM, respectively. These experiments establish that the C15PentOPP probe can be used successfully in combination with GGTase-I inhibitors to identify protein targets potentially involved in this specific type of prenylation.

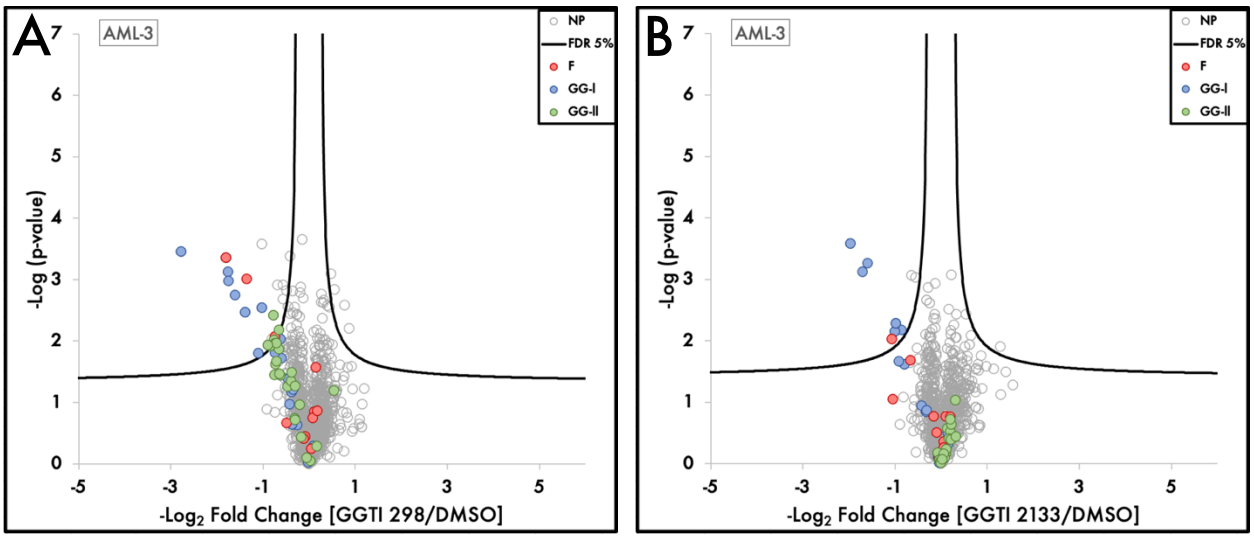

Figure 8. Volcano plots for inhibition of GG-I with the C15PentOPP probe.
(A) GGTI 298 inhibition showing 14 geranylgeranylated type-I proteins. **(B)** GGTI 2133 inhibition showing 10 geranylgeranylated type-I proteins. All treatments were performed in AML-3 cells at n = 3 and 10 μM probe/GGTI final concentration. DMSO was used as the control comparison in all cases with FDR = 0.05, s0 = 0.1 parameters.

2. 2. 6. In-vivo Labeling

2. 2. 6. 1. Experiment Design

Next, metabolic labeling was investigated in mice. If efficient labeling of prenylated proteins could be accomplished in such experiments, it would greatly increase the types of diseases and biological question that could be investigated. Earlier experiments had been conducted using the alcohol form of the probe (C15AlkOH) prepared as an emulsion in 5% Tween 80 since early metabolic labeling experiments had been carried out using that form of the probe. Prior to injection, mice were dosed with simvastatin 24 h before probe administration (either intraperitoneal or subcutaneous injection); after allowing 24 h for probe incorporation, the mice were sacrificed and brains, kidneys, liver and spleen were harvested. Cell lysis followed by click reaction with TAMRA-N_3, SDS-PAGE fractionation and fluorescent scanning revealed the presence of some labeling in the kidney and liver. Unfortunately, subsequent prenylomic analysis revealed only two potentially prenylated proteins. More recent metabolic labeling results demonstrated that the diphosphate form of the probe (C15AlkOPP) was more efficient than the alcohol form for labeling prenylated proteins in cell culture. That was reproduced in the metabolic labeling experiments described above. In addition, effective labeling of 37 different prenylated proteins in the mouse brain had been accomplished via intracerebroventricular infusion of C15AlkOPP directly into the brain (over a 2-week period).[32] Encouraged by those observations, experiments to label peripheral organs in mice were undertaken here. Given the aforementioned results obtained via subcutaneous injection of C15AlkOH,

efforts focused on that mode of administration. Accordingly, C15AlkOPP and C15PentOPP were injected subcutaneously in APP/PS1 mice either once followed by organ harvesting after 24 h or 3 times at 24 h intervals followed by harvesting after an additional 24 h. Labeling was observed with the C15AlkOPP probe in the liver and kidney (Fig. 9B).

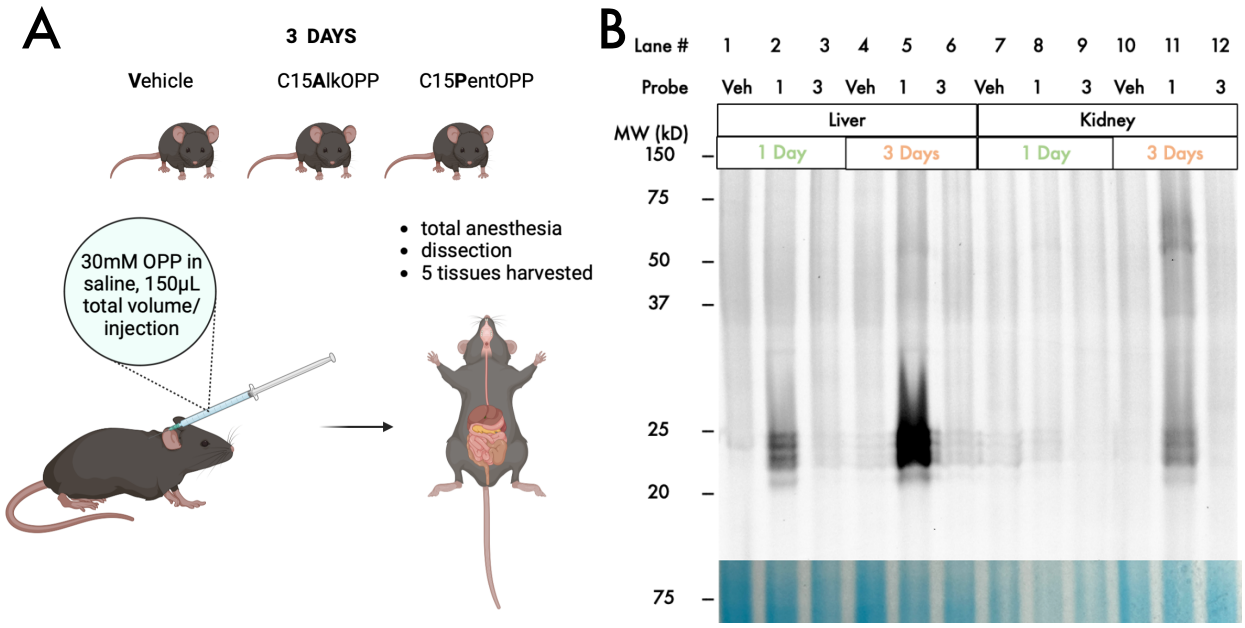

Figure 9. Animal experiment schematic and initial in-gel fluorescence results in the liver and kidney after 1 day and after 3 days.
Probe 1 = C15AlkOPP, probe 3 = C15PentOPP, Veh = vehicle control. All lanes were subjected to click reaction with TAMRA-N_3, followed by electrophoretic separation on 12% SDS-PAGE gels.

2. 2. 6. 2. In-gel Fluorescence Comparison Between E3/E4

To test the labeling potency of the C15AlkOPP probe in vivo, we wanted to answer a biological question, relevant for Alzheimer's Disease (AD). It is known that the E4 gene, when present in patients, increases their risk of developing AD up to 15-fold, whereas the E3 isoform does not have an impact on AD development.[16,18]

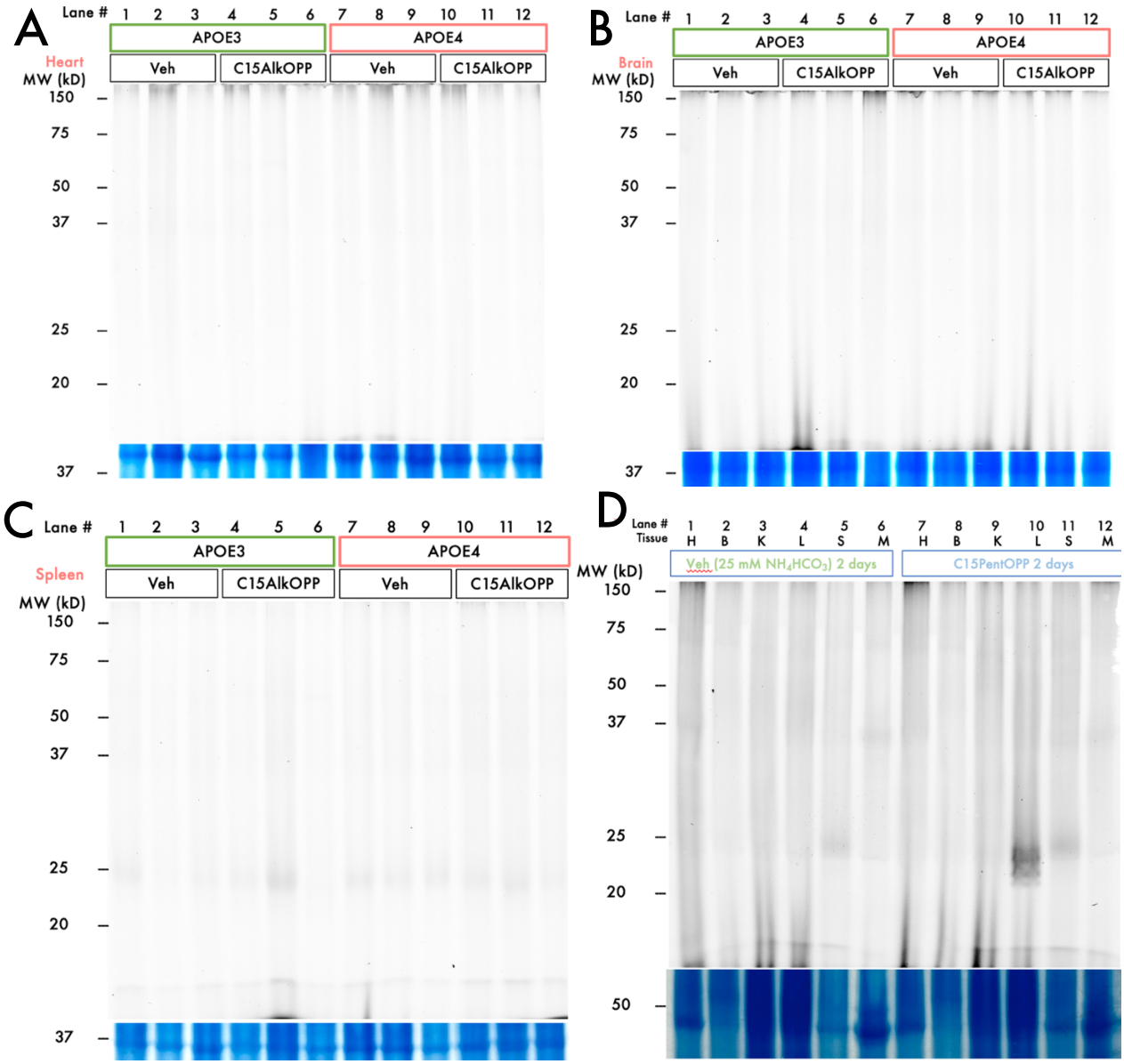

Figure 10. In gel fluorescence for different tissues and probes.
(A) C15AlkOPP in Heart after 3 days **(B)** C15AlkOPP in Brain after 3 days **(C)** C15AlkOPP in Spleen after 3 days **(D)** C15PentOPP in Heart, Brain, Kidney, Liver, Spleen and skeletal muscle after 2 days. All lanes were subjected to click reaction with TAMRA-N_3, followed by electrophoretic separation on 12% SDS-PAGE gels.

To determine whether prenylation levels vary in response to different APOE isoforms, humanized mice expressing either APOE3 or APOE4 were chosen for study. The mice were injected subcutaneously with 150 µL of C15AlkOPP or FPP control solution at 24 h intervals. After 72 h, the mice were dissected and the heart, brain, kidney,

liver and spleen tissues were collected and homogenized. The tissues were lysed and reacted with TAMRA-N_3, followed by SDS-PAGE fractionation and in-gel fluorescence scanning. The heart, brain and spleen tissues showed no probe incorporation above the control (Fig. 10A, 10B and 10C). The kidney and the liver samples were the only tissues to show labeling after subjecting the tissue lysates to the in-gel fluorescence workflow. Labeling was observed across the 3 replicates between 20 and 75 kDa in the kidney in both E3 and E4 samples, with a tendency of E3 labeling (1.8 relative intensity) to be stronger that E4 labeling (1.3 relative intensity) when quantifying the band intensities via densitometry (Fig. 11A). In contrast, in the liver, labeling was localized around the 20-25 kDa region in both E3 and E4 replicates, and labeling was more pronounced in E4 (2.2 relative intensity) than in E3 (1.9 relative intensity) when quantifying intensities of the bands via densitometry (Fig. 11B).

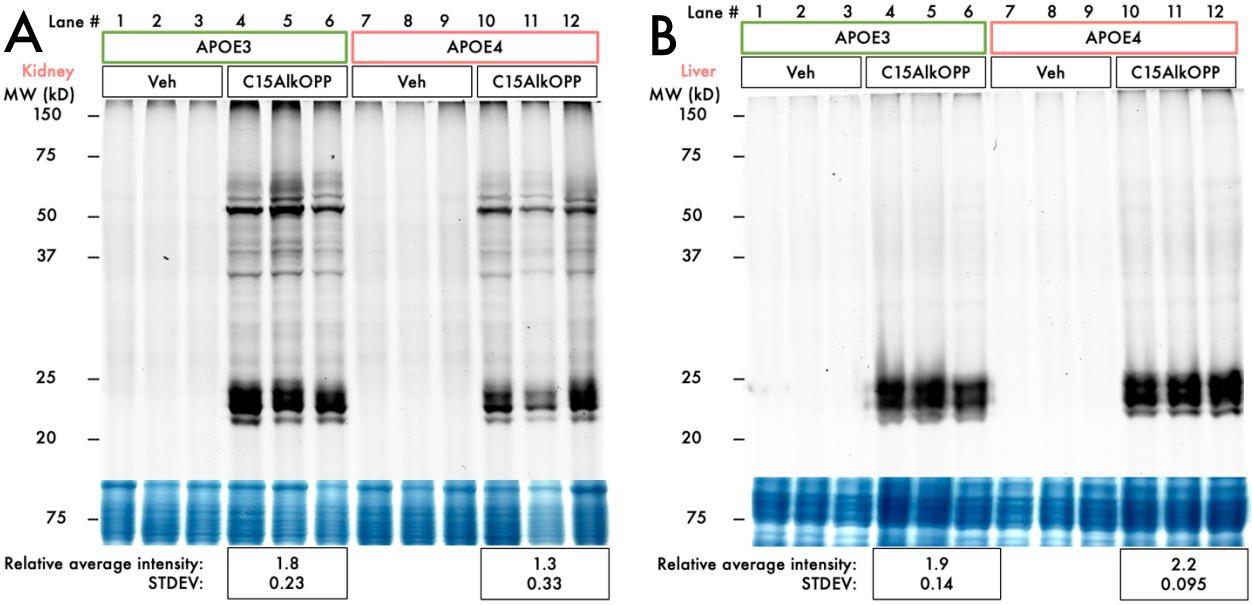

Figure 11. In-gel fluorescence data for APOE3 and APOE4 mice showing different labeling patterns in kidney and liver with the C15AlkOPP probe.
(A) Kidney E3/E4 comparison. **(B)** Liver E3/E4 comparison. All lanes were subjected to click reaction with TAMRA-N_3, followed by electrophoretic separation on 12% SDS-PAGE gels.

2. 2. 6. 3. Mouse Liver Proteomics with C15AlkOPP

Having seen potential differences in the labeling patters in the liver and kidney, and given that the liver is the only place in the periphery where APOE is synthesized,[20,21] we were excited to first examine the liver samples through proteomic profiling analysis. For both E3 and E4, less background was observed than in the cell-based experiments, with only prenylated proteins being found significantly enriched at an FDR of 1% (Fig. 12A and 12B, colored dots). There were 24 significantly enriched prenylated proteins in the E3 dataset and 23 in the E4 dataset. Of those, 20 proteins were found in common between the 2 datasets, with 9 of them having various degrees of statistically significant differences in their fold change values (Fig. 12C, right side of plot). The highest changes were observed though in the proteins solely identified in one dataset or another, namely RAB1C, RAB22A, RAB35 (geranylgeranylated type-II) and YKT6 (farnesylated/geranylgeranylated type-I) were only found significantly enriched in E3, and RAB21, RAB2B (geranylgeranylated type-II) and PEX19 (farnesylated) being found significantly enriched only in the E4 dataset (Fig. 12C, left side of plot). It must also be noted that, interestingly, 5 of these proteins found in higher levels in E4 mice with high confidence (RAB1A, RAB1B, RAB2A, RAB2B and RAB6A) were also found to be present in higher levels in a previous study that examined protein prenylation in the brains of AD mice.[32]

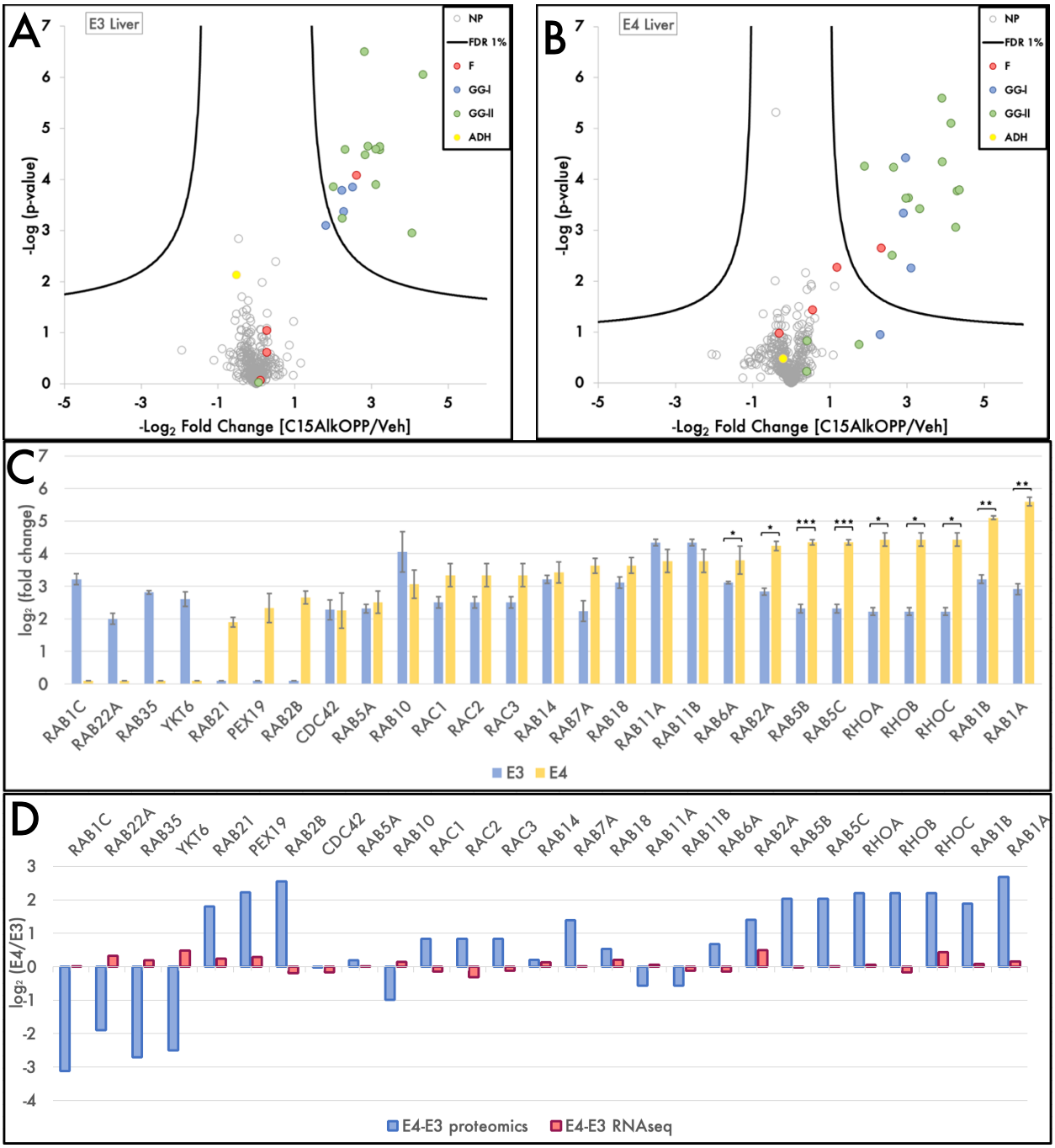

Figure 12. Proteomic profiling data for APOE3 and APOE4 mouse liver with the C15AlkOPP probe.

(A) Volcano plot for the E3 liver. **(B)** Volcano plot for the E4 liver. **(C)** Bar graph of protein identity versus fold change of significantly enriched proteins in E3 and E4. **(D)** Bar graph showing protein identities and difference in fold change between E3 and E4 in the proteomic experiment (blue bars) and in transcriptomic data (red bars). All treatments were performed subcutaneously at n = 3 and 1 daily 150 µL injection at 33 mM for 3 days. 25mM NH_4HCO_3 was used as the control and statistical data analysis was performed with stringent FDR = 0.01, s0 = 0.5 parameters. ADH (yellow dot) was the internal standard. Significance in the bar graph was tested using a two-tailed, unpaired t-test and is indicated

as *P< 0.05, **P< 0.01, and ***P<0.001. Error bars show standard error. The first 7 proteins are unique in only one of the data sets, but the respective fold change is represented as 0.1 just for illustration purposes only. RNAseq data was obtained from Gene Expression Omnibus dataset GSE42930 by Graeser *et al* in the liver of targeted gene replacement mice.

To validate the changes in prenylation observed for the 27 proteins plotted in Figure 12C do not originate in the differential expression levels of those genes in the E3 and E4 genotypes, a comparison with RNAseq data was performed. In Figure 12D, the difference in the $\log_2$ fold changes for the 27 genes are plotted for the proteomic data obtained above (blue bars) and for the transcriptomic data (red bars) obtained from the Gene Expression Omnibus dataset GSE42930 by Graeser *et al* in the livers of targeted replacement APOE3 and APOE4 mice. What is important to note is that the difference in fold change in the proteomic data is much greater than that observed in the transcriptomic data, where the respective proteins didn't have significantly higher/lower levels of expression. Importantly, this indicates that the changes in prenylation levels observed in the proteomic analysis were not due to differential (higer/lower) gene expression in each APOE genotype, but indeed a direct implication of upregulation/downregulation of prenylation itself. This validates the results obtained in the proteomic analysis and opens the door for further studies using the statistically significant proteins as drug targets in the context of Alzheimer's disease.

2. 2. 6. 4. Mouse Kidney Proteomics with C15AlkOPP

For the kidney proteomic analysis, there were 16 significantly enriched prenylated proteins in the E3 dataset and 11 in the E4 dataset, all of which were found in E3 (Fig. 13).

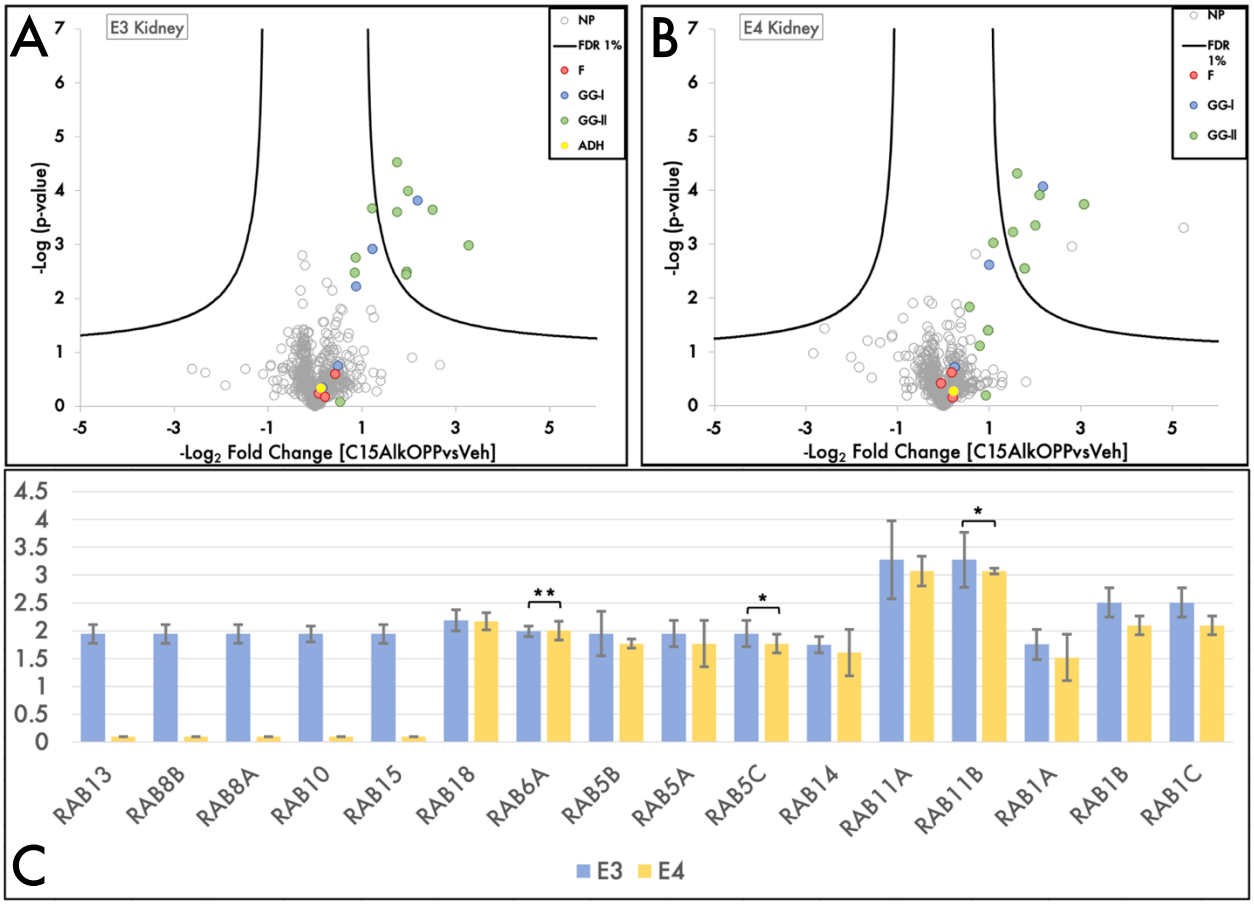

Figure 13. Proteomic profiling data for APOE3 and APOE4 mouse kidney with the C15AlkOPP probe.
(A) Volcano plot for the E3 kidney. **(B)** Volcano plot for the E4 kidney. **(C)** Bar graph of protein identity versus fold change of significantly enriched proteins in E3 and E4. All treatments performed at n = 3 and 1 daily 150 µL injection at 33 mM for 3 days. 25mM NH_4HCO_3 was used as the control and statistical data analysis was performed with FDR = 0.01, s0 = 0.5 parameters. ADH (yellow dot) was the internal standard. Significance in the bar graph was tested using a two-tailed, unpaired t-test and is indicated as *P< 0.05, **P< 0.01, and ***P<0.001. Error bars show standard error. The first 5 proteins are unique in only one of the data sets, but the respective fold change is represented as 0.1 just for illustration purposes only.

The changes in prenylation between the 2 datasets of E3 and E4 were much more modest, with just three proteins identified overall as having a statistically significant fold change from one genotype to another (Fig. 13).

2. 2. 6. 5. Interpretation of E3/E4 Differences

Apolipoprotein E (APOE) is a protein with a major role in the metabolism and transport of fats in mammals. In the brain, it is the main carrier of cholesterol.[44] In humans, there are three main alleles: E2 (8% world frequency), E3 (78% world frequency) and E4 (14% frequency).[17] The presence of the E2 isoform is indicative of lower risk for AD development and the E3 allele is considered to be neutral, whereas the presence of the E4 allele is a predictor, suggesting increasing risk of late onset AD by up to 15-33 fold when homozygous in different populations.[45] In an AD brain, the naturally occurring amyloid-β (Aβ) protein is found in abnormally high levels with the proteins associating, resulting in the formation of plaques that impair neuronal function. Fibrillar Aβ increases lipid droplets in the brain, a mechanism dependent on APOE4.[46]

Multiple RAB proteins have been linked with AD, some being upregulated in AD patients (RAB4A, RAB5, RAB6A, RAB7, RAB10, RAB27) and others having direct regulatory effects, interactions or increasing production of Aβ (RAB1A/B, RAB3A/B, RAB5, RAB6A, RAB11A/B, RAB39B).[47] The prenylated forms of RAB proteins found significantly enriched in E4 versus E3 in the liver proteomic analysis include: RAB1A, RAB1B, RAB2A, RAB5B, RAB5C, RAB6A. RAB1A and RAB1B prenylation is essential for their cellular functions that include protein transport, cell autophagy, cell signaling and,

importantly, intracellular trafficking of the amyloid-ß precursor protein.[48] This means that RAB1A/B proteins are directly involved in Aβ production, and their elevated detection in the E4 liver suggests that prenylation of RAB1A/B may be linked to AD. The RAB5B/C family serves a role in early endosome regulation. It is known that in AD, the RAB5 proteins are upregulated, which leads to enlarged endosomes.[49] Upregulation of RAB5 proteins has also been linked to increasing the production of Aβ protein, further connecting it with AD.[50] RAB6A, another protein that is upregulated in AD,[51] is known to interact with presenilin 1 (PSEN1),[52] one of the main proteins that regulates the production of the amyloid-ß precursor protein and hence, the production of Aβ. Thus, RAB6A may be indirectly related to AD development. The Rho family signaling pathway has been linked to promoting AD onset by increasing β-secretase activity and promoting amyloid-beta (Aβ) production.[53] Lastly, another protein found only in the E4 dataset is PEX19 whose farnesylation is essential for its role in peroxisomal function.[54] Peroxisomal dysfunctions have been correlated with early AD onset and accelerated brain aging,[55] therefore linking PEX19 directly with AD.

2. 3. Conclusions

In this work, two different alkyne-containing isoprenoid probes of different lengths (C15AlkOPP and C15PentOPP) were synthesized to study protein prenylation. The C15AlkOPP probe was able to identify via metabolic labeling and subsequent prenylomic analysis a plethora of prenylated proteins with high confidence in different cell lines, including COS-7 and AML-3. The C15PentOPP probe is longer and was designed to

selectively label geranylgeranylated proteins, which it does most successfully in the absence of statin. The proteins identified by the C15PentOPP probe are a subset of those labeled by the C15AlkOPP probe, further demonstrating the broader labeling ability of the latter probe. Both probes have been able to identify some proteins that others in the field were able to identify with different probes using comparable methods and experimental conditions, further validating the applicability of our probes and method. The C15PentOPP was responsive in labeling sets of geranylgeranylated type-I proteins in the presence of potent GGTase type-I inhibitors (GGTI 298 and GGTI 2133), revealing with high confidence prenylated targets of these inhibitory compounds.

When studying the two probes for prenylation *in vivo*, the C15AlkOPP probe showed labeling after one injection and more intense labeling after 3 days of daily injections in the liver and kidney, with the C15PentOPP probe showing weaker labeling after 2 days compared to the C15AlkOPP labeling after one day. The APOE gene has been associated with AD, so an experiment comparing protein prenylation in transgenic mice with the E3 allele of the APOE gene versus mice with the E4 allele revealed differences in prenylation in the liver, the main location for the endogenous synthesis of peripheral APOE. Out of the 27 proteins identified as significantly enriched with high confidence in the two datasets (E3 and E4), 4 were found only in E3, 3 were found only in E4 and 20 were found in both E3 and E4. From the 20 proteins found in common, 9 of them had fold changes that were statistically significant, with all these 9 proteins having a higher fold change value in the E4 dataset, along with implications in either APOE regulation/transport or AD pathology.

2. 4. Experimental Procedures

2. 4. 1. Synthetic Procedure for the C15PentOPP Probe

2-(((2E,6E)-3,7,11-trimethyldodeca-2,6,10-trien-1-yl)oxy)tetrahydro-2H-pyran (5)

This synthetic procedure follows a previously published protocol.[1] To a stirred solution of farnesol (5 g, 22.5 mmol, 1 equiv) in dry CH_2Cl_2 (50 mL), DHP (2,3-dihydropyran) (2.9 g, 33.8 mmol, 1.5 equiv) was added at rt. After that PPTS (0.6 g, 2.25 mmol, 0.1 equiv) was added to the reaction mixture at rt. The resulting solution was stirred at rt for 3 h. The reaction was quenched with saturated aqueous $NaHCO_3$ and extracted with CH_2Cl_2 (3 x 25 mL). The combined organic layer was dried over Na_2SO_4 and concentrated, affording compound **7** as a clear oil (6.8 g, 99%). Spectral data obtained were in good agreement with those reported in the literature.[1]

(2E,6E,10E)-2,6,10-trimethyl-12-((tetrahydro-2H-pyran-2-yl)oxy)dodeca-2,6,10-trien-1-ol (6)

This synthetic procedure follows a previously published protocol.[1] To a stirred solution of THP-protected farnesol **7** (6.8 g, 22.2 mmol, 1 equiv) in dry CH_2Cl_2 (50 mL), SeO_2 (225 mg, 2.22 mmol, 0.1 equiv) and salicylic acid (307 mg, 2.22 mmol, 0.1 equiv) were added at rt. After that, *t*-BuOOH (6 g, 66.6 mmol, 3 equiv) was added dropwise to the reaction mixture at rt. The resulting solution was stirred at rt overnight. The reaction was quenched with saturated aqueous $NaHCO_3$ and extracted with CH_2Cl_2 (3 x 25 mL).

The combined organic layer was dried over Na_2SO_4 and concentrated. The resulting crude product was dissolved in CH_3OH and subjected to $NaBH_4$ reduction: 1 equiv was added portion wise over the course of 1 h, while the reaction mixture was being stirred slowly on an ice bath. Then, the methanol was evaporated, and the reaction was extracted with EtOAc (3 x 25 mL). The combined organic layer was dried over Na_2SO_4, concentrated, and then purified by flash column chromatography on silica gel using 20% EtOAc/hexanes (v/v) to afford the desired allylic alcohol **6** (2 g, 28%). Spectral data obtained were in good agreement with those reported in the literature.[1]

2-(((2E,6E,10E)-12-chloro-3,7,11-trimethyldodeca-2,6,10-trien-1-yl)oxy)tetrahydro-2H-pyran (7)

NCS (2.5 g, 18.6 mmol, 3 equiv) was dissolved in dry CH_2Cl_2 (40 mL) under N_2. The resulting solution was placed on an ice bath and was stirred about 15 min until it reached 0 ºC. Then, $(CH_3)_2S$ (1.2 g, 18.6 mmol, 3 equiv) was added and the resulting mixture was stirred at 0 ºC for 30 min. Then, the ice bath was removed, and the mixture was allowed to reach rt (45 min). After that, the mixture was cooled back down to 0 ºC. The allylic alcohol **6**, dissolved in 10 mL of dry CH_2Cl_2, was then added dropwise over a period of 15 min (2 g, 6.2 mmol, 1 equiv). When the addition was complete, the ice bath was removed, and the reaction was allowed to reach rt. After stirring at rt for 3 h, the reaction was quenched with H_2O (50 mL) and extracted with CH_2Cl_2 (3 x 50 mL). The organic layer was dried over Na_2SO_4, concentrated, and then purified by flash column

chromatography on silica gel using 5% EtOAc/hexanes (v/v) to afford the desired allylic chloride **5** (1.5 g, 71%).

^{1}H NMR (500 MHz, $CDCl_3$): δ = 1.51-1.93 (m, 6H), 1.62 (s, 3H), 1.70 (s, 3H), 1.75 (s, 3H), 2.01-2.19 (m, 8H), 3.50-3.57 (m, 1H), 3.88-3.95 (m, 1H), 4.05-4.09 (m, 1H), 4.26 (dd, 1H, J = 8.0, 8.7), 4.65 (t, 1H, J = 4.5), 5.14 (t, 1H, J = 8.0), 5.38 (t, 1H, J = 7.5), 5.52 (t, 1H, J = 8.0).

^{13}C NMR (125 MHz, CDCl3): δ = 14.3, 16.0, 16.5, 19.7, 25.5, 26.3, 26.6, 30.7, 38.9, 39.6, 52.6, 62.3, 63.7, 97.9, 120.87, 124.5, 130.7, 131.6, 134.5, 140.1.

HRMS (ESI) m/z for $C_{20}H_{33}O_2ClNa^+$: calculated 363.2067, found 363.2077 $[M+Na]^+$.

2-(((2E,6E,10E)-3,7,11-trimethyl-12-(pent-4-yn-1-yloxy)dodeca-2,6,10-trien-1-yl)oxy)tetrahydro-2H- pyran (8)

First, 4-pentyn-1-ol (1.5 g, 17.6 mmol, 4 equiv) was dissolved in dry THF (30 mL) on an ice bath. Then, *t*-BuOK (2 g, 17.6 mmol, 4 equiv) was added slowly and the resulting mixture was placed under N_2. Then, 18-crown-6 ether (120 mg, 0.44 mmol, 0.1 equiv) was added and the reaction was stirred at 0 ºC for 15 min. After that, the allylic chloride **5** was added dropwise (1.5 g, 4.4 mmol, 1 equiv, dissolved in 10 mL dry THF) and the reaction was stirred for 1h at 0 ºC. The ice bath was then removed and the reaction was stirred at rt overnight. Then, the THF was removed *in vacuo* and the reaction was extracted with CH_2Cl_2. The organic layer was dried over Na_2SO_4, concentrated and then purified by flash column chromatography on silica gel using 5% EtOAc/hexanes (v/v) to afford the desired protected ether **4** (1.2 g, 70%).

^{1}H NMR (500 MHz, $CDCl_3$): δ = 1.62 (s, 3H), 1.66 (s, 3H), 1.70 (s, 3H), 1.78-1.81 (m, 6H), 2.00-2.17 (m, 8H), 2.39-2.47 (m, 4H), 3.44 (t, 2H, J = 7.0), 3.50-3.56 (m, 1H), 3.66 (td, 2H, J=7.1, 6.5), 4.05-4.09 (m, 1H), 4.26 (dd, 1H, J= 8.0, 8.7), 4.64 (t, 1H, J = 3.0), 5.13 (t, 1H, J = 7.5), 5.38 (q, 2H, J= 6.5).

^{13}C NMR (125MHz, CDCl3): δ = 13.8, 16.0, 16.4, 19.6, 20.2, 25.5, 26.3, 28.6, 30.7, 39.3, 39.6, 62.3, 63.7, 66.5, 67.9, 76.0, 89.5, 96.2, 97.8, 120.6, 124.2, 128.2, 132.0, 134.9, 140.2.

HRMS (ESI) m/z for $C_{25}H_{40}O_3Na^+$: calculated 411.2875, found 411.2895 $[M+Na]^+$.

((2E,6E,10E)-3,7,11-trimethyl-12-(4-pent-1-yl)oxy)dodeca-2,6,10-trien-1-ol (4)

To a solution of THP protected alcohol **4** (1.2 g, 3.1 mmol, 1 equiv) in 50 mL of ethanol, PPTS (0.8 g, 3.1 mmol, 1 equiv) was added at rt. Then the reaction mixture was heated to 65 ºC and stirred for 3 h. The solvent was evaporated and then purified by flash column chromatography on silica gel using 20% EtOAc/hexanes (v/v) to afford the desired deprotected ether **3** (450 mg, 47%).

^{1}H NMR (500 MHz, CDCl3): δ = 1.62 (s, 3H), 1.66 (s, 3H), 1.70 (s, 3H), 2.02-2.17 (m, 10H), 2.39 - 2.46 (m, 3H), 3.88 (s, 2H), 4.14 (d, 2H, J = 7.5), 4.18 (d, 2H, J = 7.5), 5.14 (t, 1H, J = 7.5), 5.39 (t, 1H, J = 6.5) 5.44 (t, 1H, J = 6.0).

^{13}C NMR (125 MHz, CDCl3): δ = 13.8, 16.0, 16.3, 20.1, 21.1, 23.1, 26.3, 39.3, 39.5, 59.4, 60.4, 61.4, 68.0, 76.0, 123.4, 124.1, 128.1, 132.0, 135.1, 139.7.

HRMS (ESI) m/z for $C_{20}H_{32}O_2Na^+$: calculated 327.2300, found 327.2259 $[M+Na]^+$.

1-(((2E,6E,10E)-12-bromo-3,7,11-trimethyldodeca-2,6,10-trien-1-yl)oxy)pent-4-yne (9)

PPh_3 (resin-bound, 1.2 g, 4.4 mmol, 3 equiv) was suspended in 10 mL CH_2Cl_2 and the mixture was stirred for 45 min at rt under N_2 atmosphere. After that, the deprotected alcohol **3** (450 mg, 1.46 mmol in 10 ml CH_2Cl_2) was added to the suspension and stirred at rt for 15 min. Afterwards, CBr_4 (1.5 g, 4.4 mmol in 10 ml CH_2Cl_2) was added to the reaction, allowing for further stirring for 3 h under N_2 at rt. After that, the resin was removed by filtration (using filter paper) and the resulting mixture was concentrated to yield the desired bromide **2** (crude, 600 mg, 1.64 mmol). This was directly used in the next step without purification due to the bromide's high instability.

((2E,6E,10E)-3,7,11-trimethyl-12-(4-pent-1-yl)oxy)dodeca-2,6,10-trien-1-yl diphosphate (3)

The crude bromide **2** was dissolved in 15 mL of dry acetonitrile (assuming quantitative conversion) and a solution of $(n\text{-}Bu_4N)_3HP_2O_7$ (1.8 g, 2 mmol, 1.2 equiv) in 5 mL of dry acetonitrile was added to the reaction mixture at rt under N_2 atmosphere. After 4 h, the reaction mixture was concentrated and then passed directly through a Dowex Resin (ion-exchange column, Amberchrome® 50WX8 100-200H, hydrogen form, 50-100 mesh).

To prepare this, the resin was packed into a column, washed with 3 bed volumes of conc. NH_4OH, and equilibrated with 4 bed volumes of 25 mM NH_4HCO_3/*i*-PrOH (98/2, v/v). Then, the crude product was loaded on the ion-exchange column and eluted with 250 mL of 25 mM NH_4HCO_3/*i*-PrOH (98/2, v/v). The compound containing fractions were combined and lyophilized.

After that, the crude was resuspended in 3 mL of 0.1 M NH_4HCO_3 and 12 mL of CH_3CN:IPA (1/1, v/v). The mixture was vortexed and then centrifuged for 10 min. Then the supernatant was collected and the solvent was evaporated.

The crude was further purified by cellulose column. The column (2.5 x 18 cm) was packed with cellulose (Cellulose fibers, (medium), Sigma-Aldrich C6288) and equilibrated with 90:10 THF: 0.1 M NH_4HCO_3 (v/v).

Next, the crude mixture was added to the column and 200 mL of 90:10 THF:0.1M NH_4HCO_3 (v/v) was eluted. Then 200 mL 80:20 THF:0.1 M NH_4HCO_3 (v/v) and 200 mL 70:30 THF:0.1 M $NH4HCO_3$ (v/v) were eluted at a flow rate of 5.0-6.0 mL/min. The fractions were collected in 13 x 100 mL test tubes and checked by ESI mass spectrometry. The fractions containing the diphosphate were combined and the THF was evaporated, followed finally by lyophilization of the remaining aqueous buffer. The yield of the reaction was determined by the ^{31}P NMR spectroscopy using an internal standard (Na_2HPO_4) to be 21% (154 mg).

^{1}H NMR (400 MHz, D_2O): δ = 1.54 (s, 5H), 1.64 (s, 3H), 1.67 (s, 3H), 1.93-2.17 (m, 9H), 2.26 - 2.33 (m, 2H), 3.35 (t, 2H, J = 6.0), 3.81 (s, 2H), 4.39 (t, 2H, J = 5.2), 5.11 (t, 1H, J = 3.6), 5.31-5.42 (m, 2H).

^{31}P NMR (162 MHz, D_2O): δ = -6.23 (d, J = 21.1 Hz), -10.17 (d, J = 21.1 Hz).

^{13}C NMR (100 MHz, D_2O): δ = 13.3, 15.4, 15.8, 19.4, 25.7, 26.0, 38.7, 39.2, 62.6, 67.2, 76.4, 76.7, 77.7, 119.8, 124.5, 124.6, 129.1, 131.6, 135.6, 142.5.

HRMS (ESI) m/z for $C_{20}H_{33}O_8P_2^-$: calculated 463.1656; found 463.1652 $[M-H]^-$.

2. 4. 2. Metabolic Labeling in Cultured Cells

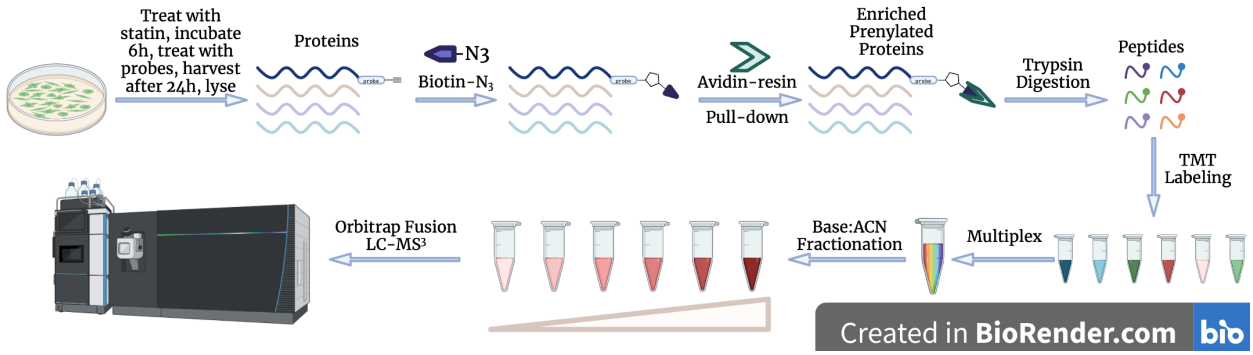

Figure 14. Proteomics workflow from cultured cells.

AML-3 cells (generously provided by Dr. David Fruman at the University of California, Irvine) were cultured in T25 vented-cap flasks (Thermo Fisher) at a density of around 1.5 x 10^6/ mL and allowed to grow for 24h in RPMI 1640 (Gibco) media supplemented with 1% L-Glutamine (Gibco), 10% fetal bovine serum (GenClone) and 1% penicillin–streptomycin (Gibco). COS-7 cells were cultured on 100 mm dishes at around 1 × 10^6 density and allowed to grow for 24h in 10 mL DMEM (Gibco) media supplemented with 10% fetal bovine serum (Gibco) and 1% penicillin–streptomycin (Gibco).

After 24h, the media was removed and replaced with 5 mL of fresh media. In the case of experiments including statin, lovastatin (Cayman Chemical) was added at this point (10 μM) and the flasks/dishes were incubated for 6 h under 5% CO_2 at 37 ºC. After the statin pre-treatment, the media was retained and the C15PentOPP (10 μM) was

added, alongside the respective GGTI (where indicated, at respective concentration). After 24h of incubation, the cells were harvested and pelleted via centrifugation.

2. 4. 3. In-gel Fluorescence Labeling

The cell pellets were suspended in 300 µL of lysis buffer (2.4 µM PMSF, 200 units/nL benzonase nuclease (Sigma-Aldrich), protease inhibitor cocktail and 1% SDS in 1X PBS) and lysed by sonicating on ice 7 times with 3-s pulses at 3-s intervals. Then, the protein concentration in each sample was quantified using a BCA assay (Thermo Fisher Scientific). For each sample, a volume containing 100 µg of protein was then subjected to a copper catalyzed alkyne-azide cycloaddition (CuAAC) reaction (click reaction) with TAMRA-N_3 (25 µM TAMRA-N_3 (BroadPharm), 1 mM TCEP (Sigma-Aldrich), 0.1 mM TBTA (Sigma-Aldrich), and 1 mM $CuSO_4$) for 2 h at rt in the dark. After that, proteins were precipitated using a ProteoExtract precipitation kit (Millipore-Sigma) following the manufacturer's procedure. After removing all liquid, the protein pellet was resuspended in 30 µL of 1X loading buffer (10% glycerol, 2% SDS, 0.02% bromophenol blue in 50 mM Tris–HCl pH 6.8) and the pellet was dissolved by heating briefly to 80 ºC and vortexing. Afterwards, the protein samples were loaded and resolved on a 12% SDS-PAGE gel at 120 V until the dye ran off. The gels were placed in deionized H_2O and immediately scanned for TAMRA fluorescence using a Typhoon FLA 9500 (GE Healthcare) gel scanner. The resulting gel images were processed in ImageJ by adjusting the brightness and contrast of lanes. The gels were stained with Coomassie blue for 12 h and then

destained with destain solution for 24 h. The final gel images were then processed and assembled in Microsoft PowerPoint.

2. 4. 4. Enrichment of Prenylated Proteins

For enrichment, a much larger protein sample was necessary than the one used for in-gel fluorescence, namely 2000 µg. The cells were cultured and treated in the same manner as described above, just on a larger scale for each replicate. The lysis and BCA assay protein concentration determination were performed in the same manner as described above as well. Then, a volume containing 2 mg of protein for each sample was subjected to a Biotin-N_3 click reaction by adding 100 µM Biotin-N_3 (BroadPharm), 1 mM TCEP, 0.1 mM TBTA, and finally 1 mM $CuSO_4$. The mixtures were rotated for 2 h at rt and then the tubes were centrifuged briefly. The proteins were precipitated on ice by adding 1 mL CH_3Cl, 4 mL CH_3OH and 3 mL 1X PBS buffer, mixing vigorously and then centrifuging for 10 min. The aqueous layers were removed gently by decanting and the resulting protein pellets were stored at -20 ºC overnight. Next, the protein pellets were resuspended in 500 µL of 1%SDS in 1X PBS buffer and dissolved by sonication, followed by a BCA assay to normalize the concentration of recovered protein in each sample.

Then, 200 µL of 0.5 mg/mL Neutravidin agarose beads (Thermo Scientific) were washed 3 times with 1%SDS in 1X PBS buffer. The volume containing 1 mg of protein was added to each tube and normalized with 1%SDS in 1X PBS buffer to a total liquid volume of 500 µL. The samples were incubated at rt for 2h, then they were spun down and the supernatant was removed.

The beads were than washed 3 times with 1 mL of 1%SDS in 1X PBS buffer, then once with 1 mL of 1X PBS buffer, removing the supernatant after each wash. Next, the beads were washed 3 times with 1 mL of 8 M Urea in 50 mM TEAB buffer followed by 3 times with 1 mL of 50 mM TEAB buffer. It is crucial during this procedure to ensure a thorough wash, as well as removing the supernatant without removing any beads.

2. 4. 5. On-Bead Digestion of Biotinylated Proteins

Digestion was immediately set up next by adding 100 µL of 50 mM TEAB buffer to each sample containing proteins bound to the resin beads and 6 µL of sequencing grade trypsin solution (ProMega Corp.). The samples were incubated at 37 ºC for 18 hours, then, the digestion was quenched by adding 2.5 µL of 20% formic acid to each sample and incubated 15 min further. The supernatant was then passed through a Pierce Spin column (ThermoFisher, not loaded with any stationary phase) and the beads were washed with 100 µL of 0.5% formic acid. The supernatant was collected again for each tube after passing through the Spin column.

Lastly, the resin was washed with 100 µL of 30% CH_3CN solution in H_2O and the whole mixture was passed through the spin column. The liquid phase collected for each fraction was then concentrated by freeze-drying and the peptides were resuspended in 40 µL 100 mM TEAB buffer.

2. 4. 6. TMT Labeling Reaction for Peptides

TMT 6-plex reagents were prepared following the manufacturer's specifications (ThermoFisher). Another BCA assay was performed in order to quantify the peptide samples' concentrations. Then, the volume necessary for 10 µg of peptides was supplemented with 3 µL of 150 fM yeast ADH1 internal standard (Waters). 10 µL of the respective TMT reagent was added to each sample and the volume was normalized to 33 µL with 100 mM TEAB buffer. After incubating at rt for 2 h, 2.5 µL of 5% NH_4OH was added to each sample and then they were incubated for 15 more min at rt to quench the reaction. Finally, samples were multiplexed by adding them all to the same tube, then concentrating via freeze-drying. The combined samples were resuspended in 300 µL of 200 mM Ammonium formate pH 10.

2. 4. 7. Reverse-Phase Fractionation

In a 200 µL pipette tip, 3 layers of SDB-XC extraction disks (3 M, 1.07 mm x 0.50 mm) were placed and gently packed in. The micro-column formed was washed with 60 µL CH_3CN and 60 µL of 200 mM Ammonium formate pH 10 by centrifugation and collecting the flowthrough in a micro-centrifuge tube. 100 µL of the TMT-labeled peptides were loaded into the micro-column and centrifuged. The flowthrough was reloaded and the centrifugation repeated. Then, a final wash of the loaded micro-column was performed with 60 µL 200 mM ammonium formate pH 10. All flowthroughs to this point were discarded. Then, the high-pH reverse-phase fractionation began, collecting and saving

each flowthrough, followed by freeze-drying of each fraction. There were 7 fractions collected, 60 µL each: 5%, 10%, 15% 20%, 22.5%, 27.5%, 80% CH_3CN in 200 mM ammonium formate. The 5% and 10% fractions were combined, each subsequent fraction was individually collected. After all fractions were lyophilized, the final total of 6 fractions were each resuspended in 30 µL of 0.1% formic acid and transferred into 300 µL fused glass insert mass spec vials for UPLC-MS^3 Fusion analysis.

2. 4. 8. UHPLC-MS^3 Fusion Data Acquisition

Data acquisition was performed by using a method that was previously reported. The TMT-labeled peptides were resolved using a flow rate of 300 nL/min on an UltiMate™ 3000 RSLCnano UHPLC System (ThermoFisher), using a reversed-phase column packed in-house (75 µm i.d., 45 cm). Each of the 6 fractions obtained above was subjected to varying gradients (from 7% to 34%) of CH_3CN with 0.1 % formic acid and 0.1% formic acid in H_2O for 80 min and sprayed directly into the Orbitrap Fusion instrument (ThermoFisher). MS1 scans were collected at 120,000 resolution in a 320–2,000 m/z range, with 100 ms maximum injection time and an automatic gain control (AGC) target of 200,000. Next, the data-dependent MS/MS scans were collected with collision-induced dissociation (CID) at a normalized collision energy (NCE) of 35% with a 1.3 m/z isolation window, with a maximum injection time of 100 ms and AGC target of 5000. Lastly, the acquisition of MS3 data was done by a synchronous selection of the top 10 precursors for fragmentation by high-collisional energy dissociation (HCD) in the

orbitrap with 55% NCE, 2.5 m/z isolation window, 120 ms maximum injection time and 50,000 AGC target.

2. 4. 9. Prenylomic Data Processing and Visual Interpretation

Using MaxQuant (version 2.0.3.1), the raw data files obtained from the UHPLC-MS^3 acquisition were uploaded and searched against a non-redundant human database (UP000005640) from Uniprot. Some parameters were modified from default as follows. Trypsin/P (Porcine origin) was used for digestion, allowing for a maximum of 3 missed cleavages with a minimum peptide length of 7 residues. Protein FDR was set to 0.5, carbamidomethyl C modifications in search were removed, and unique + razor peptides were used for quantification. Then, MaxQuant was run on 24 cores at the University of Minnesota Supercomputing Institute. From the files generated, the proteingroup.txt file was uploaded into Perseus (version 2.0.3.0) for filtering and statistical analysis. In the Perseus analysis, proteins that were only identified by site, potential contaminants or reversed were removed. The raw intensities were $\log_2$ transformed, and proteins with less than 3 out of 6 values for each TMT channel after transformation were removed. Missing values were imputed from the normal distribution of the remaining valid values. Reporter ion (TMT) values were normalized by subtracting rows by the mean value and columns by the median value. Statistical analysis was performed using a two-sample t-test at FDR = 1% and s0 = 0.5. Data was then exported to Microsoft Excel for generation of Volcano plots and further figures.

2. 4. 10. Animal injections

Mice were injected subcutaneously (subQ) with either 150 µL of sterile filtered C15AlkOPP (stock solution: 3000 µL at 30mM C15AlkOPP with 4.8 mM NH_4HCO_3 in 1x PBS) or sterile filtered vehicle (3000 µL at 4.8mM NH_4HCO_3 in 1x PBS) solution using a 1 mL syringe (Neta Scientific), and 25G needle (Fisher Scientific). Sterile filtration was performed with 0.22 µM size syringe filters (Celltreat).

2 .4. 11. Anesthesia

When the experimental timeframe was complete, mice were anesthetized using Isoflurane (Isospire) in a drop bottle method for 2-4 minutes, or until they no longer reacted to a foot pinch test.

2 .4. 12. Dissection and Animal Tissue Collection

After anesthesia, mice (all had body weights between 40-50 g) were dissected using a general dissection protocol. They were cardiac bled with a 1 mL syringe (Neta Scientific) and 25G needle (Fisher Scientific) to remove excess blood before being perfused with 20 mL of DPBS (Gibco). After perfusion, the brain was removed and placed on a glass side on ice. The brain was then dissected into 5 different sections: left front cortex (LFCrt, 50-70 mg), left back cortex (LBCrt, 50-70 mg), right cortex (RCrt, 100-120 mg), cerebellum (CB, 60-100 mg) and all else labeled as rest brain (RB, 100-160 mg). All tissues were placed in a 1.5 mL safe-lock tube (Eppendorf), weighed, and then flash-frozen in liquid nitrogen. Heart (atrium, 70-100 mg, ventricle, 50-130 mg), spleen (30-80

mg), kidney (100-200 mg), and liver (60-900 mg) samples were also collected, weighed, and then flash-frozen in the same manner as the brain.

2 .4. 13. Tissue Homogenization

Each tube (with 50-100 mg tissue) had 300 µl of lysis buffer and 100 mg of 0.5 mm diameter ZrOB05 beads (Next Advance) added. Tubes were homogenized in the Bullet Blender (Next Advance) on speed 10 and time 3 min at 4°C. Tubes were checked for unhomogenized tissue, and, if present, were homogenized for an additional 3 min. After homogenization, samples were quickly centrifugated on a tabletop centrifuge (Labnet) for 5 seconds. Tissue homogenates were then transferred to a 1.5 mL microcentrifuge tube (Eppendorf) and then sonicated using the Sonic Dismembrator (Fisher Scientific) 6 times at 10 second intervals with the tube on ice. All samples were then centrifuged (Fisher Scientific) at 10,000 x g for 15 minutes and the supernatants were collected for each sample for subsequent analysis.

Chapter 3. Proteomic Analysis with an Alkyne-modified Probe Reveals Differential Effects of Two Different GGTase Type-I Inhibitors with Implications for Anti-cancer Research.

3. 1. Introduction

Protein prenylation is an irreversible post-translational modification that involves the attachment of an isoprenoid group to the C-terminus of approximately 2% of the mammalian proteome. There is the possibility of attaching one farnesyl (C15-length) chain (Farnesylation), one geranylgeranyl (C20-length) chain (Geranylgeranylation type-I) or 2 geranylgeranyl chains (Geranylgeranylation type-II) (Fig. 1A). Given the widespread nature of prenylation, it has been implicated or linked to a variety of diseases, including blood cancer.

One of the drugs used in treating leukemia and lymphoma is the BCL2 inhibitor venetoclax. Several studies that led to clinical trials included the successful use of this drug in combination with other inhibitors to drive the apoptosis of some AML-derived cell lines.[23,24] Notably, the Fruman group observed that a synergistic effect was seen when combining venetoclax and statin. In their studies, they mention that the statin acts as an inhibitor of geranylgeranylation type-I, which upregulates AML-cell apoptosis.[22] When administering a combination of venetoclax and geranylgeranyltransferase type-1 inhibitor 298 (GGTI 298), the Fruman group observed enhanced albeit cell-dependent apoptosis that was not observed with a different inhibitor, GGTI 2133.[22] Knowing which geranylgeranylated type-I proteins are involved in this process is a key factor in

understanding the synergistic effect of venetoclax and targeting those proteins for therapeutic applications.

In order to do this, we have decided to employ our C15AlkOPP probe (Fig. 1A) for initial proteomic profiling in different cell lines and then two different GGTIs (Fig. 1B) in combination with the probe to identify differential effects between the two inhibitors. Since the C15AlkOPP probe labels all types of prenylated proteins,[40] a farnesyl transferase inhibitor (FTI) Tipifarnib was also used in the preliminary in-gel fluorescence experiments to evaluate the validity of this method for targeted protein identification (Fig. 1B).

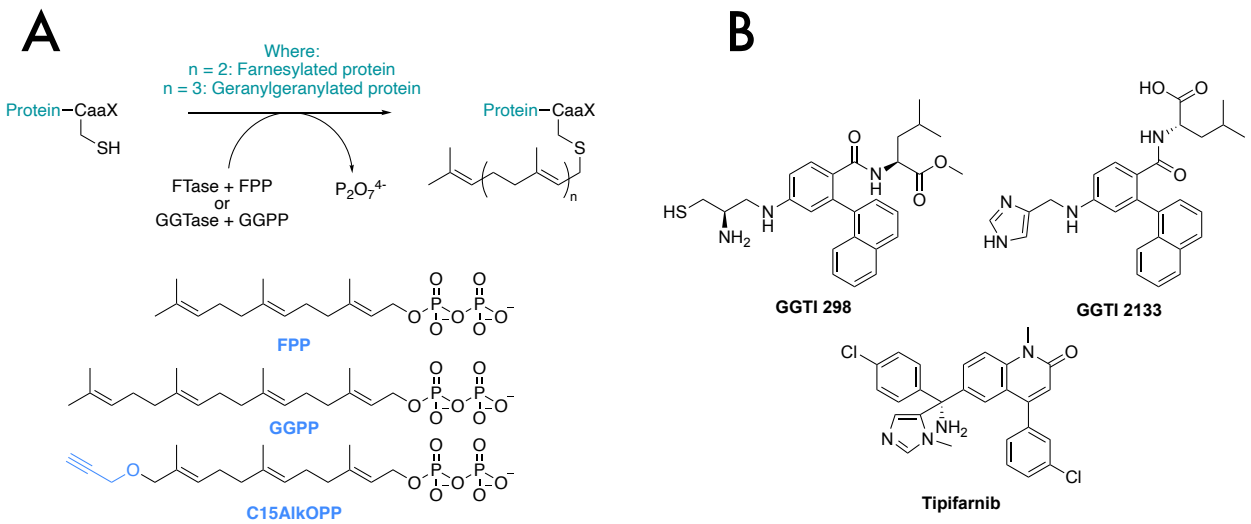

Figure 1: Prenylation mechanism and structures of the FPP endogenous substrate, C15AlkOPP probe, the two GGTase type-I inhibitors and the FTase inhibitor, along with initial in-gel fluorescence evaluation.
(A) Prenylation mechanism and chemical structures of farnesylation's endogenous substrate and the C15AlkOPP probe. **(B)** Chemical structures of the inhibitors discussed in this chapter.

3. 2. Results and Discussion

3. 2. 1. In-gel Fluorescence-based Inhibition with GGTI 298, GGTI 2133 and Tipifarnib

Initial evaluation of prenylation inhibition was done via in-gel fluorescence using our previously published protocol.[40] The C15AlkOPP probe (Fig. 1A) was synthesized and the inhibitors were purchased from Sigma-Aldrich. Initial results in AML-3 showed decreased labeling in the 20-25 kDa region, where most geranylgeranylated proteins are found, with GGTI 298 compared to no inhibitor (Fig. 2A, lanes 1 and 2).

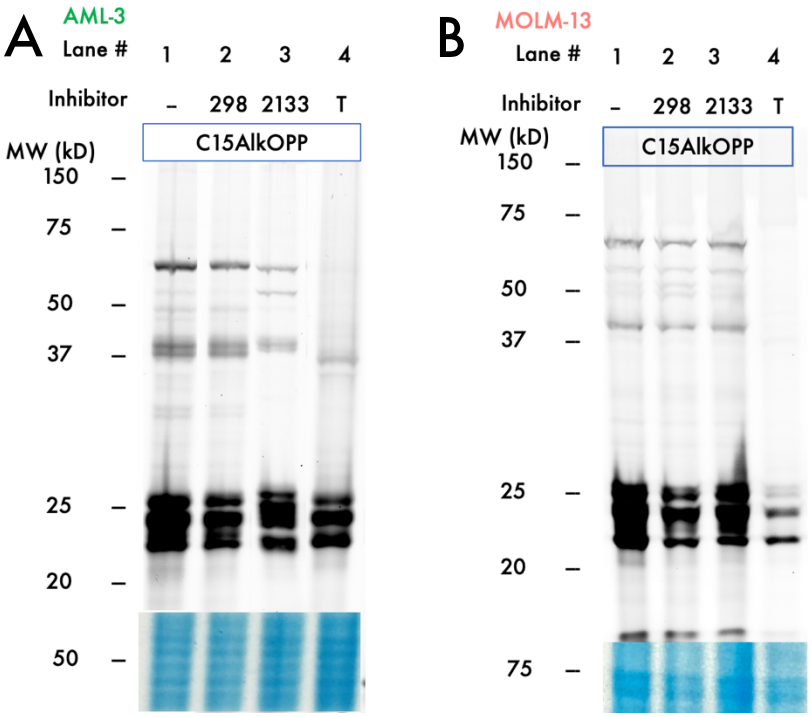

Figure 2: Initial evaluation of inhibition via in-gel fluorescence in different cell lines. **(A)** AML-3 in-gel fluorescence with inhibitors. **(B)** MOLM-13 in-gel fluorescence with inhibitors. All lanes were subjected to click reaction with TAMRA-N_3, followed by electrophoretic separation on 12% SDS-PAGE gels. All inhibitors were present at 10 μM final concentration.

GGTI 2133 had a less potent inhibitory effect in the same region, showing more labeling than GGTI 298 but less than no inhibitor (Fig. 2A, lanes 2 and 3). Lastly, Tipifarnib showed a reduction in labeling in the higher molecular weight region, where most farnesylated proteins are found, as well as a small reduction in the 20-25 kDa region that typically includes both farnesylated and geranylgeranylated proteins.For MOLM-13, a significant reduction in labeling was observed in the 20-25 kDa region with GGTI 298 (Fig. 1D, lanes 1 and 2), with GGTI 2133 having a less pronounced effect (Fig. 2C, lane 3) and Tipifarnib showing substantial reduction of labeling across the entire molecular weight range (Fig. 2C, lane 4). These results showcase the effect of inhibitors on prenylation via in-gel fluorescence, with inhibition's potency being a cell line dependent matter.

3. 2. 2. Cell Culture-based Proteomics for Protein Identification

3. 2. 2. 1. AML-3 Profiling and Inhibition with C15AlkOPP

Having seen the positive in-gel fluorescence results, the next step was to analyze four different blood cancer cell lines. Using the previously published proteomic workflow,[40] three TMT 6-plex™ proteomic experiments were performed in AML-3, an acute myeloid leukemia cell line. The first experiment involved profiling with the C15AlkOPP probe in the absence of statin to avoid any perturbations to the cell physiology, where 67 prenylated proteins were identified as significantly enriched using an FDR of 5% (Fig. 3A), 20 (30%) out of which were geranylgeranylation type-I targets (blue dots). Next, using C15AlkOPP in both the control and the inhibitor samples, we looked at the inhibition with GGTI 298 and GGTI 2133 (Fig. 3C and 3D). At FDR = 1%, there were fewer

geranylgeranylated type-I proteins found significantly enriched in profiling (18) and fewer proteins significantly depleted with GGTI 298 and GGTI 2133 (14 and 5, respectively) (Table 1) than there were at FDR = 5%.

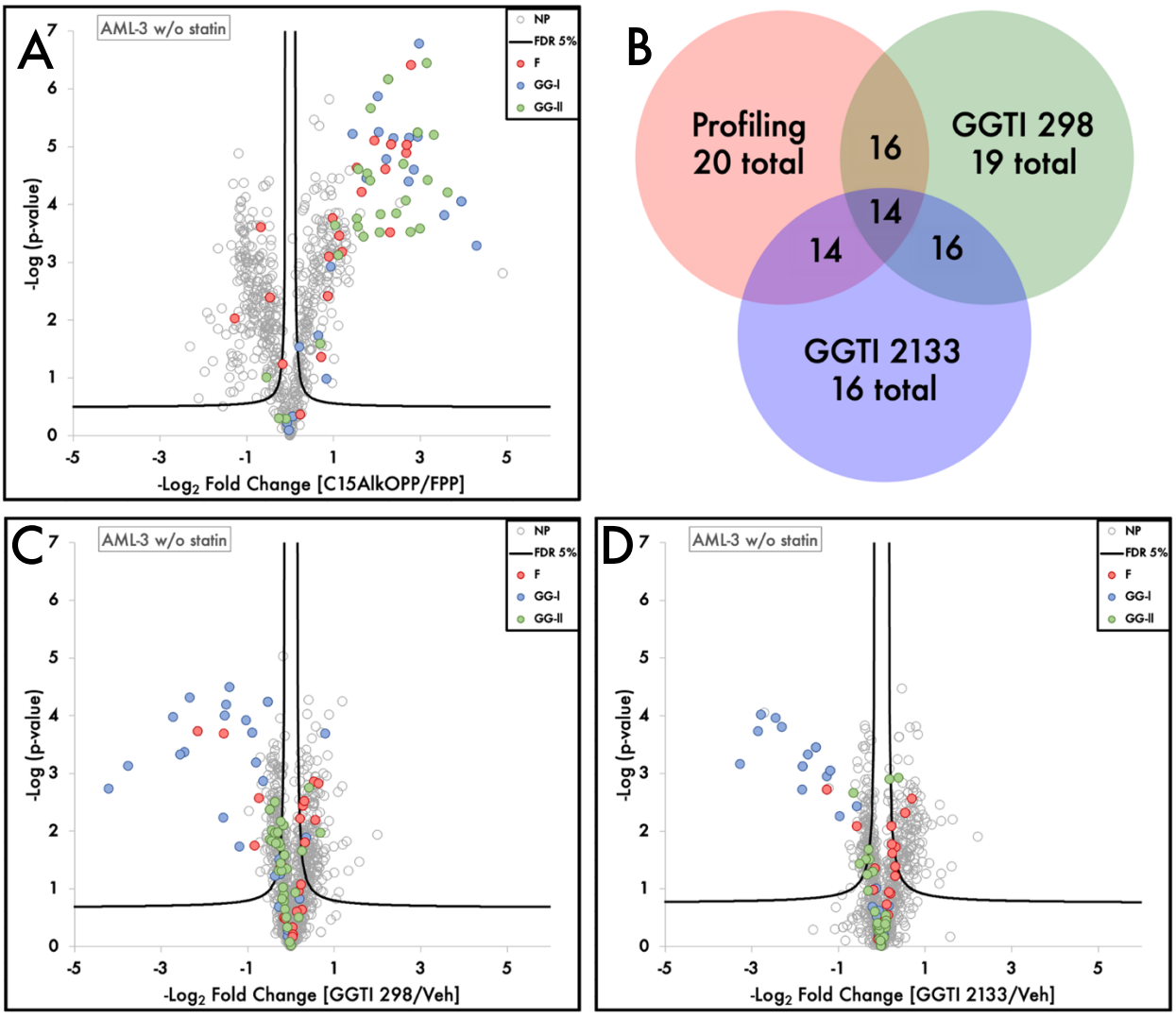

Figure 3: Volcano plots for AML-3 inhibition with GGTIs and Venn diagram for geranylgeranylated type-1 proteins.
(A) Profiling experiment in the absence of statin with C15AlkOPP **(B)** Venn diagram for geranylgeranylated type-1 proteins in profiling (red) GGTI 298 (green) and GGTI 2133 (blue), with 14 proteins being found across the 3 datasets **(C)** GGTI 298 inhibition showing significantly depleted proteins are mostly geranylgeranylated type-1 (blue dots) **(D)** GGTI 2133 inhibition showing significantly depleted proteins are mostly geranylgeranylated type-1 (blue dots). C15AlkOPP and inhibitor final concentrations were all 10 μM. All experiments are shown at t-test FDR = 0.05, s0 = 0.1.

There were 19 geranylgeranylated type-I proteins found significantly depleted using an FDR = 5% with GGTI 298 (16 (80%) in common with the 20 proteins found in profiling) and 16 with GGTI 2133 (14 in common with the 20 proteins found in profiling) (Fig. 3B and Table 1). At this FDR level, all geranylgeranylated type-I proteins inhibited by GGTI 2133 were also inhibited by GGTI 298, with GGTI 298 inhibiting 3 proteins that GGTI 2133 did not, namely RAP2C, GNG4 and GBP2 (Table 1).

Table 1. Identities of type-I geranylgeranylated proteins in AML-3 with C15AlkOPP at FDR = 1% and FDR = 5%.

	FDR 1%			FDR 5%		
No.	Profiling	GGTI 298	GGTI 2133	Profiling	GGTI 298	GGTI 2133
1	GNG12	GNG12	GNG12	GNG10	GNG10	GNG10
2		MIEN1	MIEN1	GNG12	GNG12	GNG12
3	RALA	RALA	RALA	GNG5	GNG5	GNG5
4	RAP1A	RAP1A	RAP1A	MIEN1	MIEN1	MIEN1
5	RAP1B	RAP1B	RAP1B		MRAS	MRAS
6	RAC1	RAC1		RAC1	RAC1	RAC1
7	RAC2	RAC2		RAC2	RAC2	RAC2
8	RALB	RALB		RALA	RALA	RALA
9	RAP2B	RAP2B		RALB	RALB	RALB
10	RHOA	RHOA		RAP1A	RAP1A	RAP1A
11		RHOC		RAP1B	RAP1B	RAP1B
12	RHOG	RHOG		RAP2B	RAP2B	RAP2B
13	GNG5	GNG5		RHOA	RHOA	RHOA
14		GBP2			RHOC	RHOC
15	CDC42			RHOG	RHOG	RHOG
16	GNG10			RRAS	RRAS	RRAS
17	RAB18				GBP2	
18	RAB8A			GNG4	GNG4	
19	RAP2C			RAP2C	RAP2C	
20	RRAS			UBL3		
21	UBL3			CDC42		
22				RAB18		
23				RAB8A		

When looking at the fold changes of the proteins found in common, it became apparent that there was higher enrichment with GGTI 298 (Fig. 4), the proteins having higher fold changes in that dataset than in the one generated using GGTI 2133. This suggests that AML-3 is more sensitive to GGTI 298 inhibition than to GGTI 2133 inhibition.

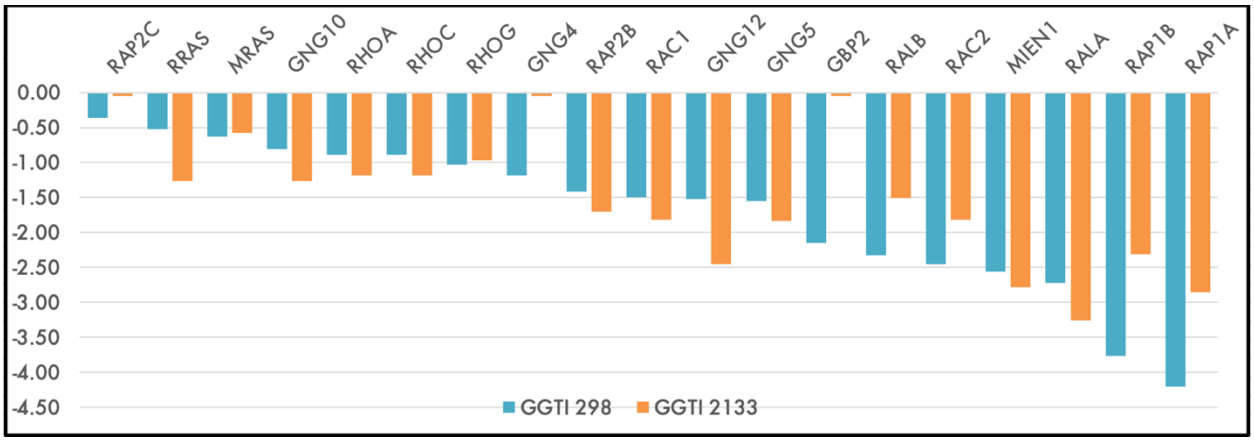

Figure 4: Bar graph plotting fold change versus protein identity in the 2 GGTI experiments for significantly depleted geranylgeranylated type-1 proteins in AML-3.
There are 16 proteins found in common between GGTI 298 and GGTI 2133, sorted by increasing order of absolute fold change values in GGTI 298. The y axis represents $\log_2$(fold change) values.

3. 2. 2. 2. MOLM-13 Profiling and Inhibition with C15AlkOPP

Next, MOLM-13, another acute myeloid leukemia cell line was analyzed. For this, the profiling experiment with the C15AlkOPP probe was performed using a TMT 6-plex™ experiment and 52 prenylated proteins were identified, 18 of which (32%) being targets for geranylgeranylation type-I (Fig. 5A, blue dots). For the inhibitors, only one TMT 10-plex™ experiment was performed, with 4 control samples containing vehicle and then 3 samples each for the two GGTIs. This approach halves the mass spectrometry experimental time and costs, but it comes at the expense of number of proteins identified, as the concentration of the samples analyzed (control/GGTI) is lower.

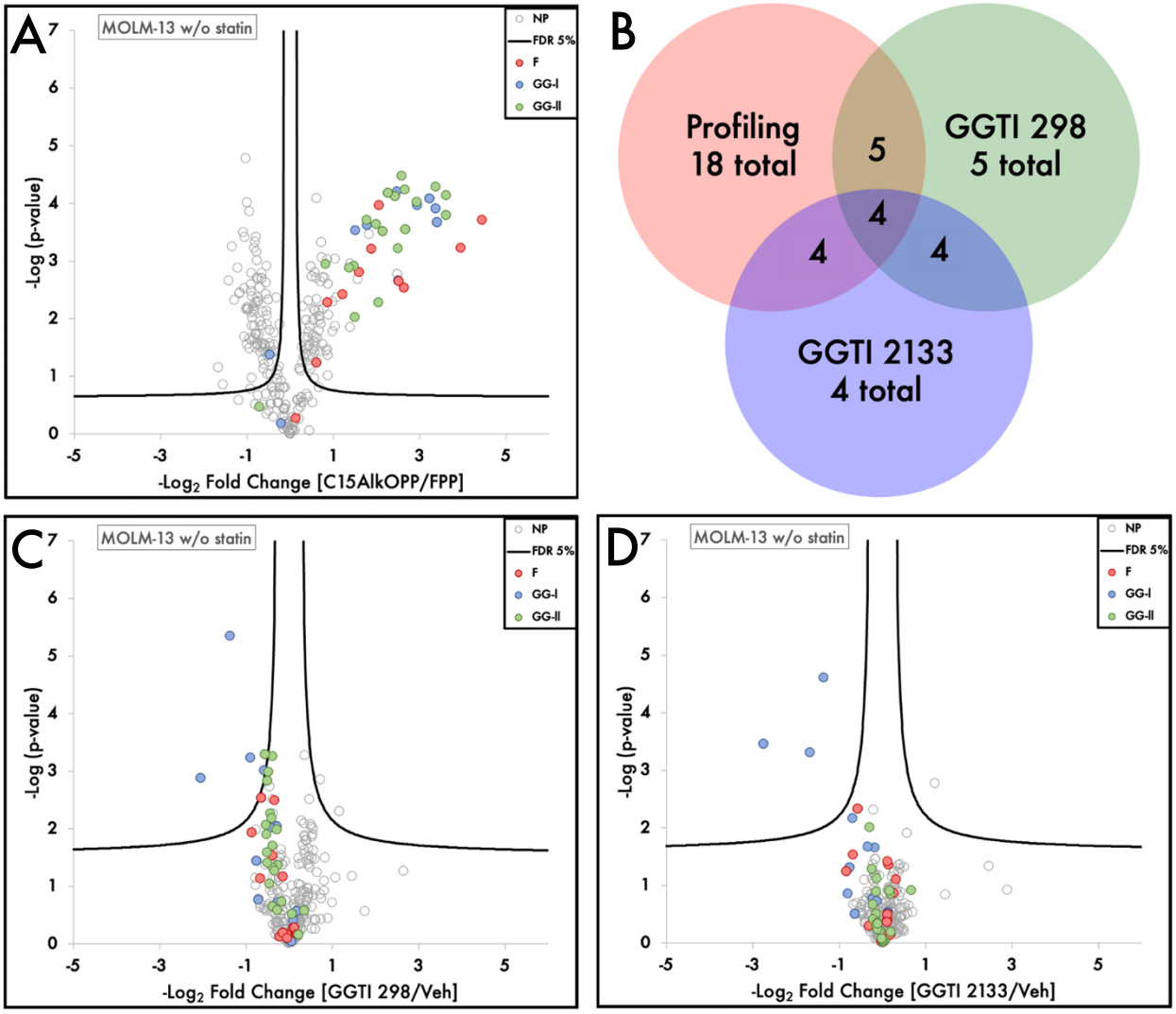

Figure 5: Volcano plots for MOLM-13 inhibition with GGTIs and Venn diagram for geranylgeranylated type-1 proteins.
(A) Profiling experiment in the absence of statin with C15AlkOPP **(B)** Venn diagram for geranylgeranylated type-1 proteins in profiling (red) GGTI 298 (green) and GGTI 2133 (blue), with 4 proteins being found across the 3 datasets **(C)** GGTI 298 inhibition showing significantly depleted proteins are mostly geranylgeranylated type-1 (blue dots) **(D)** GGTI 2133 inhibition showing significantly depleted proteins are mostly geranylgeranylated type-1 (blue dots). C15AlkOPP and inhibitor final concentrations were all 10 μM. All experiments are shown at t-test FDR = 0.05, s0 = 0.1.

At FDR 1%, there were 15 geranylgeranylation type-I targets identified in the profiling and no proteins depleted by either inhibitor (Table 2). However, at FDR = 5%, there were 18 geranylgeranylation type-I targets identified in profiling and we were able

to identify 5 geranylgeranylated type-I proteins depleted with GGTI 298 (Fig. 5C, blue dots) and 4 geranylgeranylated type-I proteins depleted with GGTI 2133 (Fig. 5D, blue dots). Both inhibitor protein datasets were a subset of the 18 total geranylgeranylated type-I proteins identified in profiling (Fig. 5A and Table 2).

Table 2. Identities of type-I geranylgeranylated proteins in MOLM-13 with C15AlkOPP at FDR = 1% and FDR = 5%.
At FDR 1%, there were no depleted proteins with either GGTI.

	FDR 1%			FDR 5%		
No.	Profiling	GGTI 298	GGTI 2133	Profiling	GGTI 298	GGTI 2133
1	RAC2	N/A	N/A	RAC2	RAC2	RAC2
2	RALA			RALA	RALA	RALA
3	RAP1A			RAP1A	RAP1A	RAP1A
4	RAP1B			RAP1B	RAP1B	RAP1B
5	RAB8A			RAB8A	RAB8A	
6	CDC42			CDC42		
7	GBP2			GBP2		
8				MIEN1		
9	RAB18			RAB18		
10	RAB8B			RAB8B		
11	RAC1			RAC1		
12	RAC3			RAC3		
13				RAP2B		
14				RAP2C		
15	RHOA			RHOA		
16	RHOB			RHOB		
17	RHOC			RHOC		
18	RHOG			RHOG		

All 4 proteins found in common using the two GGTIs had higher fold changes in the GGTI 2133 dataset, but GGTI 298 identified one extra protein that was not observed enriched in the GGTI 2133 dataset, namely RAB8A (Fig. 6). This may mean that, while

this cell line is more sensitive to GGTI 298 inhibition, GGTI 2133 is more potent in inhibiting geranylgeranylation type-I in MOLM-13.

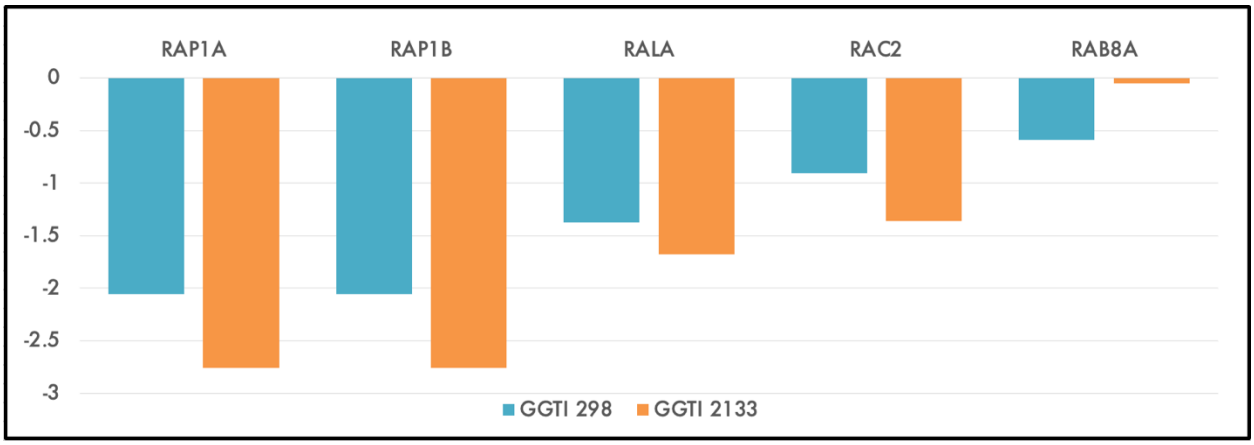

Figure 6: Bar graph plotting fold change versus protein identity in the 2 GGTI experiments for significantly depleted geranylgeranylated type-1 proteins in MOLM-13.
There are 4 proteins found in common between GGTI 298 and GGTI 2133. RAB8A was only detected by GGTI 298, the small bar is represented in GGTI 2133 just for illustration purposes. The y axis represents $\log_2$(fold change) values.

3. 2. 2. 3. L363 Profiling and Inhibition with C15AlkOPP

The next cell line analyzed was L363, a plasma cell leukemia, with all experiments performed via TMT 6-plex™. When profiling with C15AlkOPP, 63 prenylated proteins were found significantly enriched (Fig. 7A) and 23 of them (37%) were proteins prenylated by GGTase I. In the presence of GGTI 298 or GGTI 2133, there were 20 and 8, respectively, geranylgeranylated type-I proteins affected (Fig. 7C and 7D). One abnormality that must be noted, appearing for unknown reasons, is that the GGTI 298 dataset showed that labeling of the majority of all prenylated proteins was decreased, (see the left-hand side of the volcano plot) deviating from the typical behavior of observing only geranylgeranylated type-I proteins (blue dots) in that area (Fig. 7C). Overall, at FDR = 5% we identified more proteins in all three experiments, profiling, GGTI 298 and GGTI

2133 (21, 20 and 8, respectively) than at FDR = 1% (20, 17 and 8, respectively) (Table 3).

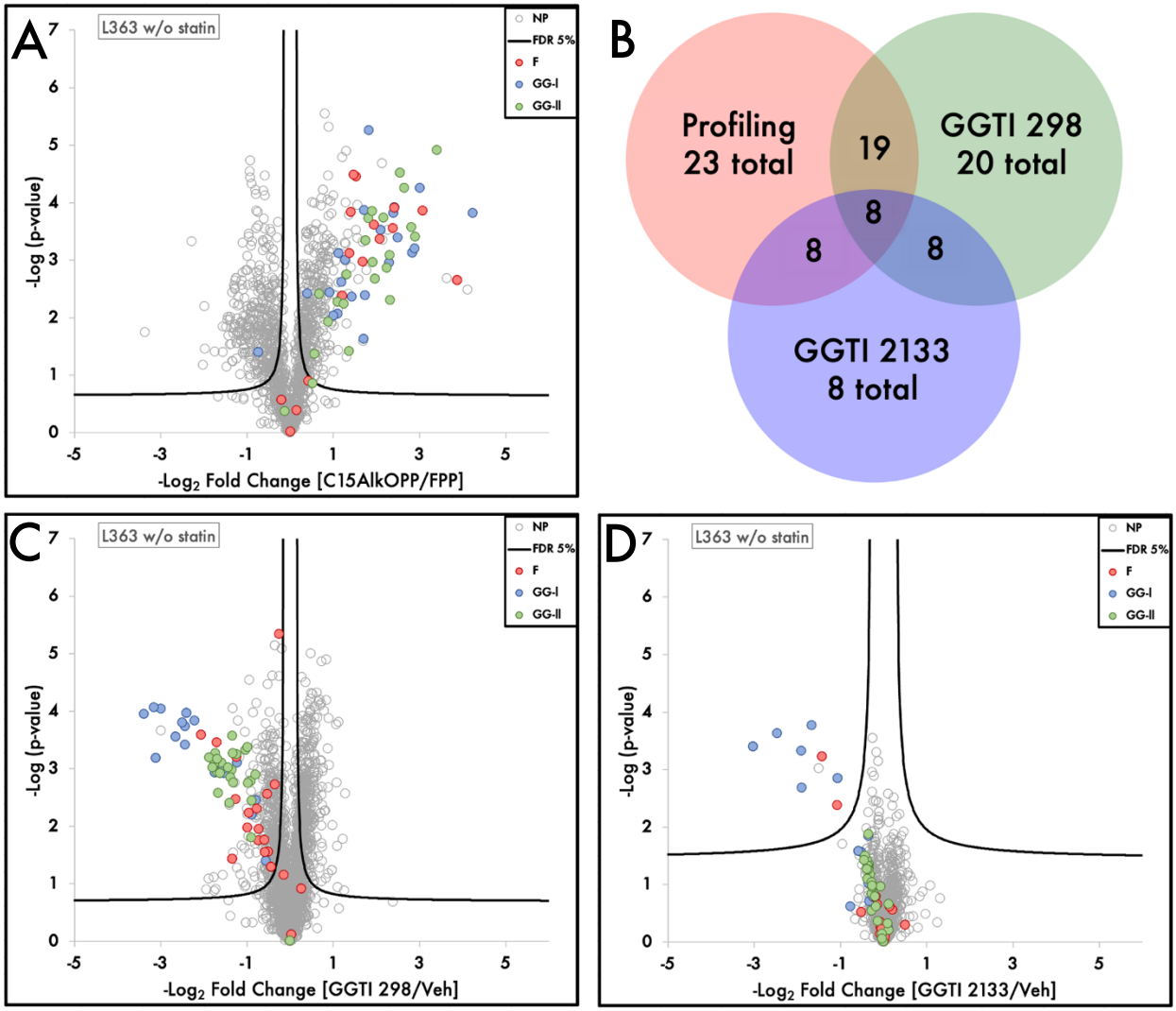

Figure 7: Volcano plots for L363 inhibition with GGTIs and Venn diagram for geranylgeranylated type-1 proteins.
(A) Profiling experiment in the absence of statin with C15AlkOPP **(B)** Venn diagram for geranylgeranylated type-1 proteins in profiling (red) GGTI 298 (green) and GGTI 2133 (blue), with 8 proteins being found across the 3 datasets **(C)** GGTI 298 inhibition showing significantly depleted proteins are mostly geranylgeranylated type-1 (blue dots) **(D)** GGTI 2133 inhibition showing significantly depleted proteins are mostly geranylgeranylated type-1 (blue dots). C15AlkOPP and inhibitor final concentrations were all 10 μM. All experiments are shown at t-test FDR = 0.05, s0 = 0.1.

At FDR = 5%, the 20 proteins in the GGTI 298 dataset included the 8 proteins that GGTI 2133 identified and there was substantial overlap between the geranylgeranylated type-I proteins depleted by the GGTIs and those observed in profiling, with all but one of the 20 proteins identified in the inhibition experiments missing from the profiling dataset (Fig. 7B and Table 3).

Table 3. Identities of type-I geranylgeranylated proteins in L363 with C15AlkOPP at FDR = 1% and FDR = 5%.
Except for GGTI 2133, where the same proteins are identified at both confidence intervals, more proteins are identified at the less stringent parameter while still at a high confidence level.

	FDR 1%			FDR 5%		
No.	Profiling	GGTI 298	GGTI 2133	Profiling	GGTI 298	GGTI 2133
1	RAC1	RAC1	RAC1	RAC1	RAC1	RAC1
2	RAC2	RAC2	RAC2	RAC2	RAC2	RAC2
3	RALA	RALA	RALA	RALA	RALA	RALA
4	RALB	RALB	RALB	RALB	RALB	RALB
5	RAP1A	RAP1A	RAP1A	RAP1A	RAP1A	RAP1A
6	RAP1B	RAP1B	RAP1B	RAP1B	RAP1B	RAP1B
7	RAP2B	RAP2B	RAP2B	RAP2B	RAP2B	RAP2B
8	RRAS	RRAS	RRAS	RRAS	RRAS	RRAS
9	CDC42	CDC42		CDC42	CDC42	
10	GNG5	GNG5		GNG5	GNG5	
11	GNG7	GNG7		GNG7	GNG7	
12	RAB18	RAB18		MIEN1	MIEN1	
13	RAB8A	RAB8A		RAB18	RAB18	
14		RAC3		RAB23	RAB23	
15	RHOA	RHOA		RAB8A	RAB8A	
16	RHOC	RHOC		RAB8B	RAB8B	
17	RHOG	RHOG			RAC3	
18	CRACR2A			RHOA	RHOA	
19	MIEN1			RHOC	RHOC	
20	RAB23			RHOG	RHOG	
21	RAB41			CRACR2A		
22	RAB8B			RAB41		
23				RHOB		
24				UBL3		

When comparing the fold changes of the 20 proteins identified by the GGTIs, we observed higher enrichment with GGTI 298 in all 8 cases of commonly found proteins in GGTI 2133 as well (Fig. 8). This indicates that GGTI 298 has a higher inhibitory effect on this cell line's geranylgeranylation type-I than GGTI 2133.

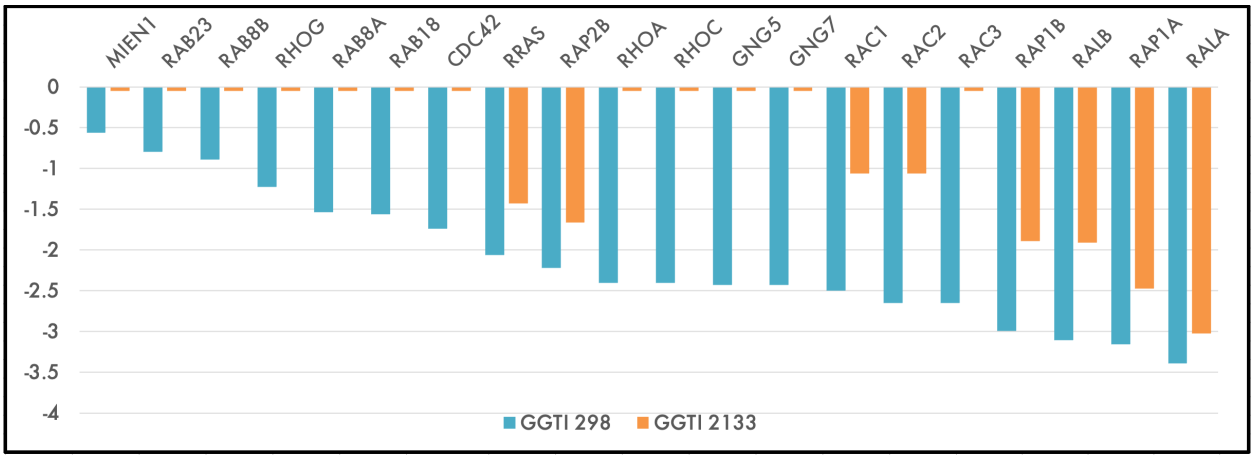

Figure 8: Bar graph plotting fold change versus protein identity in the 2 GGTI experiments for significantly depleted geranylgeranylated type-1 proteins in L363. There are 8 proteins found in common between GGTI 298 and GGTI 2133. Those detected only by GGTI 298 have a small bar represented in GGTI 2133 just for illustration purposes. The y axis represents $\log_2$(fold change) values.

3. 2. 2. 4 OPM-2 Profiling and Inhibition with C15AlkOPP

The last cell line analyzed was OPM-2, a multiple myeloma cell line, with all experiments performed via TMT 6-plex™ proteomic analysis. The initial profiling with C15AlkOPP revealed 62 prenylated proteins significantly enriched at FDR = 1% and 5% (Fig. 9A and Table 4), out of which 19 were targets for geranylgeranylation type-I (31%). However, at FDR = 1% there were 10 and 12 geranylgeranylation type-I targets significantly depleted by GGTI 298 and GGTI 2133, respectively, with those numbers increasing to 14 and 15, respectively at FDR = 5%. When looking at the inhibition data at

FDR =5 %, GGTI 298 identified 14 geranylgeranylated type-I proteins significantly depleted (Fig. 9C), whereas GGTI 2133 identified 15 (Fig. 9D and Table 4).

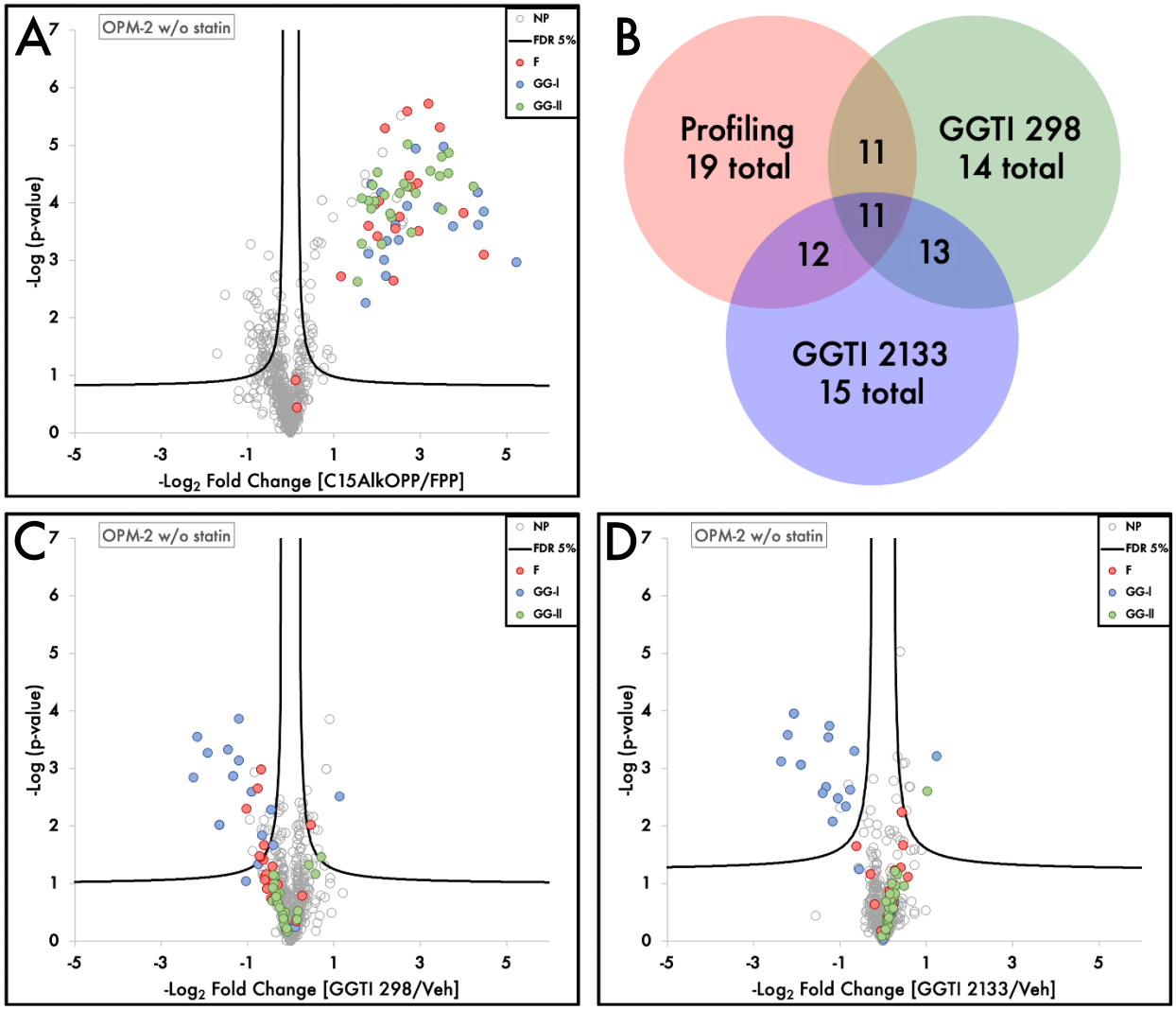

Figure 9: Volcano plots for OPM-2 inhibition with GGTIs and Venn diagram for geranylgeranylated type-1 proteins.
(A) Profiling experiment in the absence of statin with C15AlkOPP **(B)** Venn diagram for geranylgeranylated type-1 proteins in profiling (red) GGTI 298 (green) and GGTI 2133 (blue), with 11 proteins being found across the 3 datasets **(C)** GGTI 298 inhibition showing significantly depleted proteins are mostly geranylgeranylated type-1 (blue dots) **(D)** GGTI 2133 inhibition showing significantly depleted proteins are mostly geranylgeranylated type-1 (blue dots). C15AlkOPP and inhibitor final concentrations were all 10 μM. All experiments are shown at t-test FDR = 0.05, s0 = 0.1.

There was good overlap between the GGTI depleted proteins and those found in the profiling experiment with 11 and 12 found in common with the profiling for GGTI 298 and GGTI 2133 respectively at FDR 5% (Fig. 9B).

Table 4. Identities of type-I geranylgeranylated proteins in OPM-2 with C15AlkOPP at FDR = 1% and FDR = 5%.

	FDR 1%			FDR 5%		
No.	Profiling	GGTI 298	GGTI 2133	Profiling	GGTI 298	GGTI 2133
1	GNG7	GNG7			GBP2	
2	MIEN1	MIEN1	MIEN1		GNG12	GNG12
3	RAC1	RAC1	RAC1	GNG7	GNG7	GNG7
4	RALA	RALA	RALA	MIEN1	MIEN1	MIEN1
5	RALB	RALB	RALB	RAC1	RAC1	RAC1
6	RAP1A	RAP1A	RAP1A	RALA	RALA	RALA
7	RAP1B	RAP1B	RAP1B	RALB	RALB	RALB
8	RAP2B	RAP2B	RAP2B	RAP1A	RAP1A	RAP1A
9	RHOA	RHOA	RHOA	RAP1B	RAP1B	RAP1B
10		RHOC	RHOC	RAP2B	RAP2B	RAP2B
11			RRAS	RHOA	RHOA	RHOA
12			DNAJB2		RHOC	RHOC
13			GNG5	RHOG	RHOG	RHOG
14	RHOB			RRAS	RRAS	RRAS
15	RHOG					DNAJB2
16	RRAS					GNG5
17	CDC42			RHOB		
18	CRACR2A			CDC42		
19	GNG5			CRACR2A		
20	RAB18			GNG5		
21	RAB23			RAB18		
22	RAB8A			RAB23		
23	RAB8B			RAB8A		
24				RAB8B		

The intersection of all depleted proteins by the two GGTIs is shown in Figure 10 in increasing order of fold change for proteins in the GGTI 298 dataset. Unlike in the

previous cell lines, there does not seem to be an overall greater inhibitory effect with one particular GGTI, nor does it seem there is higher sensitivity towards one inhibitor in this cell line. Interestingly, GGTI 2133 identified more geranylgeranylation type-I targets than GGTI 298 at both FDR =1% and FDR = 5% (Table 4).

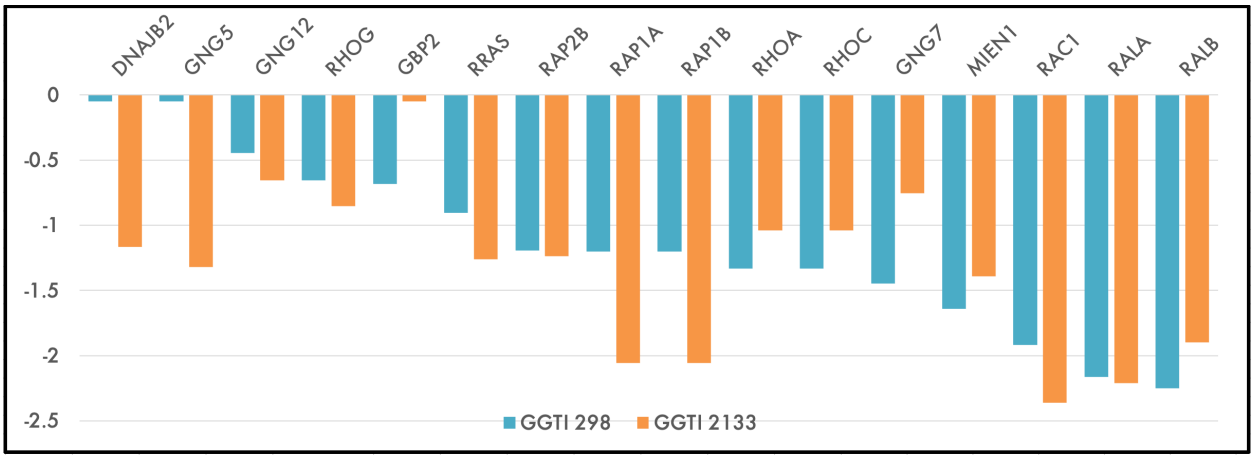

Figure 10: Bar graph plotting fold change versus protein identity in the 2 GGTI experiments for significantly depleted geranylgeranylated type-1 proteins in OPM-2. There are 13 proteins found in common between GGTI 298 and GGTI 2133. Those detected only by one GGTI have a small bar represented for the other GGTI just for illustration purposes. The y axis represents $\log_2$(fold change) values.

3. 2. 2. 5. Comparison of all Four Datasets for Geranylgeranylated Type-I Significantly Depleted Proteins with GGTI 298

When comparing the datasets of significantly depleted proteins by GGTI 298 in each of the 4 cell lines, it is interesting to note that in the case of AML-3, L363 and OPM-2 there is good overlap, with 13 proteins found in common between AML-3/L363 and AML-3/OPM-2, and 12 proteins found in common between L363/OPM-2. The identities of these proteins are listed in Table 5. There were also 11 proteins commonly found across the AML-3/L363/OPM-2 datasets, shown in Table 5 in blue, which may be of interest in further studies in the context of blood cancer.

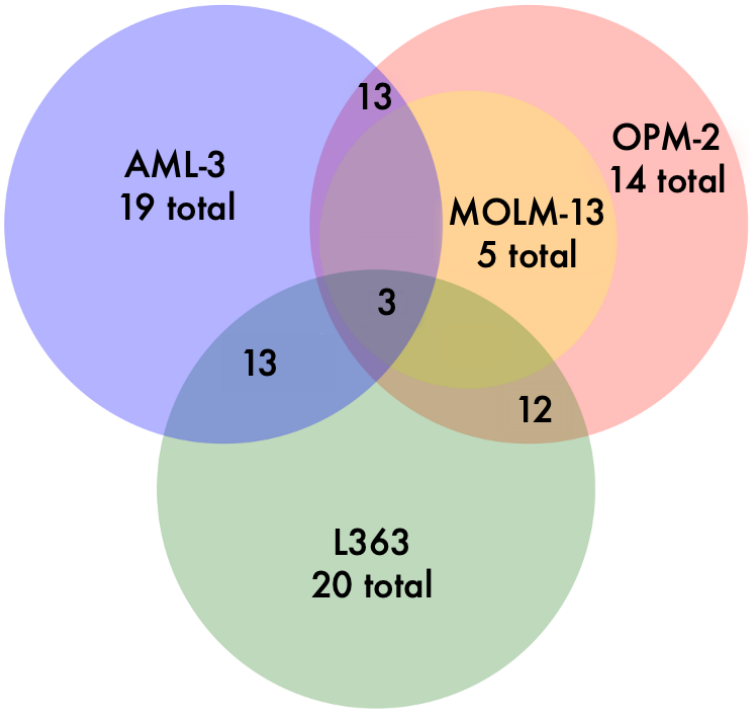

Figure 11: Venn diagram showing the intersection of all 4 datasets of significantly depleted geranylgeranylated type-I proteins with GGTI 298.
There are 3 proteins commonly found across the 4 datasets: RALA, RAP1B and RAP1A.

The MOLM-13 dataset is smaller than all the other 3 datasets. It is comprised of only 5 proteins (RAP1A, RAP1B, RALA, RAC2, RAB8A) and 3 of those are commonly found across all 4 datasets, namely RALA, RAP1B and RAP1A.

Table 5. Identities of type-I geranylgeranylated proteins across the 4 cell lines studied herein with GGTI 298 and C15AlkOPP at FDR = 5%.
There are 11 proteins commonly found in AML-3 and OPM-2 and L363 (last column).

	GGTI 298							
No.	AML-3	MOLM-13	L363	OPM-2	AML-3 L363	AML-3 OPM-2	L363 OPM-2	AML-3 OPM-2 L363
1	MIEN1		MIEN1	MIEN1	MIEN1	MIEN1	MIEN1	MIEN1
2	RAC1		RAC1	RAC1	RAC1	RAC1	RAC1	RAC1
3	RALA	RALA	RALA	RALA	RALA	RALA	RALA	RALA
4	RALB		RALB	RALB	RALB	RALB	RALB	RALB
5	RAP1A	RAP1A	RAP1A	RAP1A	RAP1A	RAP1A	RAP1A	RAP1A

6	RAP1B	RAP1B	RAP1B	RAP1B	RAP1B	RAP1B	RAP1B	RAP1B
7	RAP2B		RAP2B	RAP2B	RAP2B	RAP2B	RAP2B	RAP2B
8	RHOA		RHOA	RHOA	RHOA	RHOA	RHOA	RHOA
9	RHOC		RHOC	RHOC	RHOC	RHOC	RHOC	RHOC
10	RHOG		RHOG	RHOG	RHOG	RHOG	RHOG	RHOG
11	RRAS		RRAS	RRAS	RRAS	RRAS	RRAS	RRAS
12	GBP2			GBP2		GBP2		
13	GNG12			GNG12		GNG12		
14			GNG7	GNG7			GNG7	
15	GNG5		GNG5		GNG5			
16	RAC2	RAC2	RAC2		RAC2			
17		RAB8A	RAB8A					
18			CDC42					
19			RAB18					
20			RAB23					
21			RAB8B					
22			RAC3					
23	GNG4							
24	GNG10							
25	MRAS							
26	RAP2C							

3. 3. Conclusions

After our collaborators in the Fruman lab observed the synergistic effect of GGTIs with the anti-cancer drug venetoclax, we set out to explore the prenylated proteins affected by these inhibitors, with a goal of identifying which ones are common across different cell lines. Using the C15AlkOPP probe, we metabolically labeled prenylated proteins in the absence of statin in profiling experiments across 4 different blood cancer cell types: AML-3, MOLM-13, L363 and OPM-2, with 67, 52, 63 and 62 proteins found significantly enriched with high confidence, respectively. For each dataset, 20, 18, 23 and 19 respectively were geranylgeranylation type-I substrates. Proteomic experiments in the presence of C15AlkOPP probe and GGTI 298 or GGTI 2133 showed good overlap

between the significantly depleted proteins identified and geranylgeranylation type-I substrates found when profiling, with GGTI 298 having overall more potent inhibition. Importantly, there were 3 proteins found with high confidence across all 4 cell types as depleted by GGTI 298 (RALA, RAP1B and RAP1A), which will be used as knock-out targets by our collaborators in order to determine whether they are in fact related to the synergistic effects of GGTIs and venetoclax.

3. 4. Experimental Procedures

3. 4. 1. Metabolic Labeling in Cultured Cells

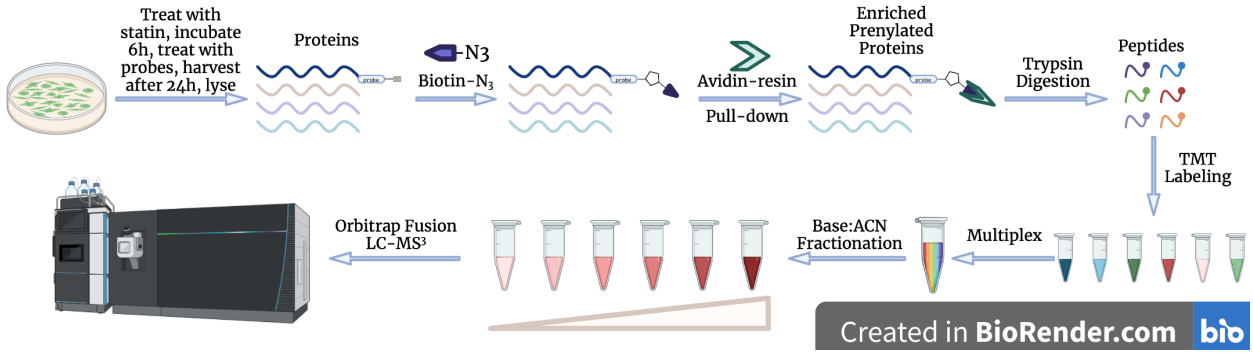

Figure 12. Proteomics workflow starting from cultured cells.

AML-3, MOLM-13, OPM2 cells (generously provided by Dr. David Fruman at the University of California, Irvine) were cultured in T25 vented-cap flasks (Thermo Fisher) at a density of around 1.5 x 10^6 /mL and allowed to grow for 24h in RPMI 1640 (Gibco) media supplemented with 1% L-Glutamine (Gibco), 10% fetal bovine serum (GenClone) and 1% penicillin–streptomycin (Gibco). COS-7 cells were cultured on 100 mm dishes at around

1×10^6 density and allowed to grow for 24h in 10 mL DMEM (Gibco) media supplemented with 10% fetal bovine serum (Gibco) and 1% penicillin–streptomycin (Gibco).

After 24h, the media was removed and replaced with 5 mL of fresh media. In the case of experiments including statin, lovastatin (Cayman Chemical) was added at this point (10 μM) and the flasks/dishes were incubated for 6 h under 5% CO_2 at 37 ºC. After the statin pre-treatment, the media was retained and the C15PentOPP (10 μM) was added, alongside the respective GGTI (where indicated, at respective concentration). After 24h of incubation, the cells were harvested and pelleted via centrifugation.

3. 4. 2. In-gel Fluorescence Labeling

The cell pellets were suspended in 300 μL of lysis buffer (2.4 μM PMSF, 200 units/nL benzonase nuclease (Sigma-Aldrich), protease inhibitor cocktail and 1% SDS in 1X PBS) and lysed by sonicating on ice 7 times with 3-s pulses at 3-s intervals. Then, the protein concentration in each sample was quantified using a BCA assay (Thermo Fisher Scientific). For each sample, a volume containing 100 μg of protein was then subjected to a copper catalyzed alkyne-azide cycloaddition (CuAAC) reaction (click reaction) with TAMRA-N_3 (25 μM TAMRA-N_3 (BroadPharm), 1 mM TCEP (Sigma-Aldrich), 0.1 mM TBTA (Sigma-Aldrich), and 1 mM $CuSO_4$) for 2 h at rt in the dark. After that, proteins were precipitated using a ProteoExtract precipitation kit (Millipore-Sigma) following the manufacturer's procedure. After removing all liquid, the protein pellet was resuspended in 30 μL of 1X loading buffer (10% glycerol, 2% SDS, 0.02% bromophenol blue in 50 mM Tris–HCl pH 6.8) and the pellet was dissolved by heating briefly to 80 ºC and vortexing.

Afterwards, the protein samples were loaded and resolved on a 12% SDS-PAGE gel at 120 V until the dye ran off. The gels were placed in DI H_2O and immediately scanned for TAMRA fluorescence using a Typhoon FLA 9500 (GE Healthcare) gel scanner. The resulting gel images were processed in ImageJ by adjusting the brightness and contrast of lanes. The gels were stained with Coomassie blue for 12 h and then destained with destain solution for 24 h. The final gel images were then processed and assembled in Microsoft PowerPoint.

3. 4. 3. Enrichment of Prenylated Proteins

For enrichment, a much larger protein sample was necessary than the one used for in-gel fluorescence, namely 2000 µg. The cells were cultured and treated in the same manner as described above, just on a larger scale for each replicate. The lysis and BCA assay protein concentration determination were performed in the same manner as described above as well. Then, a volume containing 2 mg of protein for each sample was subjected to a Biotin-N_3 click reaction by adding 100 µM Biotin-N_3 (BroadPharm), 1 mM TCEP, 0.1 mM TBTA, and finally 1 mM $CuSO_4$. The mixtures were rotated for 2 h at rt and then the tubes were centrifuged briefly. The proteins were precipitated on ice by adding 1 mL CH_3Cl, 4 mL CH_3OH and 3 mL 1X PBS buffer, mixing vigorously and then centrifuging for 10 min. The aqueous layers were removed gently by decanting and the resulting protein pellets were stored at -20 ºC overnight. Next, the protein pellets were resuspended in 500 µL of 1%SDS in 1X PBS buffer and dissolved by sonication, followed by a BCA assay to normalize the concentration of recovered protein in each sample. Then, 200 µL

of 0.5 mg/mL Neutravidin agarose beads (Thermo Scientific) were washed 3 times with 1%SDS in 1X PBS buffer. The volume containing 1 mg of protein was added to each tube and normalized with 1%SDS in 1X PBS buffer to a total liquid volume of 500 µL. The samples were incubated at rt for 2h, then they were spun down and the supernatant removed.

The beads were than washed 3 times with 1 mL of 1%SDS in 1X PBS buffer, then once with 1 mL of 1X PBS buffer, removing the supernatant after each wash. Next, the beads were washed 3 times with 1 mL of 8 M Urea in 50 mM TEAB buffer followed by 3 times with 1 mL of 50 mM TEAB buffer. It is crucial during this procedure to ensure a thorough wash, as well as removing the supernatant without removing any beads.

3. 4. 4. On-Bead Digestion of Biotinylated Proteins

Digestion was immediately set up next by adding 100 µL of 50 mM TEAB buffer to each sample containing proteins bound to the resin beads and 6 µL of sequencing grade trypsin solution (ProMega Corp.). The samples were incubated at 37 ºC for 18 hours, then, the digestion was quenched by adding 2.5 µL of 20% formic acid to each sample and incubated 15 min further. The supernatant was then passed through a Pierce Spin column (ThermoFisher, not loaded with any stationary phase) and the beads were washed with 100 µL of 0.5% formic acid. The supernatant was collected again for each tube after passing through the Spin column. Lastly, the resin was washed with 100 µL of 30% CH_3CN solution in H_2O and the whole mixture was passed through the spin column.

The liquid phase collected for each fraction was then concentrated by freeze-drying and the peptides were resuspended in 40 µL 100 mM TEAB buffer.

3. 4. 5. TMT Labeling Reaction for Peptides

TMT 6-plex reagents were prepared following the manufacturer's specifications (ThermoFisher). Another BCA assay was performed in order to quantify the peptide samples' concentrations. Then, the volume necessary for 10 µg of peptides was supplemented with 3 µL of 150 fM yeast ADH1 internal standard (Waters). 10 µL of the respective TMT reagent was added to each sample and the volume was normalized to 33 µL with 100 mM TEAB buffer. After incubating at rt for 2 h, 2.5 µL of 5% NH_4OH was added to each sample and then they were incubated for 15 more min at rt to quench the reaction. Finally, samples were multiplexed by adding them all to the same tube, then concentrating via freeze-drying. The combined samples were resuspended in 300 µL of 200 mM Ammonium formate pH 10.

3. 4. 6. Reverse-Phase Fractionation

In a 200 µL pipette tip, 3 layers of SDB-XC extraction disks (3 M, 1.07 mm x 0.50 mm) were placed and gently packed in. The micro-column formed was washed with 60 µL CH_3CN and 60 µL of 200 mM Ammonium formate pH 10 by centrifugation and collecting the flowthrough in a micro-centrifuge tube. 100 µL of the TMT-labeled peptides were loaded into the micro-column and centrifuged. The flowthrough was reloaded and

the centrifugation repeated. Then, a final wash of the loaded micro-column was performed with 60 µL 200 mM ammonium formate pH 10. All flowthroughs to this point were discarded. Then, the high-pH reverse-phase fractionation began, collecting and saving each flowthrough, followed by freeze-drying of each fraction. There were 7 fractions collected, 60 µL each: 5%, 10%, 15% 20%, 22.5%, 27.5%, 80% CH_3CN in 200 mM ammonium formate. The 5% and 10% fractions were combined, each subsequent fraction was individually collected. After all fractions were lyophilized, the final total of 6 fractions were each resuspended in 30 µL of 0.1% formic acid and transferred into 300 µL fused glass insert mass spec vials for UPLC-MS^3 Fusion analysis.

3. 4. 7. UHPLC-MS^3 Fusion Data Acquisition

Data acquisition was performed by using a method that was previously reported. The TMT-labeled peptides were resolved using a flow rate of 300 nL/min on an UltiMate™ 3000 RSLCnano UHPLC System (ThermoFisher), using a reversed-phase column packed in-house (75 µm i.d., 45 cm). Each of the 6 fractions obtained above was subjected to varying gradients (from 7% to 34%) of CH_3CN with 0.1 % formic acid and 0.1% formic acid in H_2O for 80 min and sprayed directly into the Orbitrap Fusion instrument (ThermoFisher). MS1 scans were collected at 120,000 resolution in a 320–2,000 m/z range, with 100 ms maximum injection time and an automatic gain control (AGC) target of 200,000. Next, the data-dependent MS/MS scans were collected with collision-induced dissociation (CID) at a normalized collision energy (NCE) of 35% with a 1.3 m/z isolation window, with a maximum injection time of 100 ms and AGC target of

5000. Lastly, the acquisition of MS3 data was done by a synchronous selection of the top 10 precursors for fragmentation by high-collisional energy dissociation (HCD) in the orbitrap with 55% NCE, 2.5 m/z isolation window, 120 ms maximum injection time and 50,000 AGC target.

3. 4. 8. Prenylomic Data Processing and Visual Interpretation

Using MaxQuant (version 2.0.3.1), the raw data files obtained from the UHPLC-MS^3 acquisition were uploaded and searched against a non-redundant human database (UP000005640) from Uniprot. Some parameters were modified from default as follows. Trypsin/P (Porcine origin) was used for digestion, allowing for a maximum of 3 missed cleavages with a minimum peptide length of 7 residues. Protein FDR was set to 0.5, carbamidomethyl C modifications in search were removed, and unique + razor peptides were used for quantification. Then, MaxQuant was run on 24 cores at the University of Minnesota Supercomputing Institute. From the files generated, the proteingroup.txt file was uploaded into Perseus (version 2.0.3.0) for filtering and statistical analysis. In the Perseus analysis, proteins that were only identified by site, potential contaminants or reversed were removed. The raw intensities were $\log_2$ transformed, and proteins with less than 3 out of 6 values for each TMT channel after transformation were removed. Missing values were imputed from the normal distribution of the remaining valid values. Reporter ion (TMT) values were normalized by subtracting rows by the mean value and columns by the median value. Statistical analysis was performed using a two-sample t-test at FDR = 1% and s0 = 0.5. Data was then exported to Microsoft Excel for generation of Volcano plots and further figures.

Chapter 4. A Bis Alkyne-modified Protide-like Probe Reveals Prenylation *in cellulo* and *in vivo.*

4. 1. Introduction

Protein prenylation is the irreversible attachment of farnesyl (C15-length) or geranylgeranyl (C20-length) isoprenoids to the C-terminus of approximately 2% of the mammalian proteome (Fig. 1A). This post-translational modification enables proteins to perform essential cellular functions and, has been linked to several diseases. For example, an increase in protein prenylation is associated with the formation of amyloid precursor and tau proteins, process that precedes Alzheimer's Disease.[50] The cause of this debilitating disease is not fully understood, but prenylated proteins can help decipher early steps in AD pathogenesis. Identifying prenylated proteins *in vivo* as targets for AD onset or early diagnosis can be challenging due to the nature of the probes used so far to modify prenylated proteins. In our group, we have shown that the non-charged hydrophobic alcohol form of the endogenous isoprenoid C15AlkOH (Fig. 1B) does not efficiently label mouse tissues and has a level of toxicity due to the high content of DMSO used in its formulation for administration (unpublished work). The diphosphate analogue C15AlkOPP (Fig. 1B) is soluble in water, removing any need for formulation in a nonpolar vehicle, but being a charged molecule, it does not readily cross the blood-brain barrier. When we used it to study AD in the brains of transgenic mice, an ICV bolus injection at high concentration in the left ventricle proved inefficient, leading to the need to surgically attach a pump that would inject the probe into the brain of the mice over 13 days to obtain sufficient levels of labeling.[56]

To overcome these, a prodrug approach was considered, using an established chemical scaffold used in organophosphorus protides,[26] to deliver probes of prenylation *in vivo*.[27,28] To this aim, a stable phosphoramidate prodrug form was chosen[27] and linked to the C15AlkOH scaffold to develop 2 new probes that would be activated *in vivo* by a kinase, HINT1, which is overexpressed in the liver and hydrolyzes phosphoramidates.[29]

Herein, the evaluation in different cell lines and at different concentrations of the ProAlaC15AlkOPP and BisC15AlkOPP (Fig. 1B) protides is described along with a comparison of their how labeling compares to that of C15AlkOPP and the profiling of liver tissue in transgenic APOE3 and APOE4 mice.

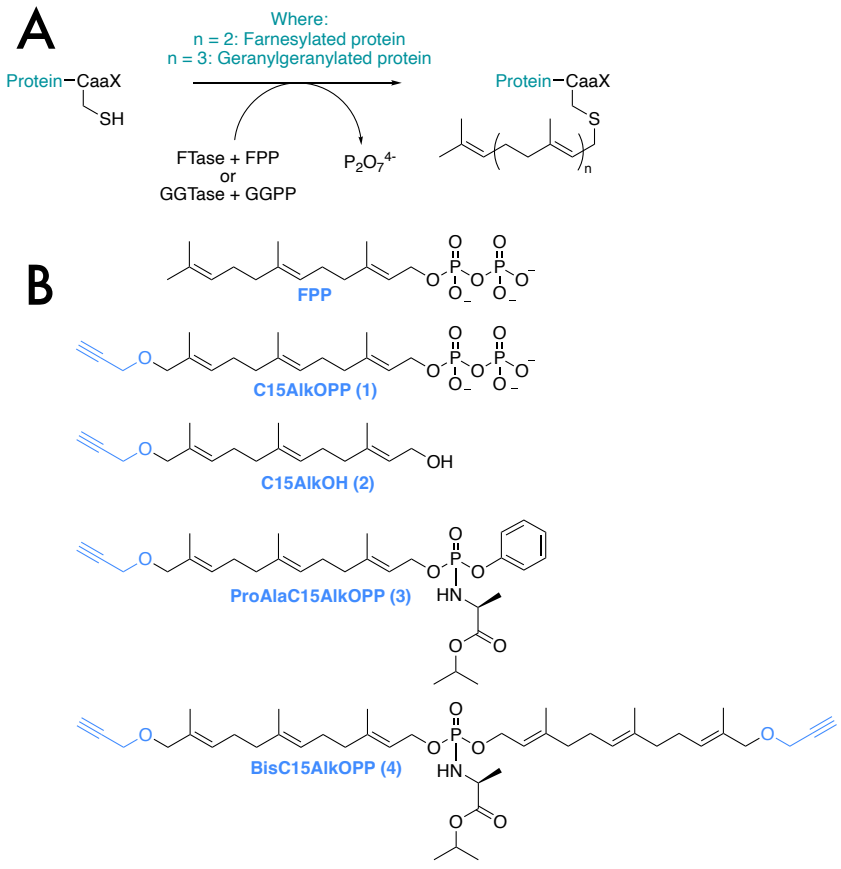

Figure 1: **(A)** General prenylation mechanism **(B)** Structures of the FPP endogenous substrate, C15AlkOPP, C15AlkOH, ProAlaC15AlkOPP and BisC15AlkOPP probes.

4. 2. Results and discussion

4. 2. 1. Comparison of Metabolic Labeling with ProAlaC15AlkOPP and BisC15AlkOPP Probes Versus C15AlkOPP in OPM-2 Cells via In-gel Fluorescence Analysis

After synthesis of ProAlaC15AlkOPP (prepared by Dr. Nyema Harmon), its metabolic labeling efficiency was tested *in cellulo* at different concentrations versus the C15AlkOPP probe and its alcohol version, C15AlkOH, with FPP serving as the control in this experiment. After treating the OPM-2 cell lysates with TAMRA-N_3 under click reaction conditions and resolving the proteins on SDS-PAGE gels, the TAMRA fluorescence was visualized. Like in previous studies, at 10 μM, the C15AlkOPP showed much superior labeling than the C15AlkOH (Fig. 2A, lanes 2 and 3).[3] Unfortunately, the ProAlaC15AlkOPP showed comparable labeling to the C15AlkOH, even at higher concentrations of 50 μM (Fig. 2A, lane 6). Increasing the concentration of ProAlaC15AlkOPP to 100 μM mostly lead to a large increase in background labeling (Fig. 2A, lane 7). Increasing the treatment time to 48 h recapitulated the observations previously made at 24 h of treatment (Fig. 2A). These observations lead to the conclusion that the ProAlaC15AlkOPP protide probe is not suitable for studying protein prenylation efficiently. It was speculated that, since the labeling obtained with ProAlaC15AlkOPP was similar to that observed with C15AlkOH, the allylic alcohol group appeared to be released during compound metabolism instead of the phenyl group, eliminating the possibility of forming the desired allylic monophosphate during the activation process. To this end, another protide probe, BisC15AlkOPP (Fig. 1B) was designed, that would force one of the allylic groups to remain linked to the phosphate group and facilitate its subsequent

activation to the required diphosphate. After synthesizing this molecule, it was compared with C15AlkOPP and ProAlaC15AlkOPP via metabolic labeling and in-gel fluorescence experiments (Fig. 2B). The new probe was able to label prenylated proteins with an efficiency comparable to C15AlkOPP (Fig. 2B, lanes 2 and 4) and significantly better than the ProAlaC15AlkOPP probe (Fig. 2B, lane 3). Statins are known to inhibit the mevalonate pathway which leads to the suppression of endogenous prenylation substrates biosynthesis, hence potentially increasing the incorporation of the artificial prenylation probes.

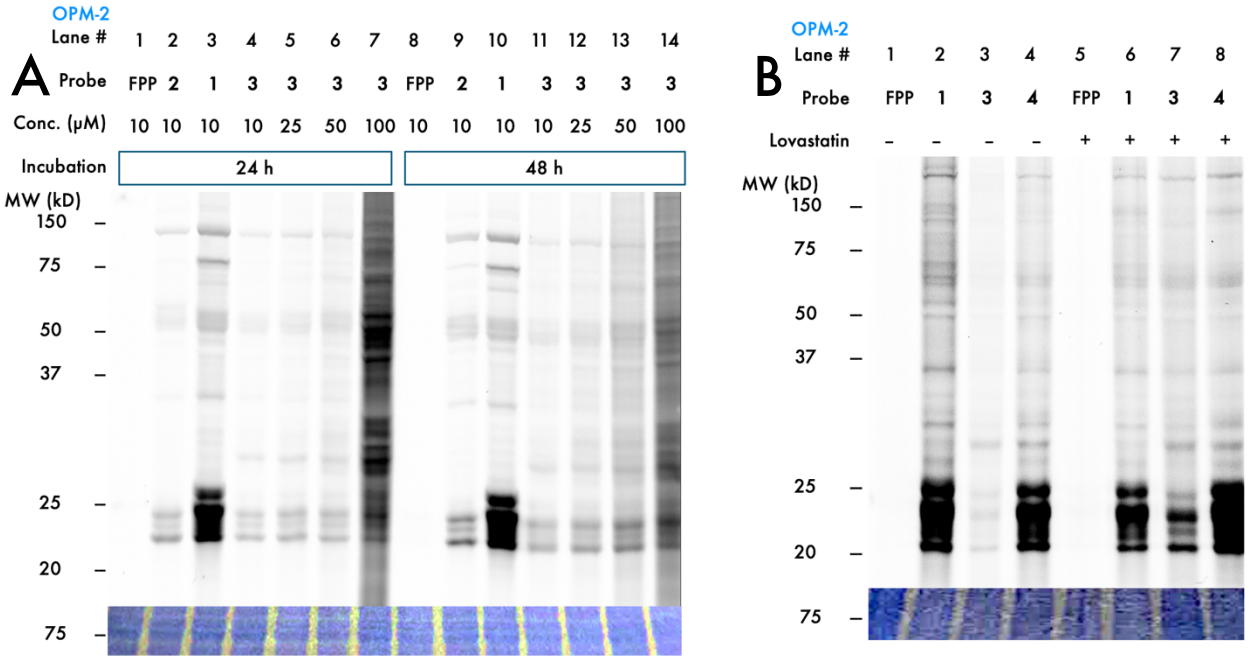

Figure 2: Initial evaluation and comparison of metabolic labeling with ProAlaC15AlkOPP **(3)** and BisC15AlkOPP **(4)** versus C15AlkOPP **(1)** via in-gel fluorescence in OPM-2 cells. **(A)** Time dependent metabolic labeling with the ProAlaC15AlkOPP **(3)** probe at varying concentrations compared with C15AlkOPP **(1)** and C15AlkOH **(2)**. The ProAlaC15AlkOPP **(3)** probe does not label as well as the C15AlkOPP **(1)**, even at higher concentrations. **(B)** C15AlkOPP **(1)**, ProAlaC15AlkOPP **(3)** and BisC15AlkOPP **(4)** labeling for 24 h at 10 μM final concentration in the presence and absence of statin pre-treatment for 6 h (10 μM final concentration). The BisC15AlkOPP probe labeling is comparable to the C15AlkOPP probe. All lanes were subjected to click reaction with TAMRA-N_3, followed by electrophoretic separation on 12% SDS-PAGE gels. Upper panels show TAMRA fluorescence, bottom panels show Coomassie total protein stain.

A 6 h pre-treatment with statin prior to the addition of the prenylation probes had a modest increase effect on the labeling with the BisC15AlkOPP probe (Fig. 2B, lanes 6-8). To avoid any potential physiological perturbations, the use of statins was not employed in any further experiments.[39] These initial evaluation experiments showed that, while the ProAlaC15AlkOPP probe does not appear to be useful for future prenylation studies, the second-generation BisC15AlkOPP protide probe was greatly improved and merited further studies.

4. 2. 2. Comparison of Metabolic Labeling with C15AlkOPP and BisC15AlkOPP in Various Cell Lines via In-gel Fluorescence Analysis

Knowing that the BisC15AlkOPP probe showed good labeling, it was tested in several different cell lines versus C15AlkOPP at 10 μM, as is typically performed. In this experiment, 7 cell lines were analyzed: MCF-7 (adenocarcinoma), COS-7 (kidney), HepG2 (young male hepatocarcinoma), Huh-7 (older male hepatocarcinoma), AML-3 (myeloid leukemia), L363 (plasma cell leukemia) and OPM-2 (multiple myeloma). In order for the BisC15AlkOPP protide probe to be incorporated into the prenylation mechanism, it must first be processed by the HINT1 enzyme, releasing the isoprenoid monophosphate for subsequent phosphorylation prior to prenyltransferase-catalyzed incorporation. Given that HINT1 is overexpressed in liver cells, attention was focused on the liver-derived HepG2 and Huh-7 cell lines (Fig. 3A and 3B, lanes 4 and 5). The labeling pattern using BisC15AlkOPP appears similar to that of C15AlkOPP in all 7 cell lines, and hence, one of them, AML-3, was chosen for subsequent experiments.

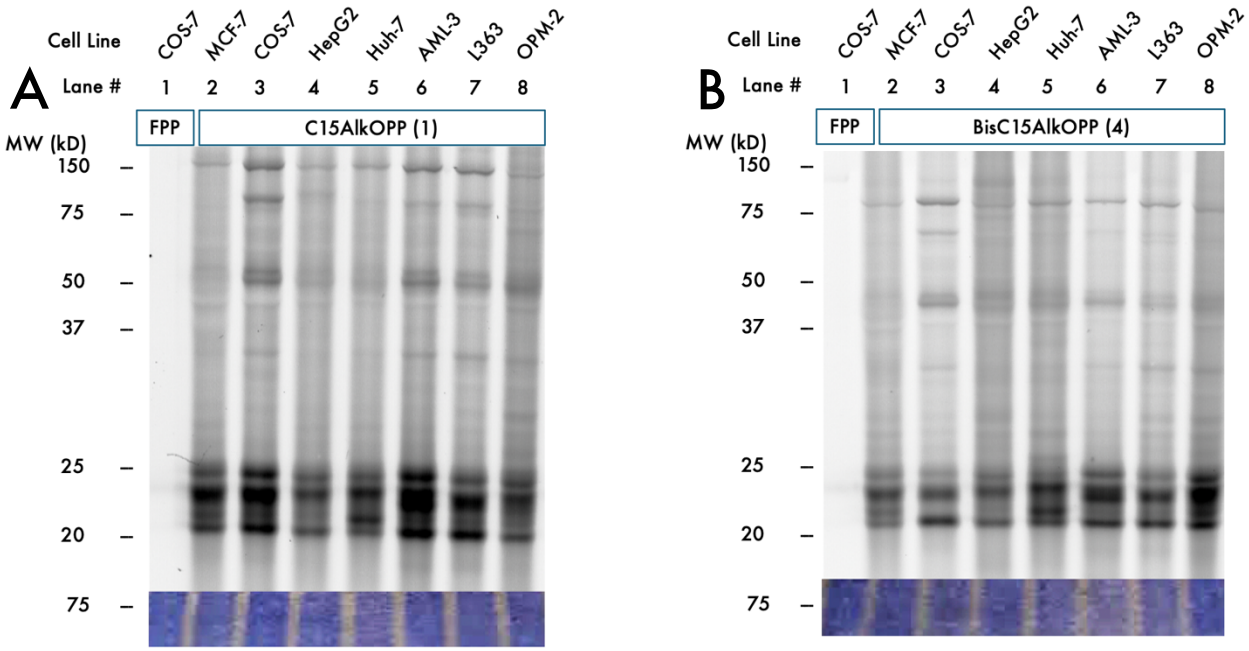

Figure 3: Comparison of metabolic labeling with C15AlkOPP and BisC15AlkOPP versus FPP via in-gel fluorescence in 7 distinct cell lines.
(A) Metabolic labeling with C15AlkOPP for 24 h at 10 μM final concentration. **(B)** Metabolic labeling with BisC15AlkOPP for 24 h at 10 μM final concentration. All lanes were subjected to click reaction with TAMRA-N_3, followed by electrophoretic separation on 12% SDS-PAGE gels. Upper panels show TAMRA fluorescence, bottom panels show Coomassie total protein stain.

4. 2. 3. Metabolic Labeling with BisC15AlkOPP at Sub-10 μM concentrations in AML-3 Cells Analyzed via In-gel Fluorescence Analysis

Next, to better understand the labeling of BisC15AlkOPP compared to the C15AlkOPP parent compound, a concentration study was performed in AML-3 cells. First, metabolic labeling with BisC15AlkOPP over a range of concentrations was compared to the labeling obtained with 10 uM C15AlkOPP. Those experiments indicated that BisC15AlkOPP exhibited better labeling at 5 μM than C15AlkOPP did at 10 μM (Fig. 4A, lanes 3 and 2). A decrease in BisC15AlkOPP labeling was observed as the concentration was lowered, with its labeling at 2.5 μM being comparable to the labeling obtained with C15AlkOPP 10 μM (Fig. 4A, lanes 4 and 2).

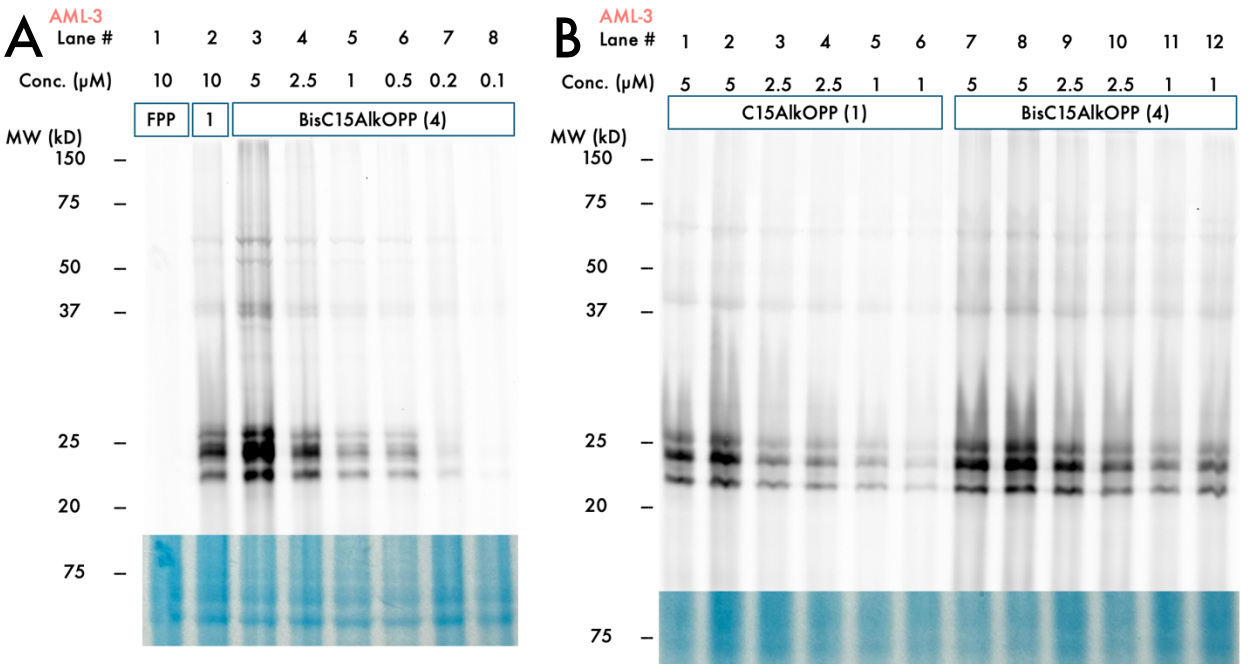

Figure 4: Comparison of metabolic labeling with C15AlkOPP and BisC15AlkOPP versus FPP via in-gel fluorescence at sub-10 μM final concentrations in AML-3 cells. **(A)** Metabolic labeling with BisC15AlkOPP for 24 h at 6 different concentrations. **(B)** Metabolic labeling with C15AlkOPP and BisC15AlkOPP for 24 h at 5, 2.5 and 1 μM final concentration. Each concentration point was performed at n = 2. All lanes were subjected to click reaction with TAMRA-N_3, followed by electrophoretic separation on 12% SDS-PAGE gels. Upper panels show TAMRA fluorescence, bottom panels show Coomassie total protein stain.

To confirm those results, a dose response experiment was performed in AML-3 cells comparing BisC15AlkOPP and C15AlkOPP at 5 μM, 2.5 μM and 1 μM, each of them being performed in duplicate (Fig. 4B). The vast majority of the labeling observed was localized in the 20-25 kDa region and only bands in that region were quantified. For each concentration, the 2 duplicate values were averaged and compared (Fig. 5). That analysis showed that labeling using BisC15AlkOPP was higher than with C15AlkOPP at all 3 concentrations, with higher relative differences as the concentration was lowered. Overall, these results suggest that in these *in vitro* experiments, the BisC15AlkOPP probe labels approximately 2-fold better than C15AlkOPP.

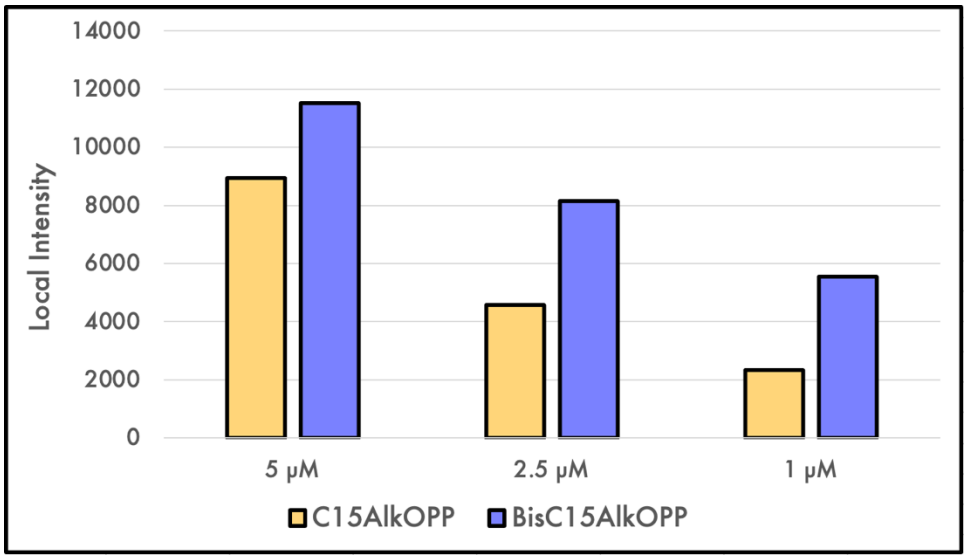

Figure 5: Quantification of labeling in Figure 4B in the 20-25 kDa region bands. All bands in the region were included in the total area quantified for each lane. The intensity shown is the average of the n = 2 replicates for each concentration point.

4. 2. 4. *In Vivo* Labeling

Given that the BisC15AlkOPP protide showed modestly improved potency in *in vitro* labeling compared with C15AlkOPP, the next step was to evaluate it in mice. The BisC15AlkOPP is a hydrophobic uncharged compound, designed to easily penetrate into cells. As a result, it is insoluble in pure aqueous solutions typically used for injection. Based on previous work in our group, we elected to used an emulsion composed of PBS supplemented with a neutral polysorbate detergent, Tween® 80. After a few solubility tests, a 5.5% (w/v) Tween® 80 solution in 1 x PBS containing BisC15AlkOPP proved to be a stable emulsion and was chosen as the formulation to be administered. Before the pilot experiment with the probe, the vehicle solution was tested by daily subcutaneous (SubQ) injections (150 μL total volume/injection) in a mouse for 3 days, where the animal survived without displaying any abnormal behavior.

4. 2. 4. 1. In-gel Fluorescence Analysis in Six Different Tissue Types

Next, a pilot experiment was designed to test the incorporation of the BisC15AlkOPP probe in different mouse tissues. Thus, 2 mice (one for the vehicle and one for the sample) were administered the probe subcutaneously and sacrificed after 24 h, and 2 other mice received daily subcutaneous injections for 3 days, being sacrificed 24 h after the last injection. For all mice, the heart, brain, kidney, liver, spleen and skeletal muscle samples were harvested and samples of ~150 mg of tissue was homogenized in each case (Fig. 6).

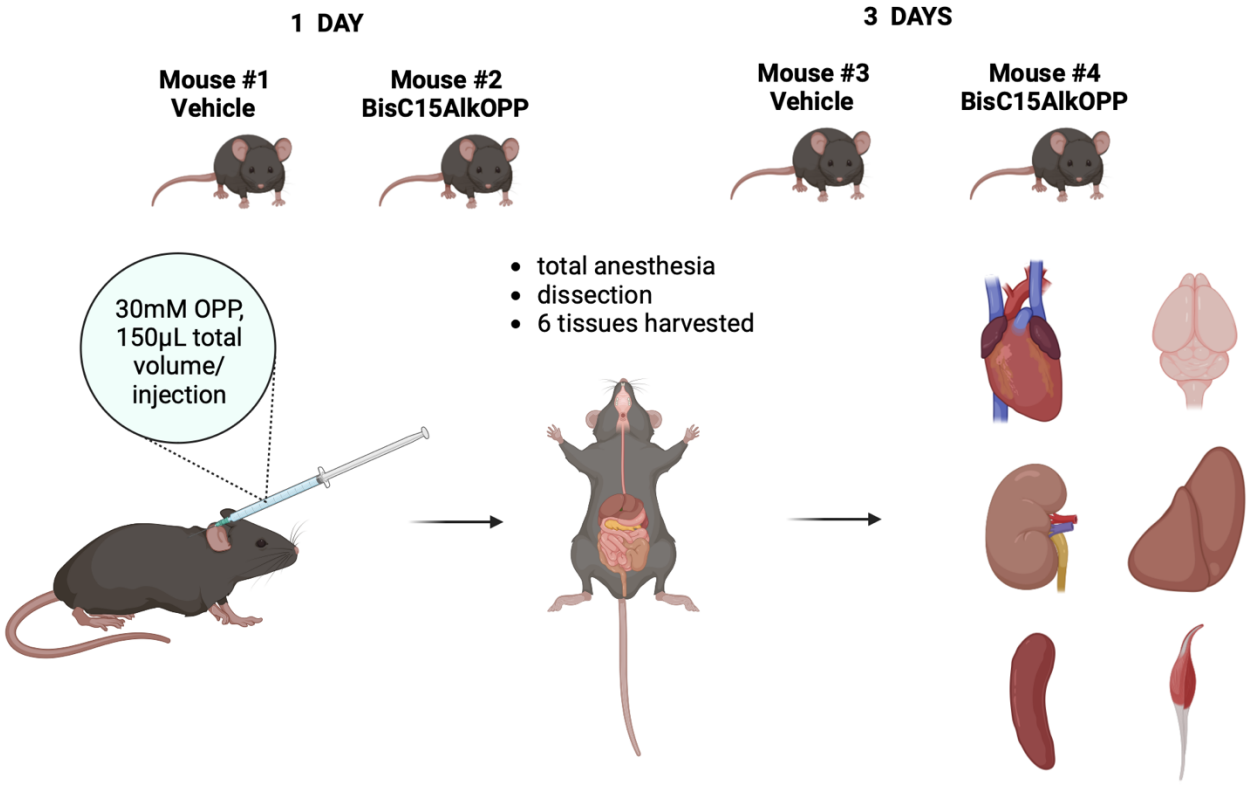

Figure 6: Schematic of the pilot animal experiments performed.
Two mice were injected once with vehicle and BisC15AlkOPP respectively and sacrificed 1 day after the injection. Two other mice were injected 3 times at 24 h intervals with vehicle and BisC15AlkOPP respectively before being sacrificed on the fourth day. The tissues harvested included heart, brain, kidney, liver, spleen and skeletal muscle. The formulation of the probe injected was a stable emulsion, 30 mM BisC15AlkOPP in 5.5 % Tween 80 (w/v) in 1 x PBS buffer. Graphic generated in BioRender.

After subjecting the homogenates to the in-gel fluorescence procedure described above that includes TAMRA-N_3 click reaction, electrophoretic resolution on SDS-PAGE gels and fluorescence imaging, labeling was observed in the liver and weaker labeling in the kidney with the BisC15AlkOPP probe after one injection (Fig. 7A, lanes 9 and 10). Encouragingly, in the mouse that received a daily injection for 3 days in a row, the liver was the most intensely labeled tissue followed by some labeling in the kidney. Low levels of labeling were also observed in the heart and spleen while there was essentially no labeling in the brain or in skeletal muscle.

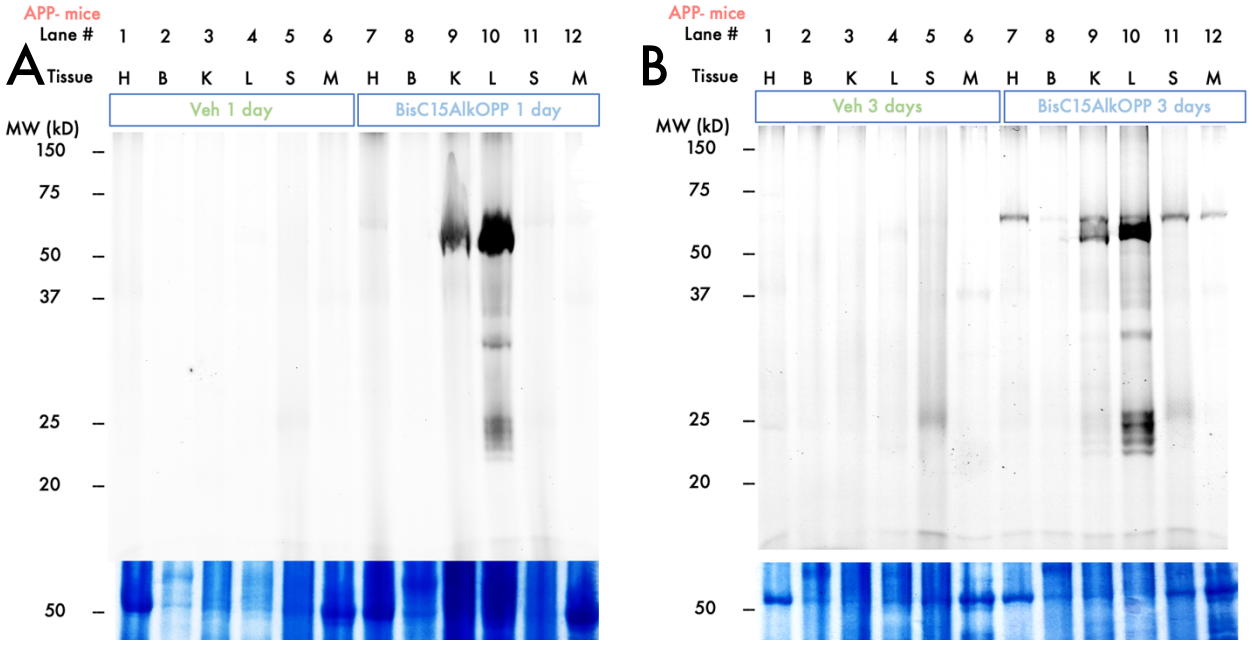

Figure 7: Pilot *in vivo* incorporation experiment with the BisC15AlkOPP probe shows labeling in the kidney and liver via in-gel fluorescence.
(A) Mice were sacrificed and tissues were harvested 24 h after one injection. **(B)** Mice were sacrificed and tissues were collected 24 h after the third daily injection. The concentration of each tissue sample homogenate was normalized via BCA assay. All lanes were subjected to click reaction with TAMRA-N_3, followed by electrophoretic separation on 12% SDS-PAGE gels. Upper panels show TAMRA fluorescence, bottom panels show Coomassie total protein stain.

Beyond labeling in the 20-25 kDa region, there was also an intensely labeled band near 75 kDa in the labeled tissue samples (Fig. 7A, lanes 9 and 10 and 7B, lanes 7, 9, 10 and 11). That latter band was even faintly present in the brain and skeletal muscle samples.

4. 2. 4. 2. Proteomic Analysis in the Liver of APOE3/APOE4 Mice

Having seen the best incorporation in the liver, we next wanted to investigate the utility of this labeling to monitor levels of protein prenylation in mice of different genotypes. In humans, the APOE4 allele has been linked to an increase of up to 33-fold of the risk of developing Alzheimer's disease compared with people that have the closely related APOE3 allele.[19] Given that in Chapter 2, the C15AlkOPP probe was used to investigate differences in prenylation levels between mice harboring the E3 or E4 alleles, it would serve as a valuable point of comparison here. Thus, quantitative prenylomic analysis was performed in mice containing either the APOE3 or APOE4 alleles. Given that the BisC15AlkOPP probe requires additional metabolic activation compared with C15AlkOPP, it is conceivable that these two probes would not necessarily yield equivalent results.

Since, as noted above, the best labeling was obtained after 3 days, those conditions were used here with labeling in the liver being the focus of the study. For this experiment, vehicle and probe (3 mice for each) were administered to mice bearing the APOE3 genotype. This was repeated with mice bearing the APOE4 genotype. An initial in-gel fluorescence analysis of the homogenates harvested from the 12 mice replicated the

labeling observed after 3 days in the pilot experiment, where labeling localized mostly in the 20-25 kDa and 50-75 kDa regions (Fig. 8), with the pattern being similar in APOE3 and APOE4 mice.

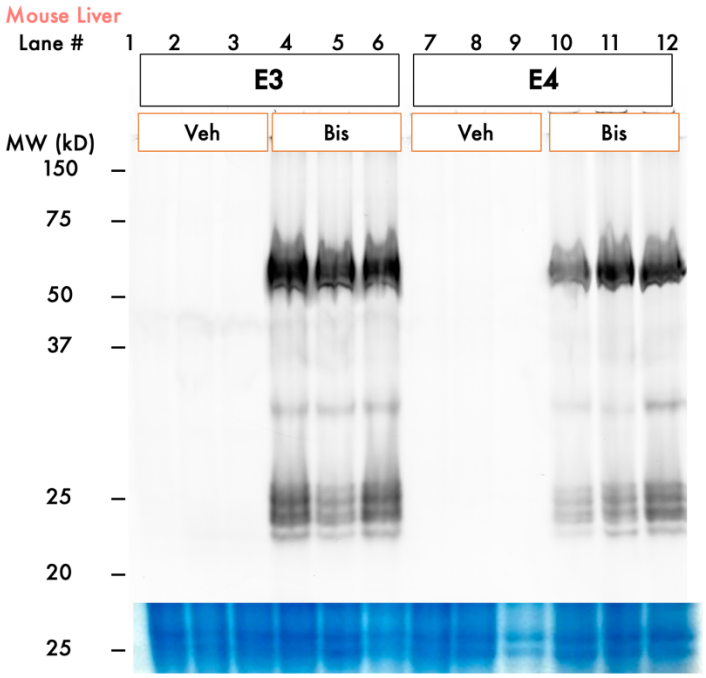

Figure 8: Mouse liver incorporation of the BisC15AlkOPP probe in APOE3 and APOE4 mice via in-gel fluorescence.
Labeling is localized mostly around the 20-25 kDa and 50-75 kDa regions. All samples were ran at n = 3. The concentration of each tissue sample homogenate was normalized via BCA assay. All lanes were subjected to click reaction with TAMRA-N_3, followed by electrophoretic separation on 12% SDS-PAGE gels. Upper panel shows TAMRA fluorescence, bottom panel shows Coomassie total protein stain. Veh = vehicle, Bis = BisC15AlkOPP.

4. 2. 4. 3. Comparison of BisC15AlkOPP/C15AlkOPP Proteomic Profiling in the Liver of APOE3/APOE4 Mice

The mouse liver homogenates were next subjected to a biotin-N_3 click reaction, followed by neutravidin pull down, trypsin digestion, TMT labeling, basic fractionation and UPLC-MS^3 analysis. Subsequent bioinformatic analysis revealed 12 and 17 significantly

enriched prenylated proteins in the APOE3 and APOE4 liver, respectively, at a stringent FDR of 1% with the BisC15AlkOPP protide (Fig. 9C and 9D, colored dots outside the FDR threshold).

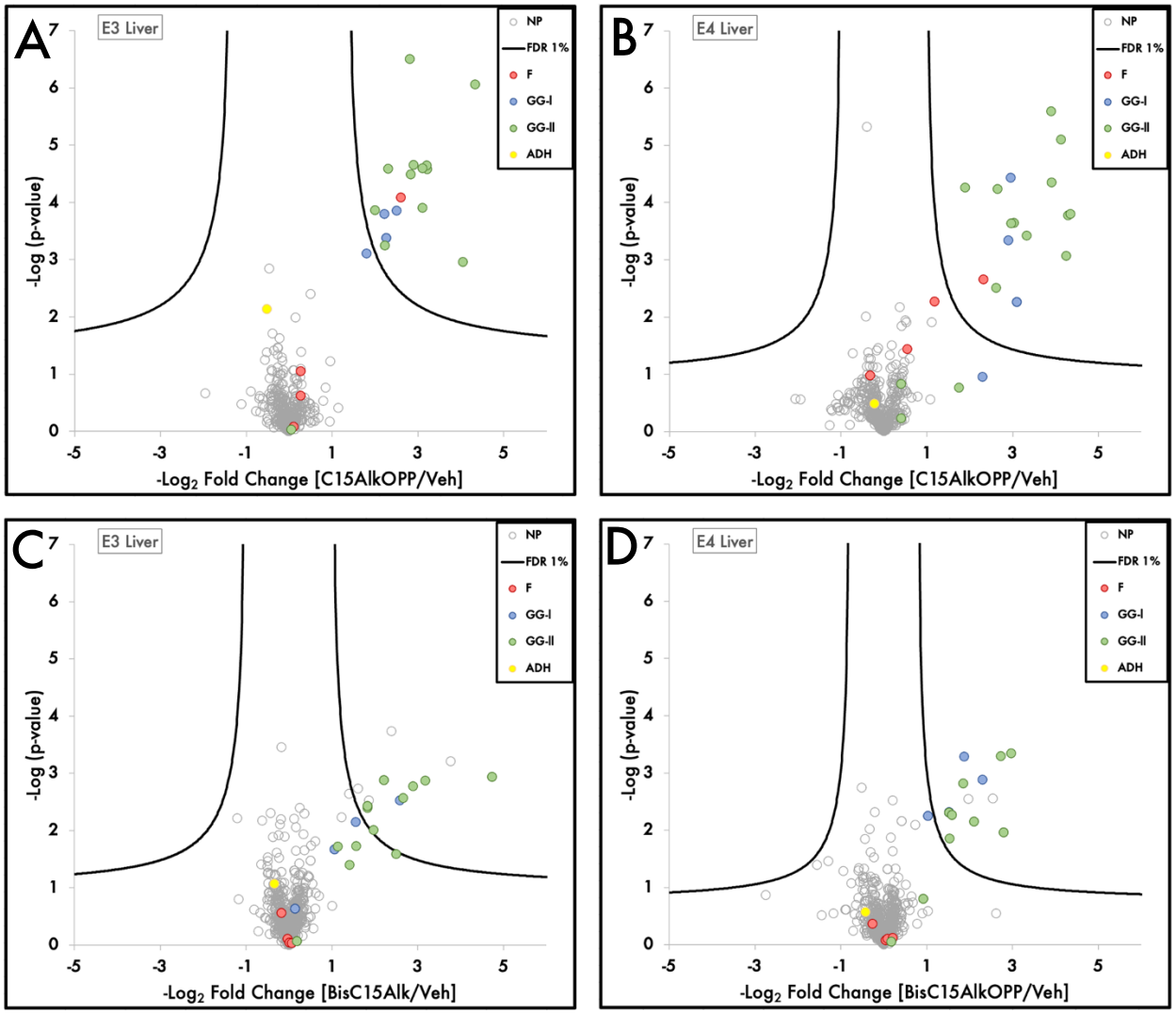

Figure 9: Volcano plots of profiling in mouse liver for E3 and E4 genotypes with C15AlkOPP and BisC15AlkOPP.
(A) APOE3 liver profiling in mice treated with C15AlkOPP reveals 24 prenylated proteins significantly enriched. **(B)** APOE4 liver profiling in mice treated with C15AlkOPP reveals 23 prenylated proteins significantly enriched. **(C)** APOE3 liver profiling in mice treated with BisC15AlkOPP reveals 12 prenylated proteins significantly enriched. **(D)** APOE4 liver profiling in mice treated with BisC15AlkOPP reveals 17 prenylated proteins significantly enriched. All experiments were done at n =3 and proteins are plotted at t-test FDR = 0.01, s0 = 0.5. ADH (yellow dot) served as an internal standard.

In the C15AlkOPP samples, at the same FDR of 1%, there were 24 and 23, respectively, significantly enriched prenylated proteins in the E3 and E4 datasets (Fig. 9A and 9B, colored dots outside the FDR threshold). The BisC15AlkOPP probe significantly identified only targets of geranylgeranylation, whereas the C15AlkOPP analogue identified some farnesylation targets as well. Unfortunately, in contrast to the *in vitro* observations, the protide probe did not appear to label more proteins *in vivo* than the C15AlkOPP parent compound.

Nevertheless, there were 31 unique prenylation targets found across the 4 datasets, and the identities of these proteins are shown in Figure 10A, with the proteins having the overall highest fold changes in the E4 C15AlkOPP dataset. There were 10 proteins found in all 4 datasets at different fold change values and 21 proteins found in at least one dataset but not in all 4.

There were 4 proteins found only in the E4 BisC15AlkOPP dataset: RAB8A, RAB8B, RAB13 and RAB15 (Fig. 10B, orange bars), indicating that their prenylation may be somehow linked to APOE4 and HINT1 expression.

For the 10 proteins found in common in all 4 datasets, the fold changes in the BisC15AlkOPP experiments were overall lower than the fold changes in the C15AlkOPP datasets (Fig. 10C). This may be indicative of the C15AlkOPP being a better prenylation substrate than the BisC15AlkOPP *in vivo*, an opposite effect than the one observed *a priori in vitro*, which might be due to different processing of the larger protide probe in an actual tissue as compared to metabolic labeling in only one type of cultured cells.

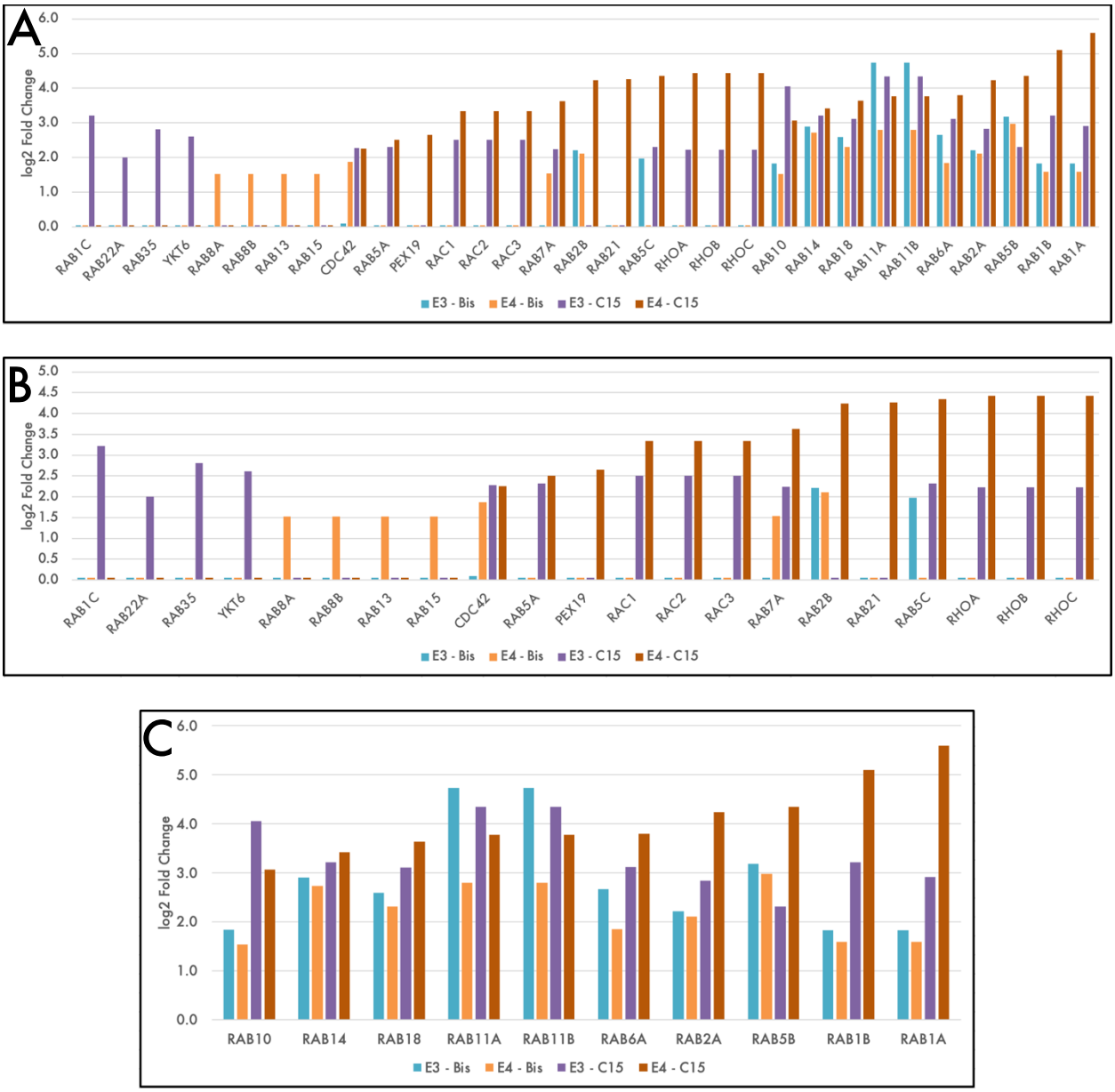

Figure 10. Bar graphs showing protein identity versus fold change for the 4 datasets. **(A)** All 31 unique proteins found across the 4 datasets with C15AlkOPP and BisC15AlkOPP. **(B)** The 21 proteins that were found in 1, 2 or 3 datasets. **(C)** The 10 proteins found in common across the 4 datasets. Protein identities were arranged in increasing order of fold changes in the C15AlkOPP E4 dataset.

The intersection of the 2 larger datasets from C15AlkOPP and the 2 smaller BisC15AlkOPP datasets is shown in the Venn diagram in Figure 11A, with 4, 2 and 4 proteins being solely found in the E3 C15AlkOPP, E4 C15AlkOPP and E4 BisC15AlkOPP

respectively. When comparing the 2 probes for each genotype, there were 13 proteins found in common in E4 and 11 found in common in E3 (Fig. 11B).

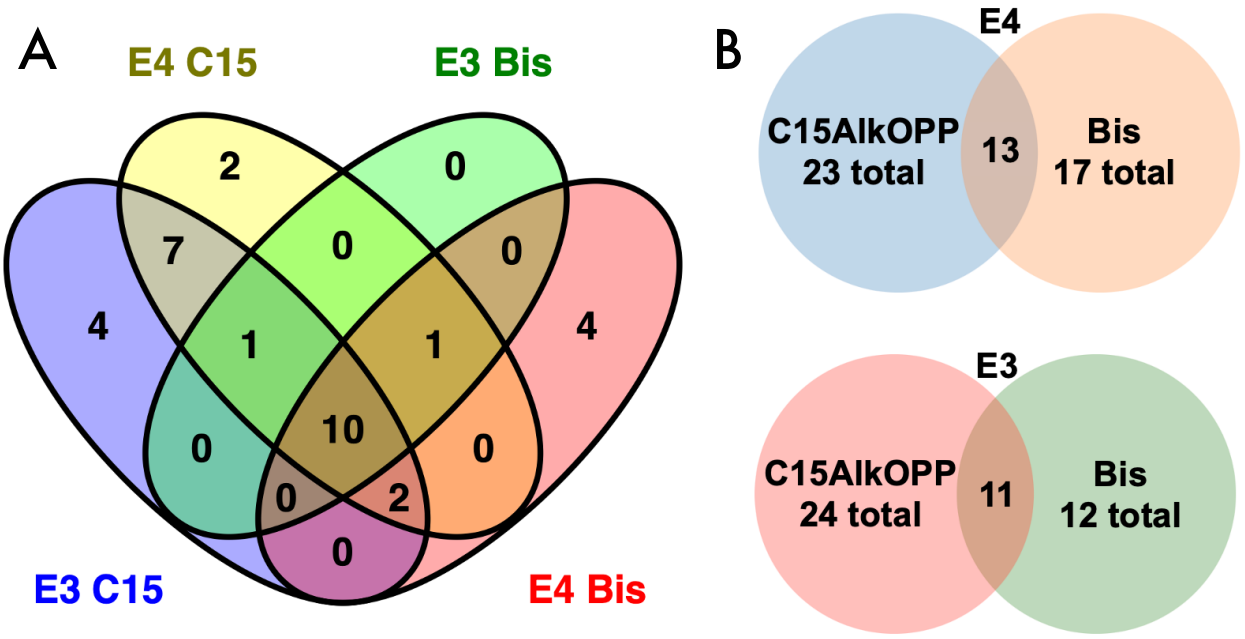

Figure 11. Venn diagrams for the 4 datasets discussed.
(A) Venn diagram showing the intersection of all 4 datasets and revealing 10 significantly enriched prenylated proteins in common across all 4 datasets. **(B)** Venn diagrams for the intersection of the C15AlkOPP and BisC15AlkOPP datasets for the E4 genotype (top, blue and orange) and the E3 genotype (bottom, red and green) showing 13 and respectively 11 proteins in common.

The identities of these proteins are shown in Table 1, with the 10 common proteins being listed first, and all fold changes for the 31 proteins discussed herein being shown in Table 2.

Table 1. Protein datasets for the C15AlkOPP and BisC15AlkOPP E3 and E4 genotypes. The first 10 proteins are the ones found across all 4 datasets. The next 21 are found in one or more sets, but not all 4. Each row is unique to only one protein. Red = farnesylation, blue = geranylgeranylation type-I, green = geranylgeranylation type-II.

C15AlkOPP		BisC15AlkOPP		
E3	E4	E3	E4	
RAB10	RAB10	RAB10	RAB10	common across all 4 datasets
RAB11A	RAB11A	RAB11A	RAB11A	
RAB11B	RAB11B	RAB11B	RAB11B	
RAB14	RAB14	RAB14	RAB14	
RAB18	RAB18	RAB18	RAB18	
RAB1A	RAB1A	RAB1A	RAB1A	
RAB1B	RAB1B	RAB1B	RAB1B	
RAB2A	RAB2A	RAB2A	RAB2A	
RAB5B	RAB5B	RAB5B	RAB5B	
RAB6A	RAB6A	RAB6A	RAB6A	
CDC42	CDC42		CDC42	
RAB5C	RAB5C	RAB5C		
RAB7A	RAB7A		RAB7A	
RAB5A	RAB5A			
RAC1	RAC1			
RAC2	RAC2			
RAC3	RAC3			
RHOA	RHOA			
RHOB	RHOB			
RHOC	RHOC			
RAB1C				
RAB22A				
RAB35				
YKT6				
	PEX19			
	RAB21			
	RAB2B	RAB2B	RAB2B	
			RAB8A	
			RAB8B	
			RAB13	
			RAB15	

Table 2. Protein datasets for the C15AlkOPP and BisC15AlkOPP E3 and E4 genotypes including the fold changes for the respective protein in that dataset.
The first 21 proteins are found in one or more sets, but not all 4. Red = farnesylation, blue = geranylgeranylation type-I, green = geranylgeranylation type-II.

BisC15AlkOPP fold change			C15AlkOPP fold change		
E3	E4	Protein ID	E3	E4	
		RAB1C	3.2		
		RAB22A	2.0		
		RAB35	2.8		
		YKT6	2.6		
	1.5	RAB8A			
	1.5	RAB8B			
	1.5	RAB13			
	1.5	RAB15			
	1.9	CDC42	2.3	2.3	
		RAB5A	2.3	2.5	
		PEX19		2.7	
		RAC1	2.5	3.3	
		RAC2	2.5	3.3	
		RAC3	2.5	3.3	
	1.5	RAB7A	2.2	3.6	
2.2	2.1	RAB2B		4.2	
		RAB21		4.3	
2.0		RAB5C	2.3	4.3	
		RHOA	2.2	4.4	
		RHOB	2.2	4.4	
		RHOC	2.2	4.4	
1.8	1.5	RAB10	4.1	3.1	common across all 4 datasets
2.9	2.7	RAB14	3.2	3.4	
2.6	2.3	RAB18	3.1	3.6	
4.7	2.8	RAB11A	4.3	3.8	
4.7	2.8	RAB11B	4.3	3.8	
2.7	1.9	RAB6A	3.1	3.8	
2.2	2.1	RAB2A	2.8	4.2	
3.2	3.0	RAB5B	2.3	4.3	
1.8	1.6	RAB1B	3.2	5.1	
1.8	1.6	RAB1A	2.9	5.6	

4. 3. Conclusions

To summarize the work described here, two new uncharged, neutral probes were developed to study prenylation employing a protide delivery mechanism. The ProAlaC15AlkOPP proved to be inefficient in metabolic labeling compared to the C15AlkOPP probe previously described in earlier work. In contrast, the BisC15AlkOPP probe showed efficient labeling *in vitro,* yielding better incorporation in metabolic labeling experiments than the C15AlkOPP probe at the same concentration of 10 μM. That was also true at lower concentrations including 2.5 μM and 5 μM. These promising results encouraged subsequent animal experiments, where the liver was the tissue was found to give the best probe incorporation.

After profiling the liver tissue in 2 different APOE genotype mice with both probes, the BisC15AlkOPP protide had fewer significantly enriched prenylated proteins than the C15AlkOPP, but the E4 genotype contained 4 geranylgeranylation targets that were not found enriched in the other 3 datasets (RAB8A, RAB8B, RAB13 and RAB15). It is possible that the prenylation of these 4 proteins may play a role in Alzheimer's disease pathogenesis, since they were only found in the mice with the deleterious isoform of the APOE gene (E4).

4. 4. Experimental Procedures

4. 4. 1. Metabolic Labeling in Cultured Cells

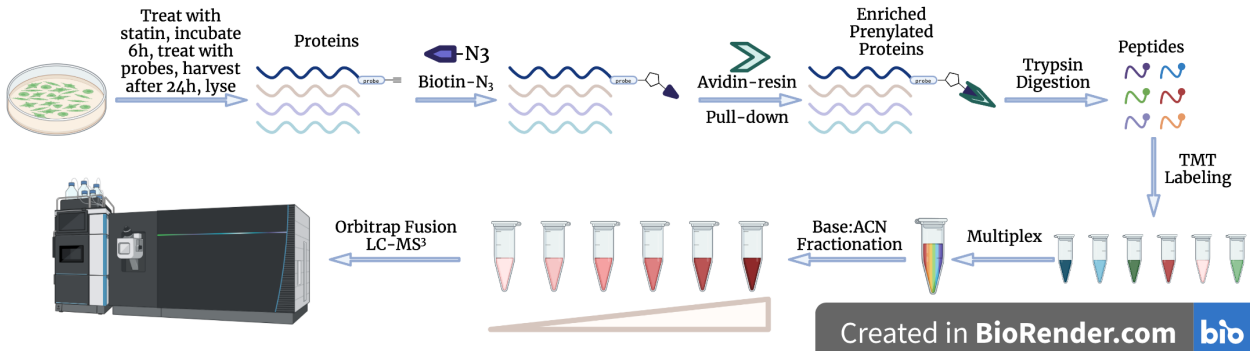

Figure 12. Proteomics workflow from cultured cells.

OPM-2, L363 and AML-3 cells (generously provided by Dr. David Fruman at the University of California, Irvine) were cultured in T25 vented-cap flasks (Thermo Fisher) at a density of around 1.5 x 10^6/ mL and allowed to grow for 24h in RPMI 1640 (Gibco) media supplemented with 1% L-Glutamine (Gibco), 10% fetal bovine serum (GenClone) and 1% penicillin–streptomycin (Gibco). COS-7 cells were cultured on 100 mm dishes at around 1 × 10^6 density and allowed to grow for 24h in 10 mL DMEM (Gibco) media supplemented with 10% fetal bovine serum (Gibco) and 1% penicillin–streptomycin (Gibco).

After 24h, the media was removed and replaced with 5 mL of fresh media. In the case of experiments including statin, lovastatin (Cayman Chemical) was added at this point (10 μM) and the flasks/dishes were incubated for 6 h under 5% CO_2 at 37 ºC. After the statin pre-treatment, the media was retained and the C15PentOPP (10 μM) was added, alongside the respective GGTI (where indicated, at respective concentration). After 24h of incubation, the cells were harvested and pelleted via centrifugation.

4. 4. 2. In-gel Fluorescence Labeling

The cell pellets were suspended in 300 µL of lysis buffer (2.4 µM PMSF, 200 units/nL benzonase nuclease (Sigma-Aldrich), protease inhibitor cocktail and 1% SDS in 1X PBS) and lysed by sonicating on ice 7 times with 3-s pulses at 3-s intervals. Then, the protein concentration in each sample was quantified using a BCA assay (Thermo Fisher Scientific). For each sample, a volume containing 100 µg of protein was then subjected to a copper catalyzed alkyne-azide cycloaddition (CuAAC) reaction (click reaction) with TAMRA-N_3 (25 µM TAMRA-N_3 (BroadPharm), 1 mM TCEP (Sigma-Aldrich), 0.1 mM TBTA (Sigma-Aldrich), and 1 mM $CuSO_4$) for 2 h at rt in the dark. After that, proteins were precipitated using a ProteoExtract precipitation kit (Millipore-Sigma) following the manufacturer's procedure. After removing all liquid, the protein pellet was resuspended in 30 µL of 1X loading buffer (10% glycerol, 2% SDS, 0.02% bromophenol blue in 50 mM Tris–HCl pH 6.8) and the pellet was dissolved by heating briefly to 80 ºC and vortexing. Afterwards, the protein samples were loaded and resolved on a 12% SDS-PAGE gel at 120 V until the dye ran off. The gels were placed in DI H_2O and immediately scanned for TAMRA fluorescence using a Typhoon FLA 9500 (GE Healthcare) gel scanner. The resulting gel images were processed in ImageJ by adjusting the brightness and contrast of lanes. The gels were stained with Coomassie blue for 12 h and then destained with destain solution for 24 h. The final gel images were then processed and assembled in Microsoft PowerPoint.

4. 4. 3. Enrichment of Prenylated Proteins

For enrichment, a much larger protein sample was necessary than the one used for in-gel fluorescence, namely 2000 µg. The cells were cultured and treated in the same manner as described above, just on a larger scale for each replicate. The lysis and BCA assay protein concentration determination were performed in the same manner as described above as well. Then, a volume containing 2 mg of protein for each sample was subjected to a Biotin-N_3 click reaction by adding 100 µM Biotin-N_3 (BroadPharm), 1 mM TCEP, 0.1 mM TBTA, and finally 1 mM $CuSO_4$. The mixtures were rotated for 2 h at rt and then the tubes were centrifuged briefly. The proteins were precipitated on ice by adding 1 mL CH_3Cl, 4 mL CH_3OH and 3 mL 1X PBS buffer, mixing vigorously and then centrifuging for 10 min. The aqueous layers were removed gently by decanting and the resulting protein pellets were stored at -20 ºC overnight. Next, the protein pellets were resuspended in 500 µL of 1%SDS in 1X PBS buffer and dissolved by sonication, followed by a BCA assay to normalize the concentration of recovered protein in each sample.

Then, 200 µL of 0.5 mg/mL Neutravidin agarose beads (Thermo Scientific) were washed 3 times with 1%SDS in 1X PBS buffer. The volume containing 1 mg of protein was added to each tube and normalized with 1%SDS in 1X PBS buffer to a total liquid volume of 500 µL. The samples were incubated at rt for 2h, then they were spun down and the supernatant removed.

The beads were than washed 3 times with 1 mL of 1%SDS in 1X PBS buffer, then once with 1 mL of 1X PBS buffer, removing the supernatant after each wash. Next, the beads were washed 3 times with 1 mL of 8 M Urea in 50 mM TEAB buffer followed by 3

times with 1 mL of 50 mM TEAB buffer. It is crucial during this procedure to ensure a thorough wash, as well as removing the supernatant without removing any beads.

4. 4. 4. On-Bead Digestion of Biotinylated Proteins

Digestion was immediately set up next by adding 100 µL of 50 mM TEAB buffer to each sample containing proteins bound to the resin beads and 6 µL of sequencing grade trypsin solution (ProMega Corp.). The samples were incubated at 37 ºC for 18 hours, then, the digestion was quenched by adding 2.5 µL of 20% formic acid to each sample and incubated 15 min further. The supernatant was then passed through a Pierce Spin column (ThermoFisher, not loaded with any stationary phase) and the beads were washed with 100 µL of 0.5% formic acid. The supernatant was collected again for each tube after passing through the Spin column. Lastly, the resin was washed with 100 µL of 30% CH_3CN solution in H_2O and the whole mixture was passed through the spin column. The liquid phase collected for each fraction was then concentrated by freeze-drying and the peptides were resuspended in 40 µL 100 mM TEAB buffer.

4. 4. 5. TMT Labeling Reaction for Peptides

TMT 6-plex reagents were prepared following the manufacturer's specifications (ThermoFisher). Another BCA assay was performed in order to quantify the peptide samples' concentrations. Then, the volume necessary for 10 µg of peptides was supplemented with 3 µL of 150 fM yeast ADH1 internal standard (Waters). 10 µL of the

respective TMT reagent was added to each sample and the volume was normalized to 33 µL with 100 mM TEAB buffer. After incubating at rt for 2 h, 2.5 µL of 5% NH_4OH was added to each sample and then they were incubated for 15 more min at rt to quench the reaction. Finally, samples were multiplexed by adding them all to the same tube, then concentrating via freeze-drying. The combined samples were resuspended in 300 µL of 200 mM Ammonium formate pH 10.

4. 4. 6. Reverse-Phase Fractionation

In a 200 µL pipette tip, 3 layers of SDB-XC extraction disks (3 M, 1.07 mm x 0.50 mm) were placed and gently packed in. The micro-column formed was washed with 60 µL CH_3CN and 60 µL of 200 mM Ammonium formate pH 10 by centrifugation and collecting the flowthrough in a micro-centrifuge tube. 100 µL of the TMT-labeled peptides were loaded into the micro-column and centrifuged. The flowthrough was reloaded and the centrifugation repeated. Then, a final wash of the loaded micro-column was performed with 60 µL 200 mM ammonium formate pH 10. All flowthroughs to this point were discarded. Then, the high-pH reverse-phase fractionation began, collecting and saving each flowthrough, followed by freeze-drying of each fraction. There were 7 fractions collected, 60 µL each: 5%, 10%, 15% 20%, 22.5%, 27.5%, 80% CH_3CN in 200 mM ammonium formate. The 5% and 10% fractions were combined, each subsequent fraction was individually collected. After all fractions were lyophilized, the final total of 6 fractions were each resuspended in 30 µL of 0.1% formic acid and transferred into 300 µL fused glass insert mass spec vials for UPLC-MS^3 Fusion analysis.

4. 4. 7. UHPLC-MS^3 Fusion Data Acquisition

Data acquisition was performed by using a method that was previously reported. The TMT-labeled peptides were resolved using a flow rate of 300 nL/min on an UltiMate™ 3000 RSLCnano UHPLC System (ThermoFisher), using a reversed-phase column packed in-house (75 μm i.d., 45 cm). Each of the 6 fractions obtained above was subjected to varying gradients (from 7% to 34%) of CH_3CN with 0.1 % formic acid and 0.1% formic acid in H_2O for 80 min and sprayed directly into the Orbitrap Fusion instrument (ThermoFisher). MS1 scans were collected at 120,000 resolution in a 320–2,000 m/z range, with 100 ms maximum injection time and an automatic gain control (AGC) target of 200,000. Next, the data-dependent MS/MS scans were collected with collision-induced dissociation (CID) at a normalized collision energy (NCE) of 35% with a 1.3 m/z isolation window, with a maximum injection time of 100 ms and AGC target of 5000. Lastly, the acquisition of MS3 data was done by a synchronous selection of the top 10 precursors for fragmentation by high-collisional energy dissociation (HCD) in the orbitrap with 55% NCE, 2.5 m/z isolation window, 120 ms maximum injection time and 50,000 AGC target.

4. 4. 8. Prenylomic Data Processing and Visual Interpretation

Using MaxQuant (version 2.0.3.1), the raw data files obtained from the UHPLC-MS^3 acquisition were uploaded and searched against a non-redundant human database (UP000005640) from Uniprot. Some parameters were modified from default as follows.

Trypsin/P (Porcine origin) was used for digestion, allowing for a maximum of 3 missed cleavages with a minimum peptide length of 7 residues. Protein FDR was set to 0.5, carbamidomethyl C modifications in search were removed, and unique + razor peptides were used for quantification. Then, MaxQuant was run on 24 cores at the University of Minnesota Supercomputing Institute. From the files generated, the proteingroup.txt file was uploaded into Perseus (version 2.0.3.0) for filtering and statistical analysis. In the Perseus analysis, proteins that were only identified by site, potential contaminants or reversed were removed. The raw intensities were $\log_2$ transformed, and proteins with less than 3 out of 6 values for each TMT channel after transformation were removed. Missing values were imputed from the normal distribution of the remaining valid values. Reporter ion (TMT) values were normalized by subtracting rows by the mean value and columns by the median value. Statistical analysis was performed using a two-sample t-test at FDR = 1% and s0 = 0.5. Data was then exported to Microsoft Excel for generation of Volcano plots and further figures.

4. 4. 9. Animal injections

Mice were injected subcutaneously (subQ) with either 150 µL of sterile filtered C15AlkOPP (stock solution: 3000 µL at 30mM C15AlkOPP with 4.8 mM NH_4HCO_3 in 1x PBS) or sterile filtered vehicle (3000 µL at 4.8mM NH_4HCO_3 in 1x PBS) solution using a 1 mL syringe (Neta Scientific), and 25G needle (Fisher Scientific). Sterile filtration was performed with 0.22 µM size syringe filters (Celltreat).

4. 4. 10. Anesthesia

When the experimental timeframe was complete, mice were anesthetized using Isoflurane (Isospire) in a drop bottle method for 2-4 minutes, or until they no longer reacted to a foot pinch test.

4. 4. 11. Dissection and Animal Tissue Collection

After anesthesia, mice (all had body weights between 40-50 g) were dissected using a general dissection protocol. They were cardiac bled with a 1 mL syringe (Neta Scientific) and 25G needle (Fisher Scientific) to remove excess blood before being perfused with 20 mL of DPBS (Gibco). After perfusion, the brain was removed and placed on a glass side on ice. The brain was then dissected into 5 different sections: left front cortex (LFCrt, 50-70 mg), left back cortex (LBCrt, 50-70 mg), right cortex (RCrt, 100-120 mg), cerebellum (CB, 60-100 mg) and all else labeled as rest brain (RB, 100-160 mg). All tissues were placed in a 1.5 mL safe-lock tube (Eppendorf), weighed, and then flash-frozen in liquid nitrogen. Heart (atrium, 70-100 mg, ventricle, 50-130 mg), spleen (30-80 mg), kidney (100-200 mg), and liver (60-900 mg) samples were also collected, weighed, and then flash-frozen in the same manner as the brain.

4. 4. 12. Tissue Homogenization

Each tube (with 50-100 mg tissue) had 300 µl of lysis buffer and 100 mg of 0.5 mm diameter ZrOB05 beads (Next Advance) added. Tubes were homogenized in the Bullet Blender (Next Advance) on speed 10 and time 3 min at 4°C. Tubes were checked

for unhomogenized tissue, and, if present, were homogenized for an additional 3 min. After homogenization, samples were quickly centrifugated on a tabletop centrifuge (Labnet) for 5 seconds. Tissue homogenates were then transferred to a 1.5 mL microcentrifuge tube (Eppendorf) and then sonicated using the Sonic Dismembrator (Fisher Scientific) 6 times at 10 second intervals with the tube on ice. All samples were then centrifuged (Fisher Scientific) at 10,000 x g for 15 minutes and the supernatants were collected for each sample for subsequent analysis.

5. Conclusions and Future Directions

In the second chapter, two different alkyne-containing isoprenoid probes of different lengths (C15AlkOPP and C15PentOPP) were synthesized to study protein prenylation. The C15AlkOPP probe was able to identify via metabolic labeling and subsequent prenylomic analysis a plethora of prenylated proteins with high confidence in different cell lines, including COS-7 and AML-3. The C15PentOPP was responsive in labeling sets of geranylgeranylated type-I proteins in the presence of potent GGTase type-I inhibitors (GGTI 298 and GGTI 2133), revealing with high confidence prenylated targets of these inhibitory compounds.

When studying the two probes for prenylation *in vivo*, the C15AlkOPP probe showed the best labeling and was used in a subsequent proteomic experiment. The APOE gene has been highly implicated with AD, so an experiment comparing protein prenylation in transgenic mice with the E3 allele of the APOE gene versus mice with the E4 allele revealed differences in prenylation in the liver, the main location for the endogenous synthesis of peripheral APOE. Out of the 27 proteins identified as significantly enriched with high confidence in the two datasets (E3 and E4), 4 were found only in E3, 3 were found only in E4 and 20 were found in both E3 and E4. From the 20 proteins found in common, 9 of them had fold changes that were statistically significant, with all these 9 proteins having a higher fold change value in the E4 dataset, along with implications in either APOE regulation/transport or AD pathology. Future work will focus on validating these protein targets via comparison with RNAseq levels of expression and western blot analysis to confirm their levels of prenylation.

In the third chapter, work was focused on exploring the prenylated proteins affected by GGTIs in blood cancers, with a goal of identifying which ones are common across different cell lines and potentially responsible for the synergistic effect our collaborators noted in cytotoxicity assays. Using the C15AlkOPP probe, we metabolically labeled prenylated proteins in the absence of statin in proteomic profiling experiments across 4 different blood cancer cell types: AML-3, MOLM-13, L363 and OPM-2, with 67, 52, 63 and 62 proteins respectively found significantly enriched with high confidence. For each dataset, 20, 18, 23 and 19 respectively were geranylgeranylation type-I targets. Proteomic experiments in the presence of C15AlkOPP probe and GGTI 298 or GGTI 2133 have shown good overlap between the significantly depleted proteins identified and the geranylgeranylation type-I targets found when profiling, with GGTI 298 having overall more potent inhibition. Importantly, there were 3 proteins found with high confidence across all 4 cell types as depleted by GGTI 298 (RALA, RAP1B and RAP1A). Future work will focus on validating these results in knock-out genetic cells followed by a cytotoxicity assay where loss of synergy will serve as confirmation that the respective protein was indeed a correct target.

In the last chapter, two new uncharged, neutral probes were developed to study prenylation employing a protide delivery mechanism in order to overcome previous challenges of monitoring prenylation *in vivo*. The ProAlaC15AlkOPP probe inefficient in metabolic labeling, but the BisC15AlkOPP probe showed efficient labeling *in vitro,* yielding better incorporation in than the C15AlkOPP probe at the same concentration. These promising results encouraged subsequent animal experiments, where the best probe incorporation was in the. After profiling the liver tissue in APOE3 and APOE4

genotype mice, the BisC15AlkOPP protide had fewer significantly enriched prenylated proteins than the C15AlkOPP, but the E4 genotype contained 4 geranylgeranylation targets that were not found enriched in the other 3 datasets (RAB8A, RAB8B, RAB13 and RAB15). It is possible that the prenylation of these 4 proteins may play a role in Alzheimer's disease pathogenesis, since they were only found in the mice with the deleterious isoform of the APOE gene (E4). Future work will focus on validating these proteins as targets, as well as longer periods of daily injections in order to increase incorporation in the other tissues and potentially observing labeling in the brain, assuming that the neutral probe crosses the blood-brain barrier.

6. Bibliography

(1) Farnsworth, C. C.; Wolda, S. L.; Gelb, M. H.; Glomset, J. A. Human Lamin B Contains a Farnesylated Cysteine Residue. *J. Biol. Chem.* **1989**, *264* (34), 20422–20429. https://doi.org/10.1016/S0021-9258(19)47079-8.

(2) Wolda, S. L.; Glomset, J. A. Evidence for Modification of Lamin B by a Product of Mevalonic Acid. *J. Biol. Chem.* **1988**, *263* (13), 5997–6000. https://doi.org/10.1016/S0021-9258(18)68736-8.

(3) Suazo, K. F.; Hurben, A. K.; Liu, K.; Xu, F.; Thao, P.; Sudheer, Ch.; Li, L.; Distefano, M. D. Metabolic Labeling of Prenylated Proteins Using Alkyne-Modified Isoprenoid Analogues. *Curr. Protoc. Chem. Biol.* **2018**, *10* (3), e46. https://doi.org/10.1002/cpch.46.

(4) Ownby, S. E.; Hohl, R. J. Farnesol and Geranylgeraniol: Prevention and Reversion of Lovastatin-induced Effects in NIH3T3 Cells. *Lipids* **2002**, *37* (2), 185–192. https://doi.org/10.1007/s11745-002-0879-1.

(5) Schmidt, R. A.; Schneider, C. J.; Glomset, J. A. Evidence for Post-Translational Incorporation of a Product of Mevalonic Acid into Swiss 3T3 Cell Proteins. *J. Biol. Chem.* **1984**, *259* (16), 10175–10180. https://doi.org/10.1016/S0021-9258(18)90945-2.

(6) Palsuledesai, C. C.; Distefano, M. D. Protein Prenylation: Enzymes, Therapeutics, and Biotechnology Applications. *ACS Chem. Biol.* **2015**, *10* (1), 51–62. https://doi.org/10.1021/cb500791f.

(7) Kuchay, S.; Wang, H.; Marzio, A.; Jain, K.; Homer, H.; Fehrenbacher, N.; Philips, M. R.; Zheng, N.; Pagano, M. GGTase3 Is a Newly Identified Geranylgeranyltransferase Targeting a Ubiquitin Ligase. *Nat. Struct. Mol. Biol.* **2019**, *26* (7), 628–636. https://doi.org/10.1038/s41594-019-0249-3.

(8) Zhang, F. L.; Casey, P. J. PROTEIN PRENYLATION: Molecular Mechanisms and Functional Consequences.

(9) Pompliano, D. L.; Schaber, M. D.; Mosser, S. D.; Omer, C. A.; Shafer, J. A.; Gibbs, J. B. Isoprenoid Diphosphate Utilization by Recombinant Human Farnesyl:Protein Transferase: Interactive Binding between Substrates and a Preferred Kinetic Pathway. *Biochemistry* **1993**, *32* (32), 8341–8347. https://doi.org/10.1021/bi00083a038.

(10) Dolence, J. M.; Poulter, C. D. A Mechanism for Posttranslational Modifications of Proteins by Yeast Protein Farnesyltransferase. *Proc. Natl. Acad. Sci.* **1995**, *92* (11), 5008–5011. https://doi.org/10.1073/pnas.92.11.5008.

(11) Fiordalisi, J. J.; Johnson, R. L.; Weinbaum, C. A.; Sakabe, K.; Chen, Z.; Casey, P. J.; Cox, A. D. High Affinity for Farnesyltransferase and Alternative Prenylation Contribute Individually to K-Ras4B Resistance to Farnesyltransferase Inhibitors. *J. Biol. Chem.* **2003**, *278* (43), 41718–41727. https://doi.org/10.1074/jbc.M305733200.

(12) Marshall, C. J. Protein Prenylation: A Mediator of Protein-Protein Interactions. *Science* **1993**, *259* (5103), 1865–1866. https://doi.org/10.1126/science.8456312.

(13) Hottman, D. A.; Li, L. Protein Prenylation and Synaptic Plasticity: Implications for Alzheimer's Disease. *Mol. Neurobiol.* **2014**, *50* (1), 177–185. https://doi.org/10.1007/s12035-013-8627-z.

(14) Jeong, A.; Cheng, S.; Zhong, R.; Bennett, D. A.; Bergö, M. O.; Li, L. Protein Farnesylation Is Upregulated in Alzheimer's Human Brains and Neuron-Specific Suppression of Farnesyltransferase Mitigates Pathogenic Processes in Alzheimer's Model Mice. *Acta Neuropathol. Commun.* **2021**, *9* (1), 129. https://doi.org/10.1186/s40478-021-01231-5.

(15) 2021 Alzheimer's Disease Facts and Figures. *Alzheimers Dement.* **2021**, *17* (3), 327–406. https://doi.org/10.1002/alz.12328.

(16) Chernick, D.; Ortiz-Valle, S.; Jeong, A.; Qu, W.; Li, L. Peripheral versus Central Nervous System APOE in Alzheimer's Disease: Interplay across the Blood-Brain Barrier. *Neurosci. Lett.* **2019**, *708*, 134306. https://doi.org/10.1016/j.neulet.2019.134306.

(17) Liu, C.-C.; Kanekiyo, T.; Xu, H.; Bu, G. Apolipoprotein E and Alzheimer Disease: Risk, Mechanisms and Therapy. *Nat. Rev. Neurol.* **2013**, *9* (2), 106–118. https://doi.org/10.1038/nrneurol.2012.263.

(18) Corder, E. H.; Saunders, A. M.; Strittmatter, W. J.; Schmechel, D. E.; Gaskell, P. C.; Small, G. W.; Roses, A. D.; Haines, J. L.; Pericak-Vance, M. A. Gene Dose of Apolipoprotein E Type 4 Allele and the Risk of Alzheimer's Disease in Late Onset Families. *Science* **1993**, *261* (5123), 921–923. https://doi.org/10.1126/science.8346443.

(19) Farrer, L. A. Effects of Age, Sex, and Ethnicity on the Association Between Apolipoprotein E Genotype and Alzheimer Disease: A Meta-Analysis. *JAMA* **1997**, *278* (16), 1349. https://doi.org/10.1001/jama.1997.03550160069041.

(20) Giannisis, A.; Patra, K.; Edlund, A. K.; Nieto, L. A.; Benedicto-Gras, J.; Moussaud, S.; De La Rosa, A.; Twohig, D.; Bengtsson, T.; Fu, Y.; Bu, G.; Bial, G.; Foquet, L.; Hammarstedt, C.; Strom, S.; Kannisto, K.; Raber, J.; Ellis, E.; Nielsen, H. M. Brain Integrity Is Altered by Hepatic APOE E4 in Humanized-Liver Mice. *Mol. Psychiatry* **2022**, *27* (8), 3533–3543. https://doi.org/10.1038/s41380-022-01548-0.

(21) Golden, L. R.; Johnson, L. A. Liver-Ing in Your Head Rent Free: Peripheral ApoE4 Drives CNS Pathology. *Mol. Neurodegener.* **2022**, *17* (1), 65. https://doi.org/10.1186/s13024-022-00569-1.

(22) Lee, J. S.; Roberts, A.; Juarez, D.; Vo, T.-T. T.; Bhatt, S.; Herzog, L.; Mallya, S.; Bellin, R. J.; Agarwal, S. K.; Salem, A. H.; Xu, T.; Jia, J.; Li, L.; Hanna, J. R.; Davids, M. S.; Fleischman, A. G.; O'Brien, S.; Lam, L. T.; Leverson, J. D.; Letai, A.; Schatz, J. H.; Fruman, D. A. Statins Enhance Efficacy of Venetoclax in Blood Cancers. *Sci. Transl. Med.* **2018**, *10* (445), eaaq1240. https://doi.org/10.1126/scitranslmed.aaq1240.

(23) Fiskus, W.; Daver, N.; Boettcher, S.; Mill, C. P.; Sasaki, K.; Birdwell, C. E.; Davis, J. A.; Das, K.; Takahashi, K.; Kadia, T. M.; DiNardo, C. D.; Burrows, F.; Loghavi, S.; Khoury, J. D.; Ebert, B. L.; Bhalla, K. N. Activity of Menin Inhibitor Ziftomenib (KO-539) as Monotherapy or in Combinations against AML Cells with MLL1 Rearrangement or Mutant NPM1. *Leukemia* **2022**, *36* (11), 2729–2733. https://doi.org/10.1038/s41375-022-01707-w.

(24) Rausch, J.; Dzama, M. M.; Dolgikh, N.; Stiller, H. L.; Bohl, S. R.; Lahrmann, C.; Kunz, K.; Kessler, L.; Echchannaoui, H.; Chen, C.-W.; Kindler, T.; Döhner, K.; Burrows, F.; Theobald, M.; Sasca, D.; Kühn, M. W. M. Menin Inhibitor Ziftomenib (KO-539) Synergizes with Drugs Targeting Chromatin Regulation or Apoptosis and Sensitizes Acute Myeloid Leukemia with *MLL* Rearrangement or *NPM1* Mutation to Venetoclax. *Haematologica* **2023**, *108* (10), 2837–2843. https://doi.org/10.3324/haematol.2022.282160.

(25) Haag, M. D. M.; Hofman, A.; Koudstaal, P. J.; Stricker, B. H. C.; Breteler, M. M. B. Statins Are Associated with a Reduced Risk of Alzheimer Disease Regardless of Lipophilicity. The Rotterdam Study. *J. Neurol. Neurosurg. Psychiatry* **2009**, *80* (1), 13–17. https://doi.org/10.1136/jnnp.2008.150433.

(26) Harmon, N. M.; Huang, X.; Hsiao, C.-H. C.; Wiemer, A. J.; Wiemer, D. F. Incorporation of a FRET Pair within a Phosphonate Diester. *Bioorganic Chem.* **2021**, *114*, 105048. https://doi.org/10.1016/j.bioorg.2021.105048.

(27) Davey, M. S.; Malde, R.; Mykura, R. C.; Baker, A. T.; Taher, T. E.; Le Duff, C. S.; Willcox, B. E.; Mehellou, Y. Synthesis and Biological Evaluation of (*E*)-4-Hydroxy-3-Methylbut-2-Enyl Phosphate (HMBP) Aryloxy Triester Phosphoramidate Prodrugs as Activators of Vγ9/Vδ2 T-Cell Immune Responses. *J. Med. Chem.* **2018**, *61* (5), 2111–2117. https://doi.org/10.1021/acs.jmedchem.7b01824.

(28) Wiemer, A. J.; Wiemer, D. F. Prodrugs of Phosphonates and Phosphates: Crossing the Membrane Barrier. In *Phosphorus Chemistry I*; Montchamp, J.-L., Ed.; Topics in Current Chemistry; Springer International Publishing: Cham, 2014; Vol. 360, pp 115–160. https://doi.org/10.1007/128_2014_561.

(29) Freel Meyers, C. L.; Borch, R. F. Activation Mechanisms of Nucleoside Phosphoramidate Prodrugs. *J. Med. Chem.* **2000**, *43* (22), 4319–4327. https://doi.org/10.1021/jm000302b.

(30) Ochocki, J. D.; Distefano, M. D. Prenyltransferase Inhibitors: Treating Human Ailments from Cancer to Parasitic Infections. *Med Chem Commun* **2013**, *4* (3), 476–492. https://doi.org/10.1039/C2MD20299A.

(31) Suazo, K. F.; Park, K.-Y.; Distefano, M. D. A Not-So-Ancient Grease History: Click Chemistry and Protein Lipid Modifications. *Chem. Rev.* **2021**, *121* (12), 7178–7248. https://doi.org/10.1021/acs.chemrev.0c01108.

(32) Jeong, A.; Auger, S. A.; Maity, S.; Fredriksen, K.; Zhong, R.; Li, L.; Distefano, M. D. *In Vivo* Prenylomic Profiling in the Brain of a Transgenic Mouse Model of Alzheimer's Disease Reveals Increased Prenylation of a Key Set of Proteins. *ACS Chem. Biol.* **2022**, *17* (10), 2863–2876. https://doi.org/10.1021/acschembio.2c00486.

(33) Hosokawa, A.; Wollack, J. W.; Zhang, Z.; Chen, L.; Barany, G.; Distefano, M. D. Evaluation of an Alkyne-Containing Analogue of Farnesyl Diphosphate as a Dual Substrate for Protein-Prenyltransferases. *Int. J. Pept. Res. Ther.* **2007**, *13* (1–2), 345–354. https://doi.org/10.1007/s10989-007-9090-3.

(34) Storck, E. M.; Morales-Sanfrutos, J.; Serwa, R. A.; Panyain, N.; Lanyon-Hogg, T.; Tolmachova, T.; Ventimiglia, L. N.; Martin-Serrano, J.; Seabra, M. C.; Wojciak-Stothard, B.; Tate, E. W. Dual Chemical Probes Enable Quantitative System-Wide Analysis of Protein Prenylation and Prenylation Dynamics. *Nat. Chem.* **2019**, *11* (6), 552–561. https://doi.org/10.1038/s41557-019-0237-6.

(35) DeGraw, A. J.; Hast, M. A.; Xu, J.; Mullen, D.; Beese, L. S.; Barany, G.; Distefano, M. D. Caged Protein Prenyltransferase Substrates: Tools for Understanding Protein Prenylation. *Chem. Biol. Drug Des.* **2008**, *72* (3), 171–181. https://doi.org/10.1111/j.1747-0285.2008.00698.x.

(36) Hartman, H. L.; Bowers, K. E.; Fierke, C. A. Lysine B311 of Protein Geranylgeranyltransferase Type I Partially Replaces Magnesium. *J. Biol. Chem.* **2004**, *279* (29), 30546–30553. https://doi.org/10.1074/jbc.M403469200.

(37) Long, S. B.; Casey, P. J.; Beese, L. S. Cocrystal Structure of Protein Farnesyltransferase Complexed with a Farnesyl Diphosphate Substrate†,.

(38) Terry, K. L.; Casey, P. J.; Beese, L. S. Conversion of Protein Farnesyltransferase to a Geranylgeranyltransferase. *Biochemistry* **2006**, *45* (32), 9746–9755. https://doi.org/10.1021/bi060295e.

(39) Greenwood, J.; Steinman, L.; Zamvil, S. S. Statin Therapy and Autoimmune Disease: From Protein Prenylation to Immunomodulation. *Nat. Rev. Immunol.* **2006**, *6* (5), 358–370. https://doi.org/10.1038/nri1839.

(40) Suazo, K. F.; Jeong, A.; Ahmadi, M.; Brown, C.; Qu, W.; Li, L.; Distefano, M. D. Metabolic Labeling with an Alkyne Probe Reveals Similarities and Differences in the Prenylomes of Several Brain-Derived Cell Lines and Primary Cells. *Sci. Rep.* **2021**, *11* (1), 4367. https://doi.org/10.1038/s41598-021-83666-3.

(41) Kallemeijn, W. W.; Lanyon-Hogg, T.; Panyain, N.; Goya Grocin, A.; Ciepla, P.; Morales-Sanfrutos, J.; Tate, E. W. Proteome-Wide Analysis of Protein Lipidation Using Chemical Probes: In-Gel Fluorescence Visualization, Identification and Quantification of N-Myristoylation, N- and S-Acylation, O-Cholesterylation, S-

Farnesylation and S-Geranylgeranylation. *Nat. Protoc.* **2021**, *16* (11), 5083–5122. https://doi.org/10.1038/s41596-021-00601-6.

(42) Vasudevan, A.; Qian, Y.; Vogt, A.; Blaskovich, M. A.; Ohkanda, J.; Sebti, S. M.; Hamilton, A. D. Potent, Highly Selective, and Non-Thiol Inhibitors of Protein Geranylgeranyltransferase-I. *J. Med. Chem.* **1999**, *42* (8), 1333–1340. https://doi.org/10.1021/jm9900873.

(43) Tate, E. W.; Kalesh, K. A.; Lanyon-Hogg, T.; Storck, E. M.; Thinon, E. Global Profiling of Protein Lipidation Using Chemical Proteomic Technologies. *Curr. Opin. Chem. Biol.* **2015**, *24*, 48–57. https://doi.org/10.1016/j.cbpa.2014.10.016.

(44) Puglielli, L.; Tanzi, R. E.; Kovacs, D. M. Alzheimer's Disease: The Cholesterol Connection. *Nat. Neurosci.* **2003**, *6* (4), 345–351. https://doi.org/10.1038/nn0403-345.

(45) Miyashita, A.; Kikuchi, M.; Hara, N.; Ikeuchi, T. Genetics of Alzheimer's Disease: An East Asian Perspective. *J. Hum. Genet.* **2023**, *68* (3), 115–124. https://doi.org/10.1038/s10038-022-01050-z.

(46) Haney, M. S.; Pálovics, R.; Munson, C. N.; Long, C.; Johansson, P. K.; Yip, O.; Dong, W.; Rawat, E.; West, E.; Schlachetzki, J. C. M.; Tsai, A.; Guldner, I. H.; Lamichhane, B. S.; Smith, A.; Schaum, N.; Calcuttawala, K.; Shin, A.; Wang, Y.-H.; Wang, C.; Koutsodendris, N.; Serrano, G. E.; Beach, T. G.; Reiman, E. M.; Glass, C. K.; Abu-Remaileh, M.; Enejder, A.; Huang, Y.; Wyss-Coray, T. APOE4/4 Is Linked to Damaging Lipid Droplets in Alzheimer's Disease Microglia. *Nature* **2024**. https://doi.org/10.1038/s41586-024-07185-7.

(47) Jordan, K. L.; Koss, D. J.; Outeiro, T. F.; Giorgini, F. Therapeutic Targeting of Rab GTPases: Relevance for Alzheimer's Disease. *Biomedicines* **2022**, *10* (5), 1141. https://doi.org/10.3390/biomedicines10051141.

(48) Dugan, J. M.; deWit, C.; McConlogue, L.; Maltese, W. A. The Ras-Related GTP-Binding Protein, Rab1B, Regulates Early Steps in Exocytic Transport and Processing of β-Amyloid Precursor Protein. *J. Biol. Chem.* **1995**, *270* (18), 10982–10989. https://doi.org/10.1074/jbc.270.18.10982.

(49) Ginsberg, S. D.; Mufson, E. J.; Alldred, M. J.; Counts, S. E.; Wuu, J.; Nixon, R. A.; Che, S. Upregulation of Select Rab GTPases in Cholinergic Basal Forebrain Neurons in Mild Cognitive Impairment and Alzheimer's Disease. *J. Chem. Neuroanat.* **2011**, *42* (2), 102–110. https://doi.org/10.1016/j.jchemneu.2011.05.012.

(50) Cataldo, A. M.; Barnett, J. L.; Pieroni, C.; Nixon, R. A. Increased Neuronal Endocytosis and Protease Delivery to Early Endosomes in Sporadic Alzheimer's Disease: Neuropathologic Evidence for a Mechanism of Increased ᴺʟ-Amyloidogenesis.

(51) Scheper, W.; Hoozemans, J. J. M.; Hoogenraad, C. C.; Rozemuller, A. J. M.; Eikelenboom, P.; Baas, F. Rab6 Is Increased in Alzheimer's Disease Brain and Correlates with Endoplasmic Reticulum Stress. *Neuropathol. Appl. Neurobiol.* **2007**, *33* (5), 523–532. https://doi.org/10.1111/j.1365-2990.2007.00846.x.

(52) Scheper, W.; Zwart, R.; Baas, F. Rab6 Membrane Association Is Dependent of Presenilin 1 and Cellular Phosphorylation Events. *Mol. Brain Res.* **2004**, *122* (1), 17–23. https://doi.org/10.1016/j.molbrainres.2003.11.013.

(53) Cai, R.; Wang, Y.; Huang, Z.; Zou, Q.; Pu, Y.; Yu, C.; Cai, Z. Role of RhoA/ROCK Signaling in Alzheimer's Disease. *Behav. Brain Res.* **2021**, *414*, 113481. https://doi.org/10.1016/j.bbr.2021.113481.

(54) Emmanouilidis, L.; Schütz, U.; Tripsianes, K.; Madl, T.; Radke, J.; Rucktäschel, R.; Wilmanns, M.; Schliebs, W.; Erdmann, R.; Sattler, M. Allosteric Modulation of Peroxisomal Membrane Protein Recognition by Farnesylation of the Peroxisomal Import Receptor PEX19. *Nat. Commun.* **2017**, *8* (1), 14635. https://doi.org/10.1038/ncomms14635.

(55) Uzor, N.-E.; McCullough, L. D.; Tsvetkov, A. S. Peroxisomal Dysfunction in Neurological Diseases and Brain Aging. *Front. Cell. Neurosci.* **2020**, *14*, 44. https://doi.org/10.3389/fncel.2020.00044.

(56) Jeong, A.; Auger, S. A.; Maity, S.; Fredriksen, K.; Zhong, R.; Li, L.; Distefano, M. D. *In Vivo* Prenylomic Profiling in the Brain of a Transgenic Mouse Model of Alzheimer's Disease Reveals Increased Prenylation of a Key Set of Proteins. *ACS Chem. Biol.* **2022**, *17* (10), 2863–2876. https://doi.org/10.1021/acschembio.2c00486.

7. Appendix

C15PentOPP NMR + HRMS spectra

^{1}H NMR (500 MHz, CD_3Cl) for compound

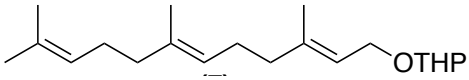

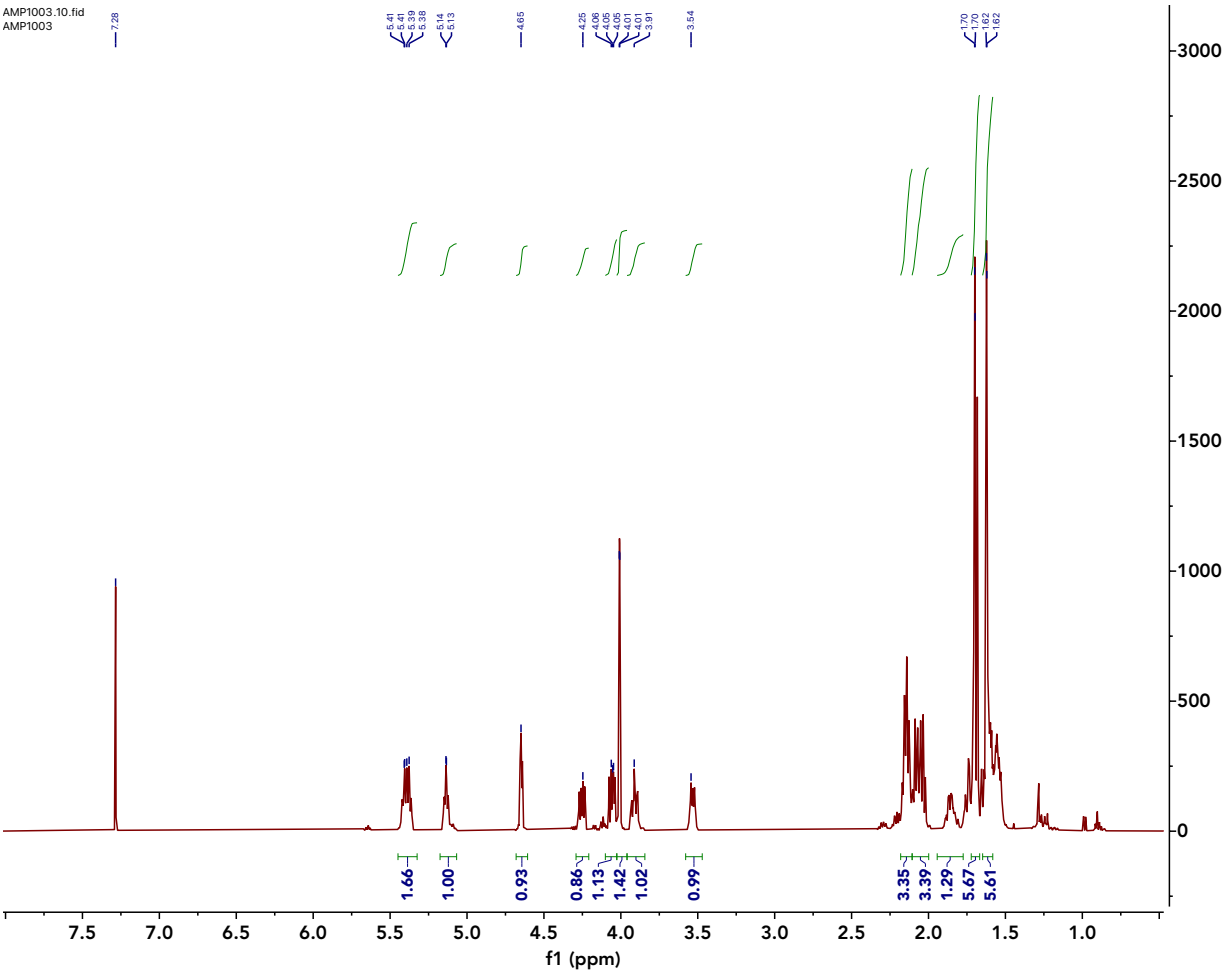

^{1}H NMR (500 MHz, CD_3Cl) for compound

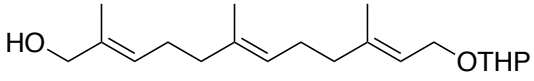

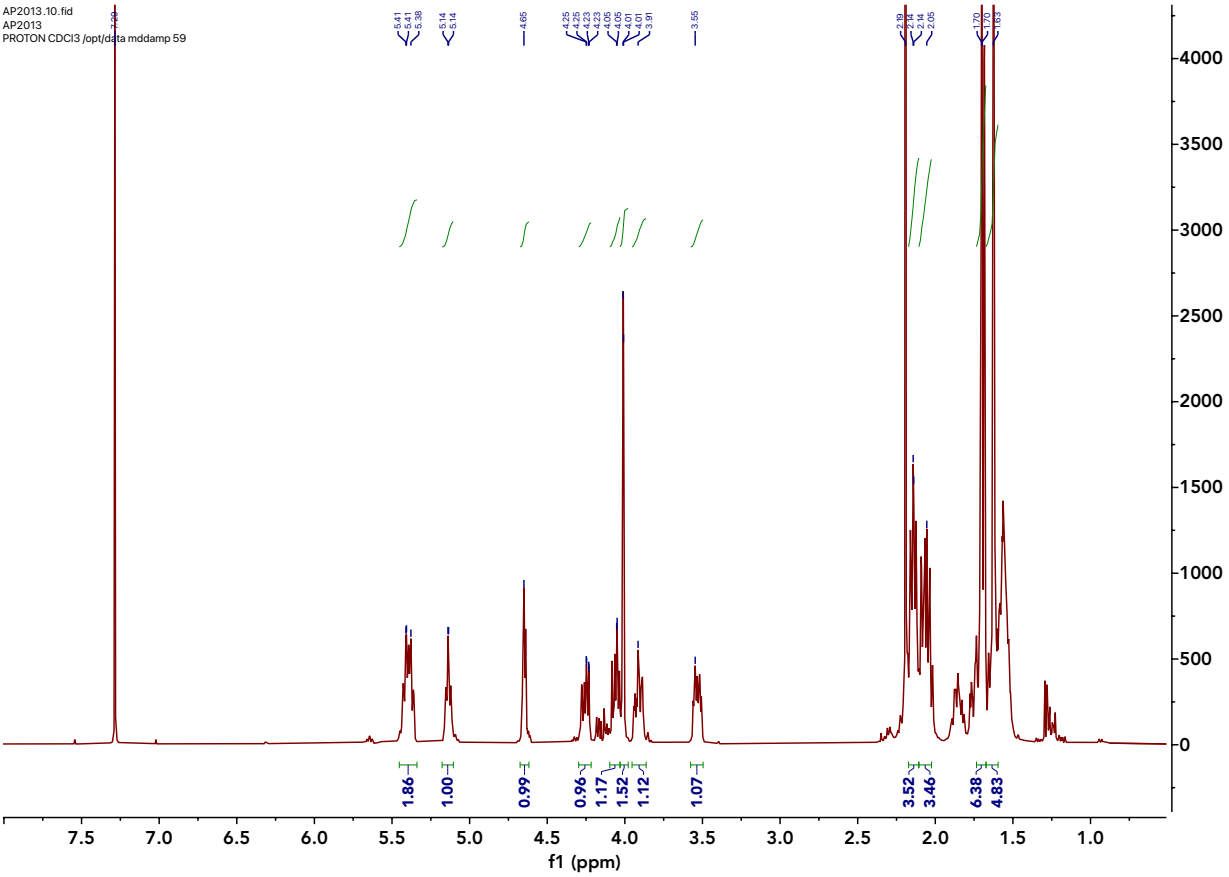

^{1}H NMR (500 MHz, CD_3Cl) for compound

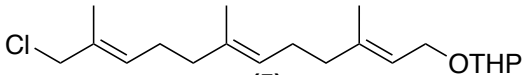

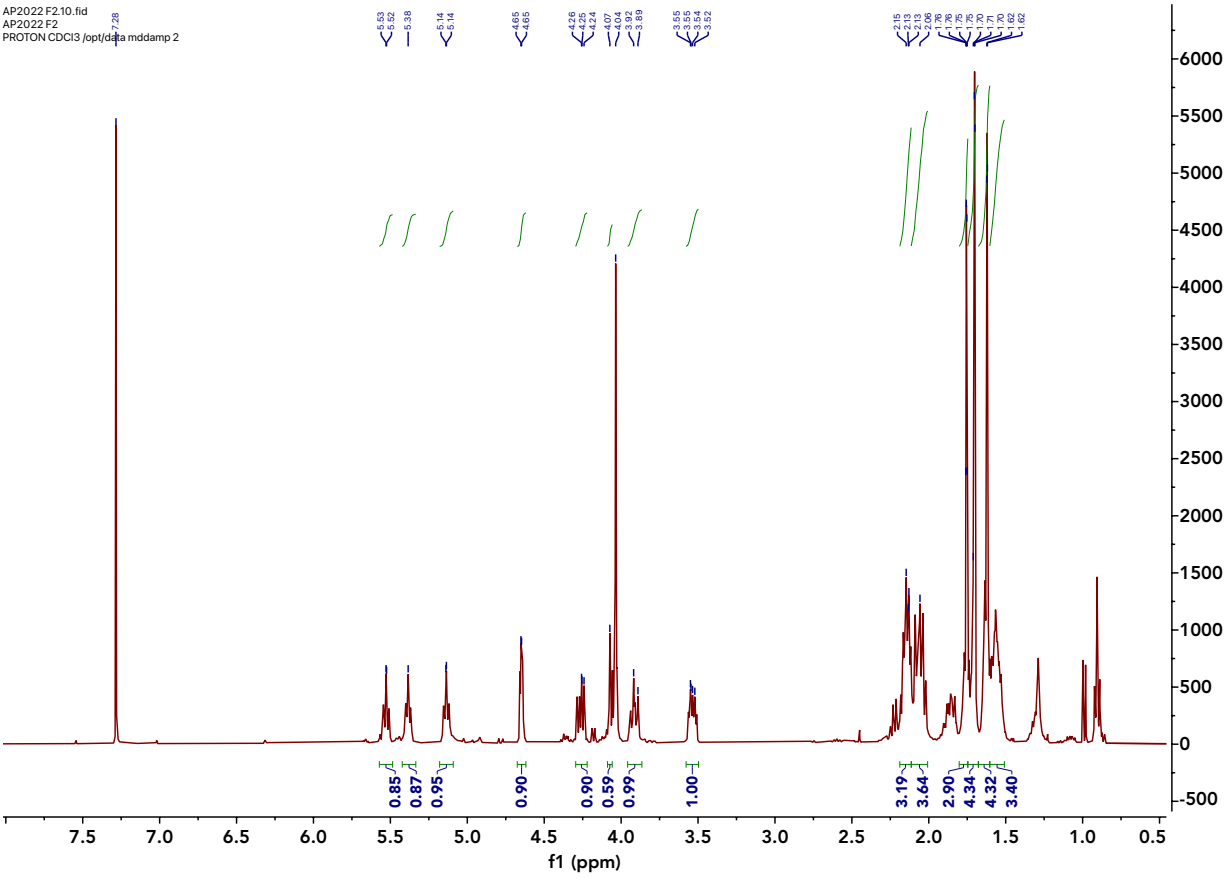

^{13}C NMR (500 MHz, CD_3Cl) for compound

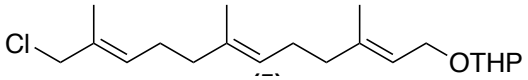

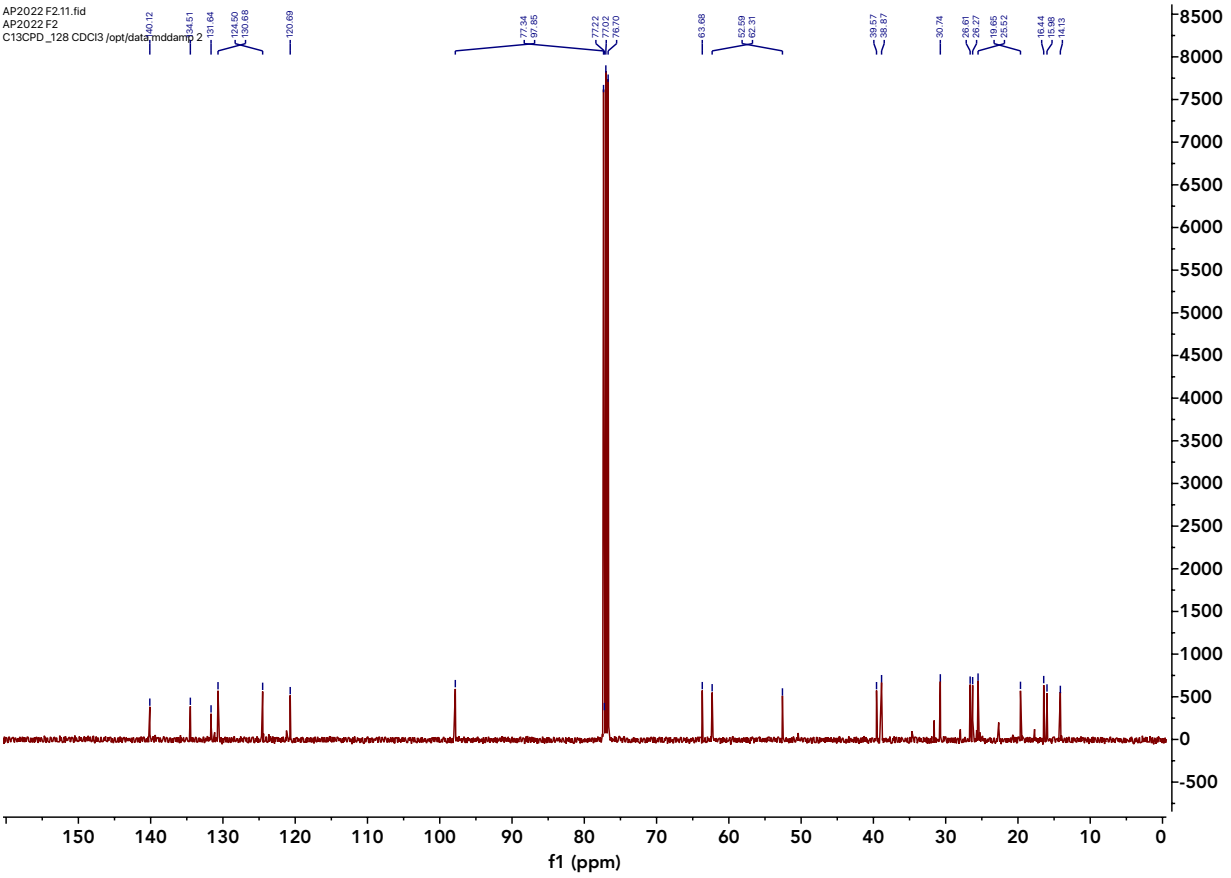

HRMS for compound

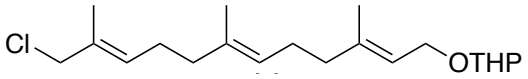

Mass Spectrum List Report

Analysis Info

Analysis Name	2	Acquisition Date	12/11/2023 12:48:20 PM
Method	positive_03102022.tofpar	Operator	operator name
Sample Name		Instrument	BioTOF II
	C15Clw/ PPG calFree format comments		

Acquisition Parameter

n/a	n/a	n/a	n/a	detbias	1750 V
EndP	-4000 V	n/a	n/a	n/a	n/a

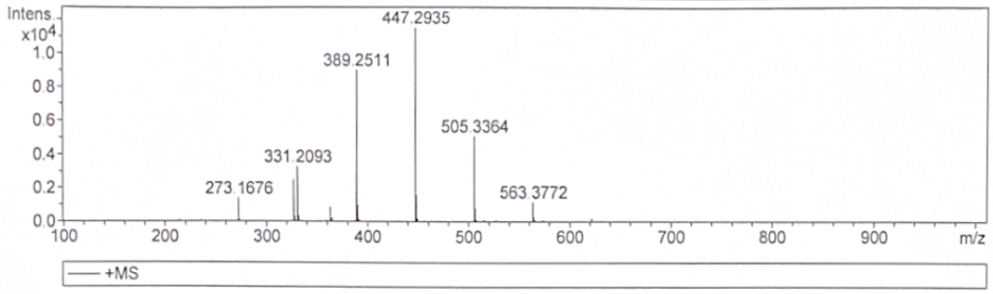

#	m/z	I
1	215.1262	100
2	273.1676	1354
3	327.2302	2458
4	328.2325	291
5	331.2093	3227
6	332.2125	291
7	363.2077	838
8	364.2096	128
9	365.2039	213
10	389.2511	8932
11	390.2540	951
12	391.2540	107
13	447.2935	11472
14	448.2975	1527
15	449.3003	174
16	505.3364	5026
17	506.3382	705
18	563.3772	1139
19	564.3792	262
20	621.4183	173

$M+Na^+$

Bruker Daltonics DataAnalysis 3.4 printed: 12/11/2023 2:16:53 PM Page 1 of 1

^{1}H NMR (500 MHz, CD_3Cl) for compound

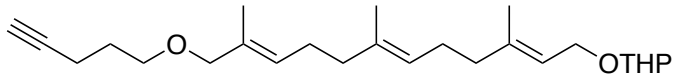

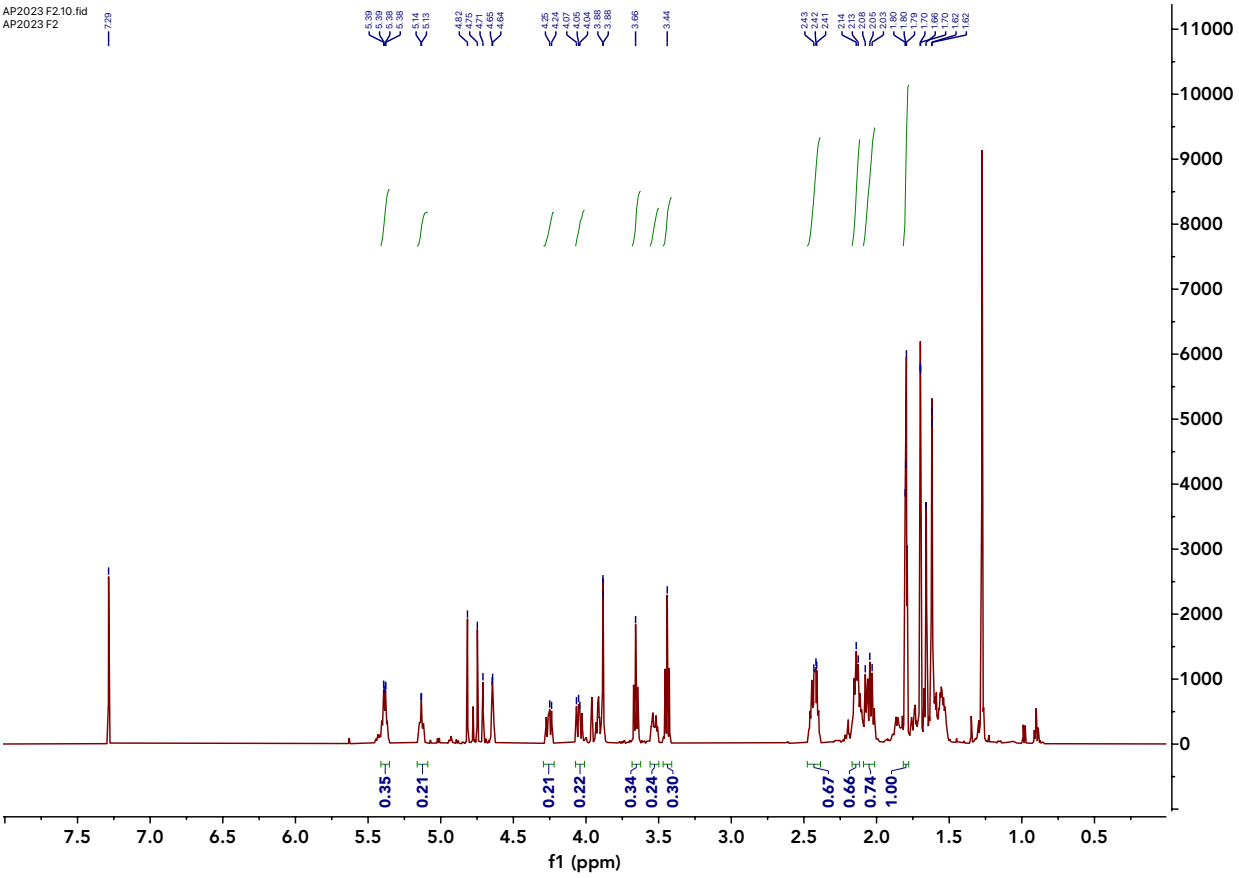

^{13}C NMR (500 MHz, CD_3Cl) for compound

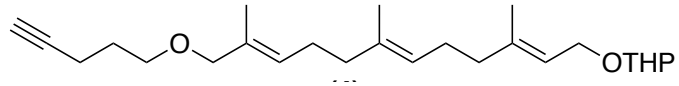

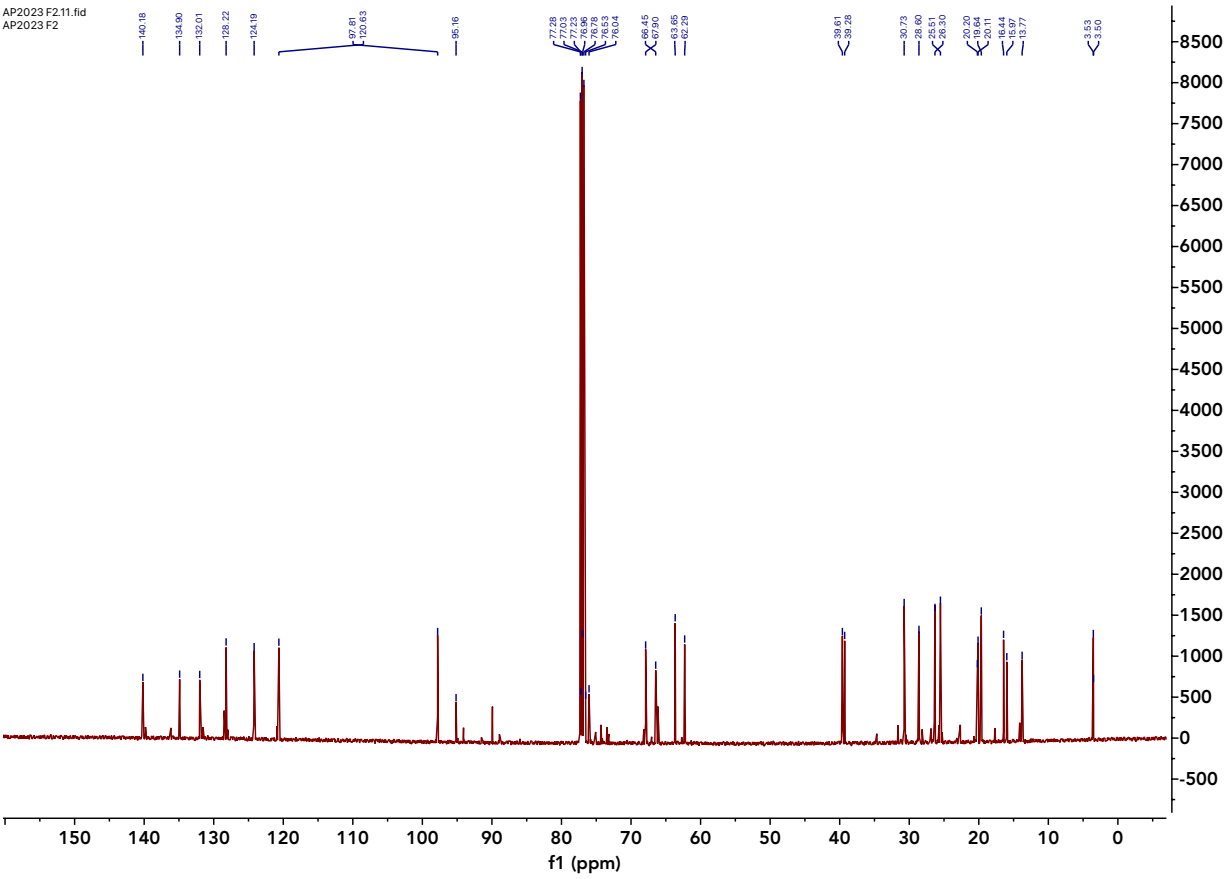

HRMS for compound

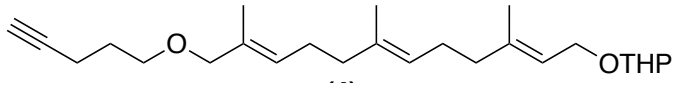

Mass Spectrum List Report

Analysis Info

Analysis Name	4	Acquisition Date	12/11/2023 12:54:09 PM
Method	positive_03102022.tofpar	Operator	operator name
Sample Name		Instrument	BioTOF II
	C15PentTHPw/ PPG calFree format comments		

Acquisition Parameter

n/a	n/a	n/a	n/a	detbias	1750 V
EndP	-4000 V	n/a	n/a	n/a	n/a

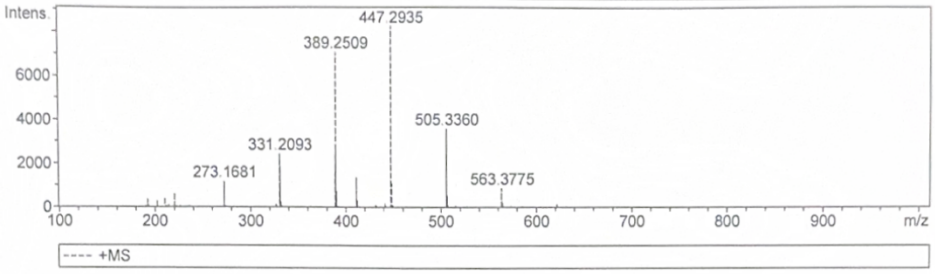

#	m/z	I
1	193.1256	333
2	203.1098	289
3	211.1356	434
4	221.1198	632
5	273.1681	1168
6	327.2341	110
7	331.2093	2408
8	332.2127	216
9	389.2509	7060
10	390.2537	711
11	411.2895	1349
12	412.2955	285
13	431.3179	132
14	441.2991	163
15	447.2935	8241
16	448.2961	1063
17	449.3009	125
18	505.3360	3557
19	506.3385	509
20	563.3775	855
21	564.3809	198
22	621.4184	129

$M+Na^+$

Bruker Daltonics DataAnalysis 3.4 printed: 12/11/2023 2:25:12 PM Page 1 of 1

^{1}H NMR (500 MHz, CD_3Cl) for compound

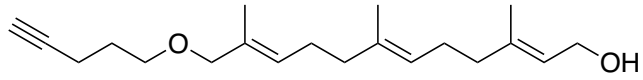

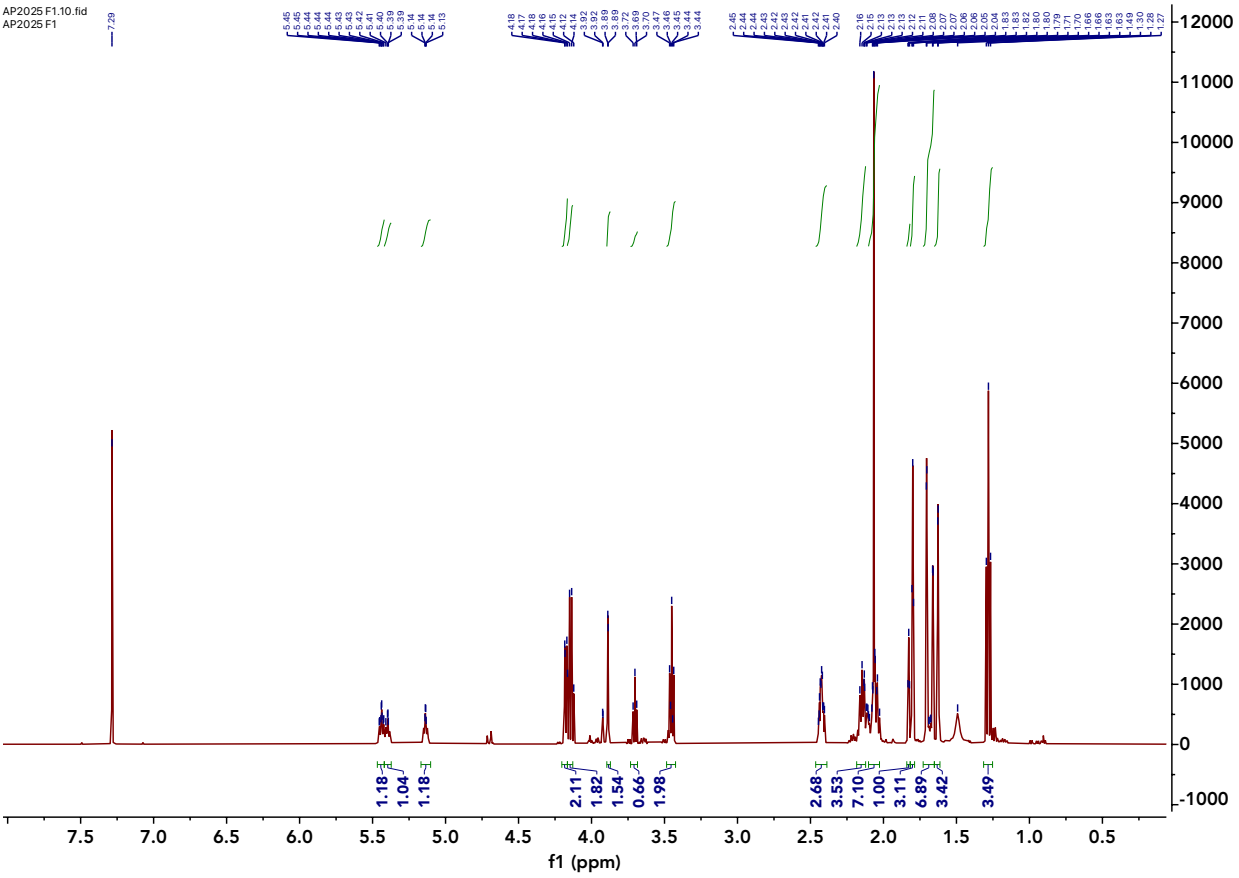

^{13}C NMR (500 MHz, CD_3Cl) for compound

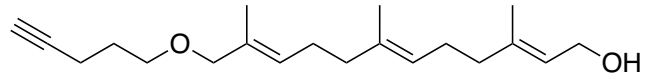

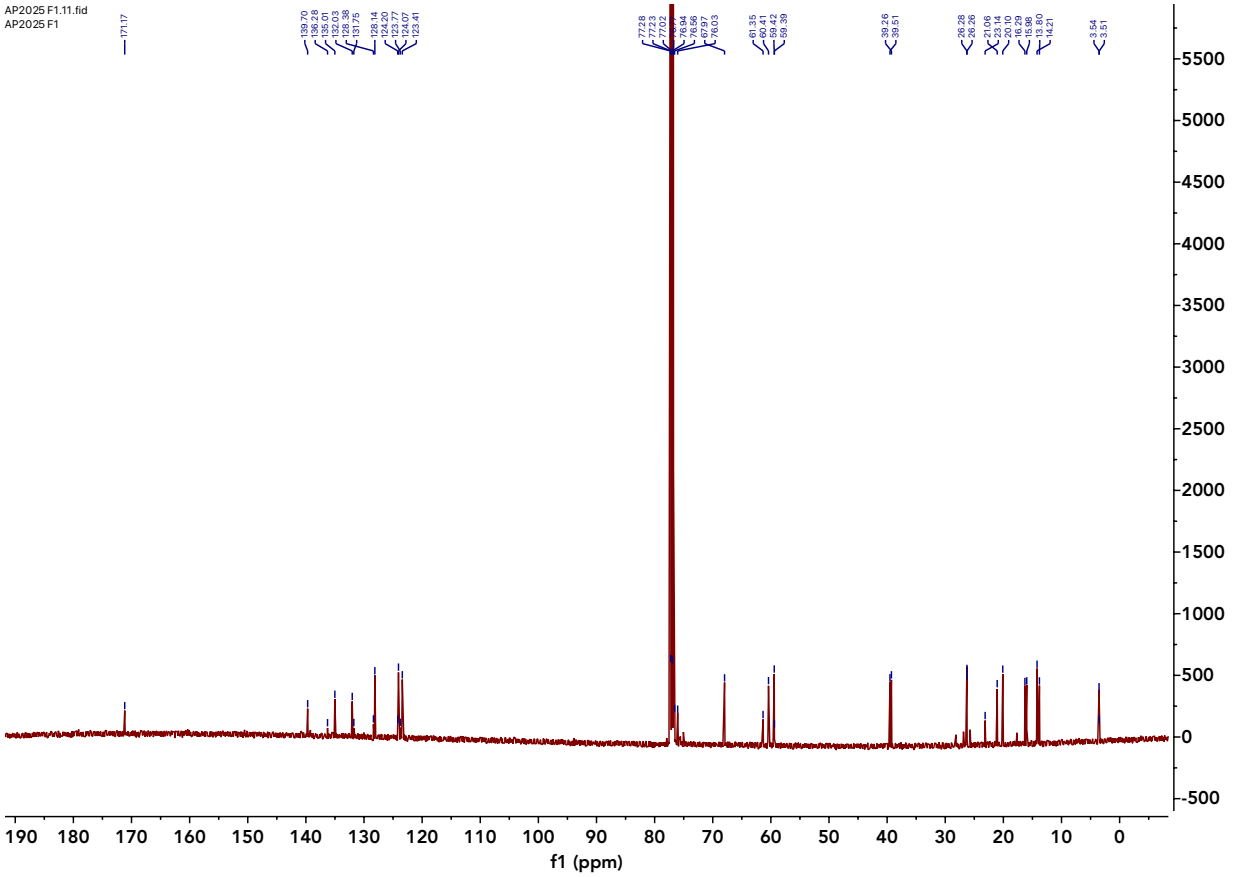

HRMS for compound

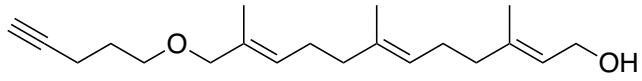

Mass Spectrum List Report

Analysis Info

Analysis Name	1	Acquisition Date	8/4/2023 10:04:36 AM
Method	pos_lowmass_03102022.tofpar	Operator	operator name
Sample Name	C15pentOH	Instrument	BioTOF II
	ppg425Free format commentsFree format comments		

Acquisition Parameter

n/a	n/a	n/a	n/a	detbias	1750 V
EndP	-4000 V	n/a	n/a	n/a	n/a

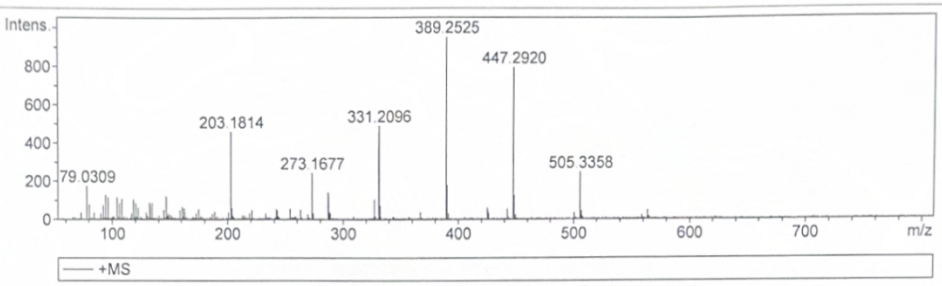

#	m/z	I
1	79.0309	174
2	95.0890	128
3	97.0699	115
4	105.0728	113
5	109.1053	106
6	119.0866	104
7	147.1188	120
8	203.1814	457
9	273.1677	240
10	287.2393	143
11	327.2259	103
12	331.2096	487
13	389.2525	949
14	390.2535	175
15	447.2920	791
16	448.2929	125
17	505.3358	245

$M+Na^+$

Bruker Daltonics DataAnalysis 3.4 printed: 8/4/2023 11:40:14 AM Page 1 of 1

^{1}H NMR (400 MHz, D_2O) for compound 1

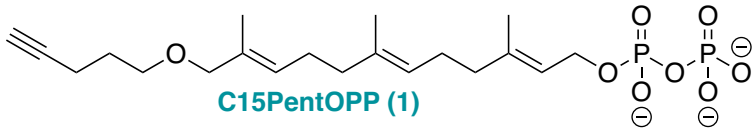

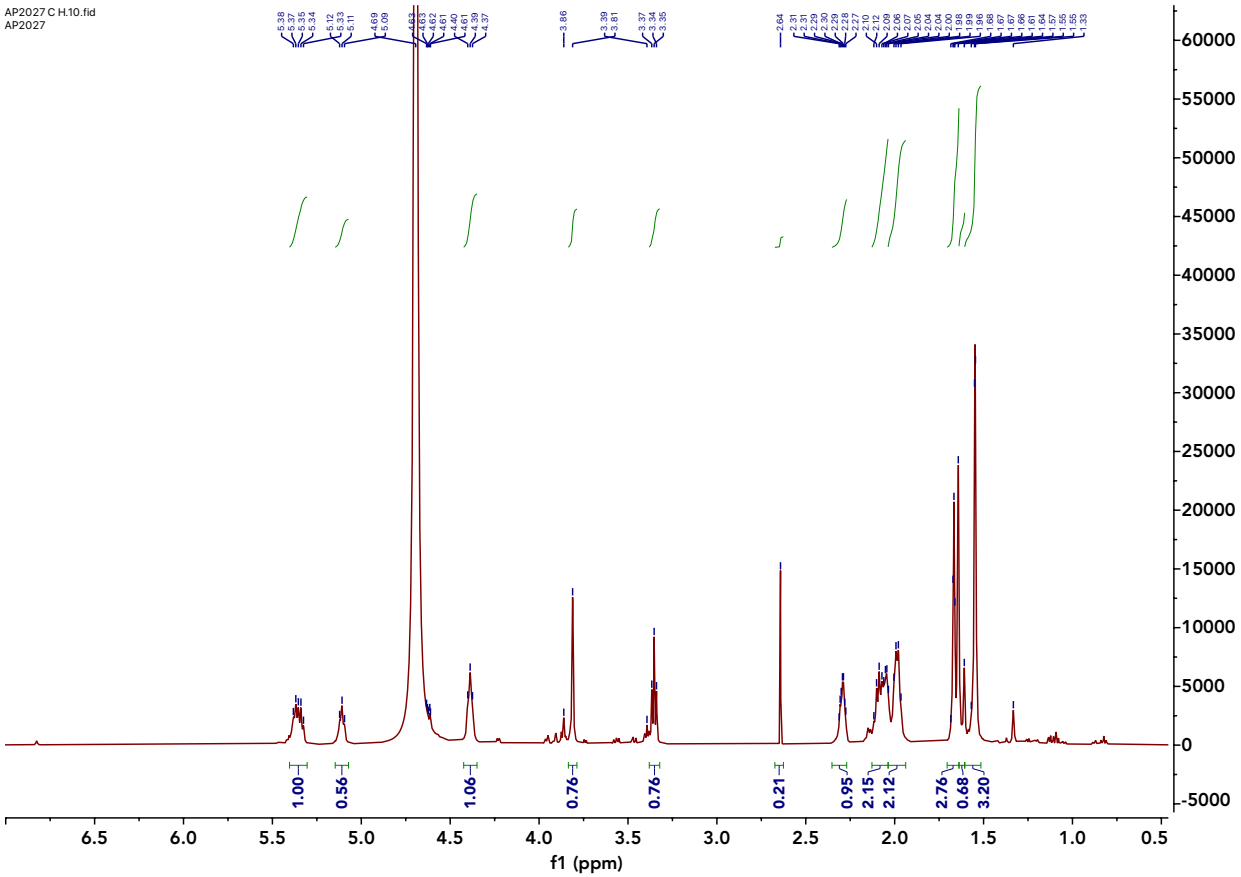

^{13}C NMR (400 MHz, D_2O) for compound 1

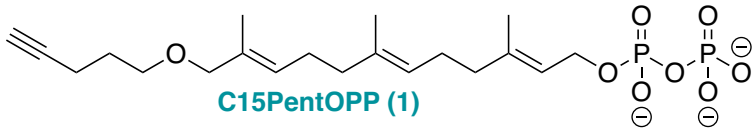

C15PentOPP (1)

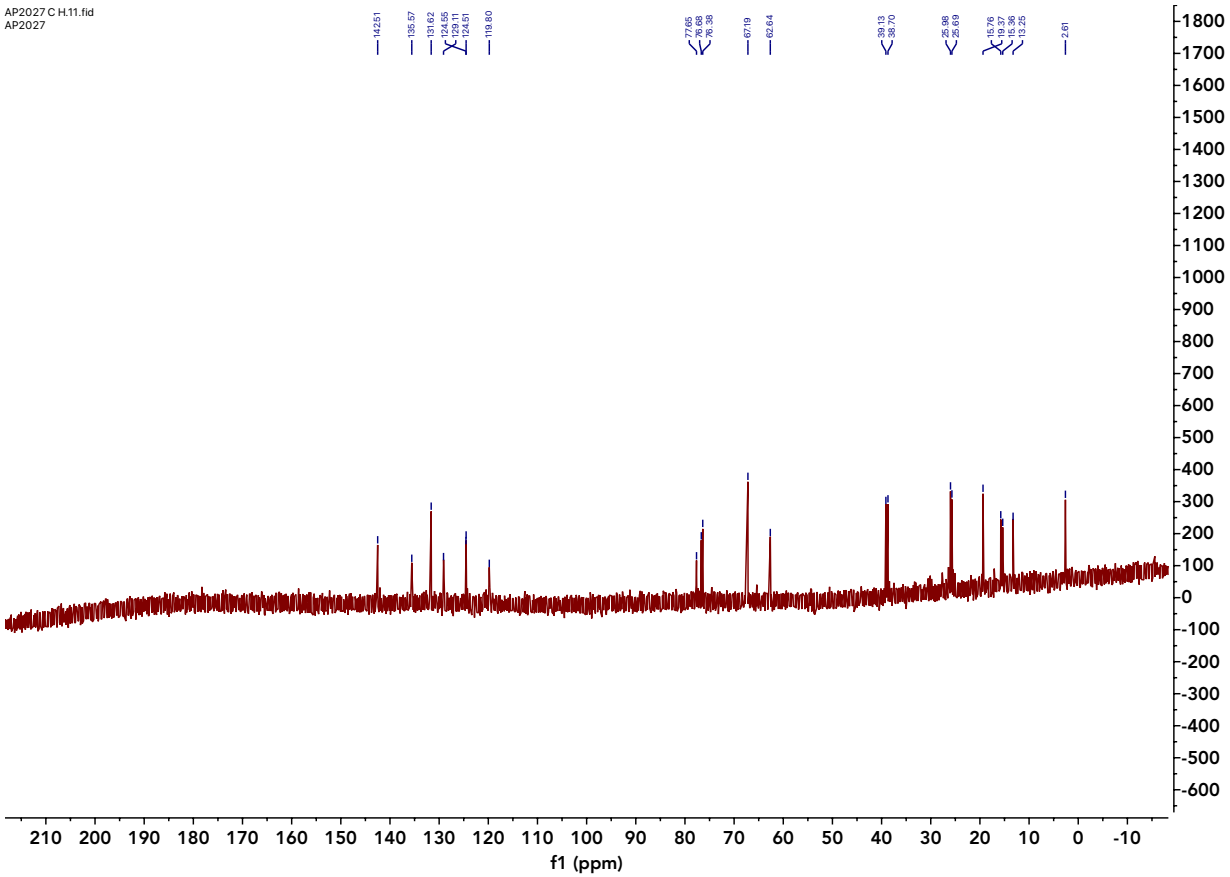

^{31}P NMR (400 MHz, D_2O) for compound 1

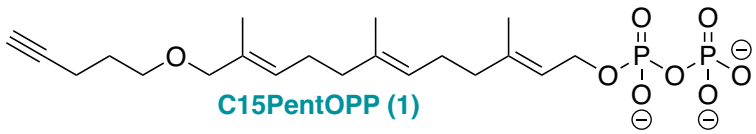

C15PentOPP (1)

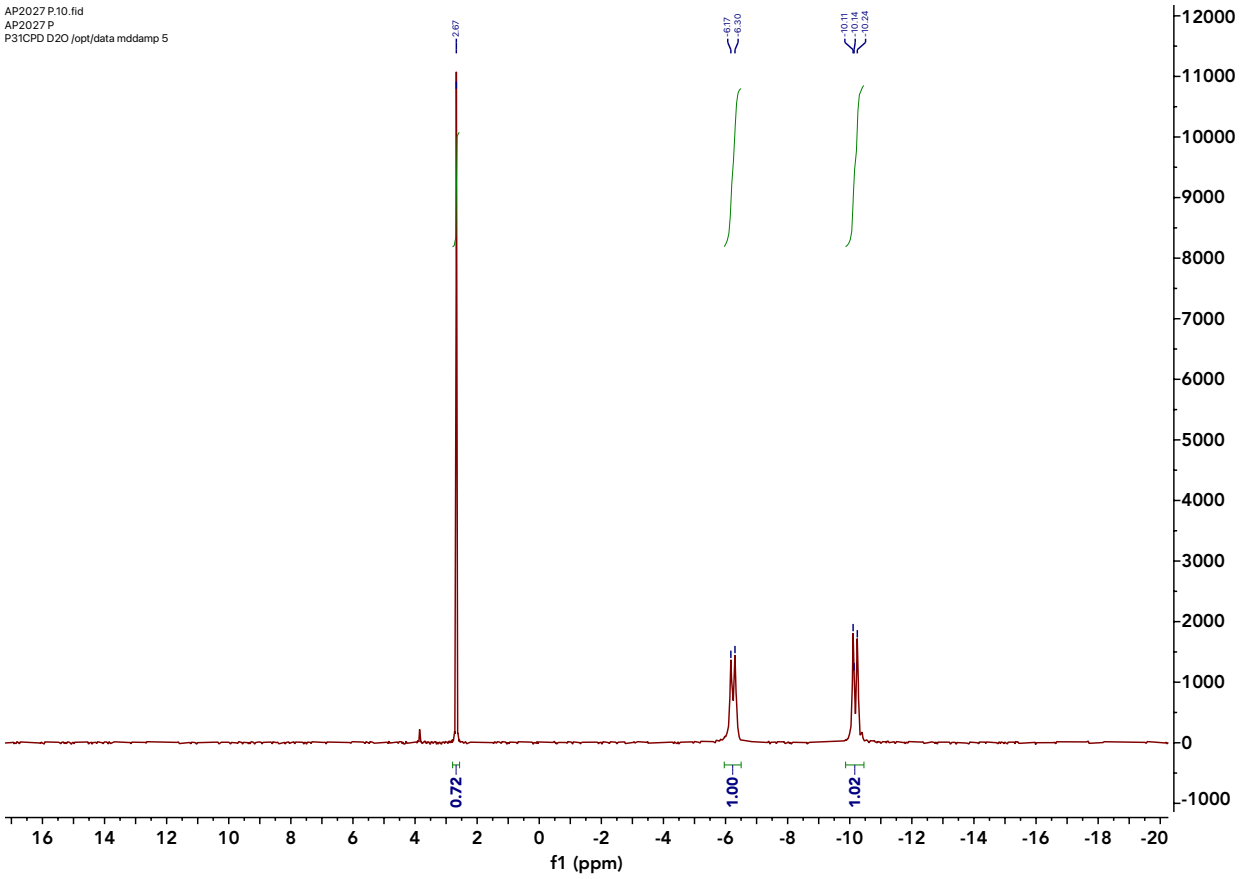

HRMS for compound 1

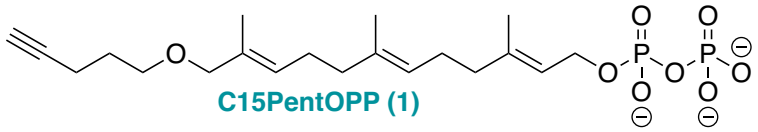

C15PentOPP (1)

Mass Spectrum List Report

Analysis Info

Analysis Name	1	Acquisition Date	8/1/2023 11:45:55 AM
Method	negative_053023.tofpar	Operator	operator name
Sample Name	ap2027hires	Instrument	BioTOF II
	TFAnaFree format commentsFree format comments		

Acquisition Parameter

n/a	n/a	n/a	n/a	detbias	1800 V
EndP	3000 V	n/a	n/a	n/a	n/a

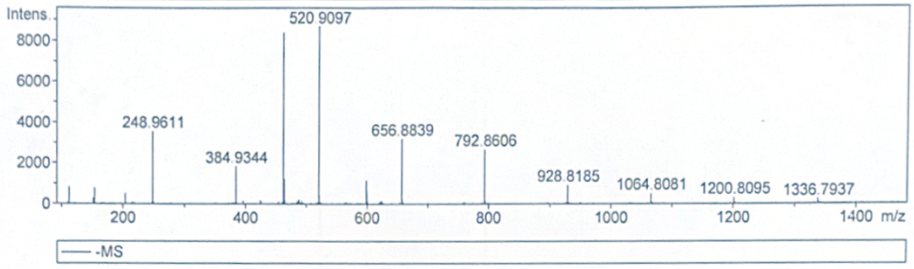

#	m/z	I
1	112.9853	796
2	152.9774	281
3	154.9735	747
4	204.9715	505
5	248.9611	3546
6	249.9650	103
7	384.9344	1806
8	397.1128	134
9	425.1458	165
10	463.1652	8369
11	464.1680	1199
12	465.1661	171
13	486.8385	162
14	488.8356	184
15	520.9097	8681
16	521.9103	389
17	599.1398	1125
18	600.1405	160
19	622.8105	136
20	624.8128	105
21	656.8839	3162
22	657.8827	183
23	792.8606	2649
24	793.8612	155
25	928.8185	907
26	1064.8081	491
27	1200.6535	223
28	1200.8095	286
29	1336.6269	170
30	1336.7937	191

Bruker Daltonics DataAnalysis 3.4 printed: 8/1/2023 1:05:42 PM Page 1 of 1

MS for compound 1

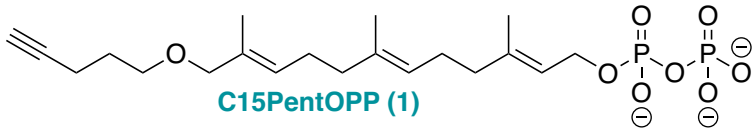

C15PentOPP (1)

Generic Display Report

Analysis Info

Analysis Name	\\DESKTOP-4FC8J8H\esi_data\alepet\130414\tt27\1	Acquisition Date	7/30/2023 2:18:21 PM
Method	negative_053023.tofpar	Operator	operator name
Sample Name	tt27	Instrument	BioTOF II
Comment	Free format commentsFree format commentsFree format comments		

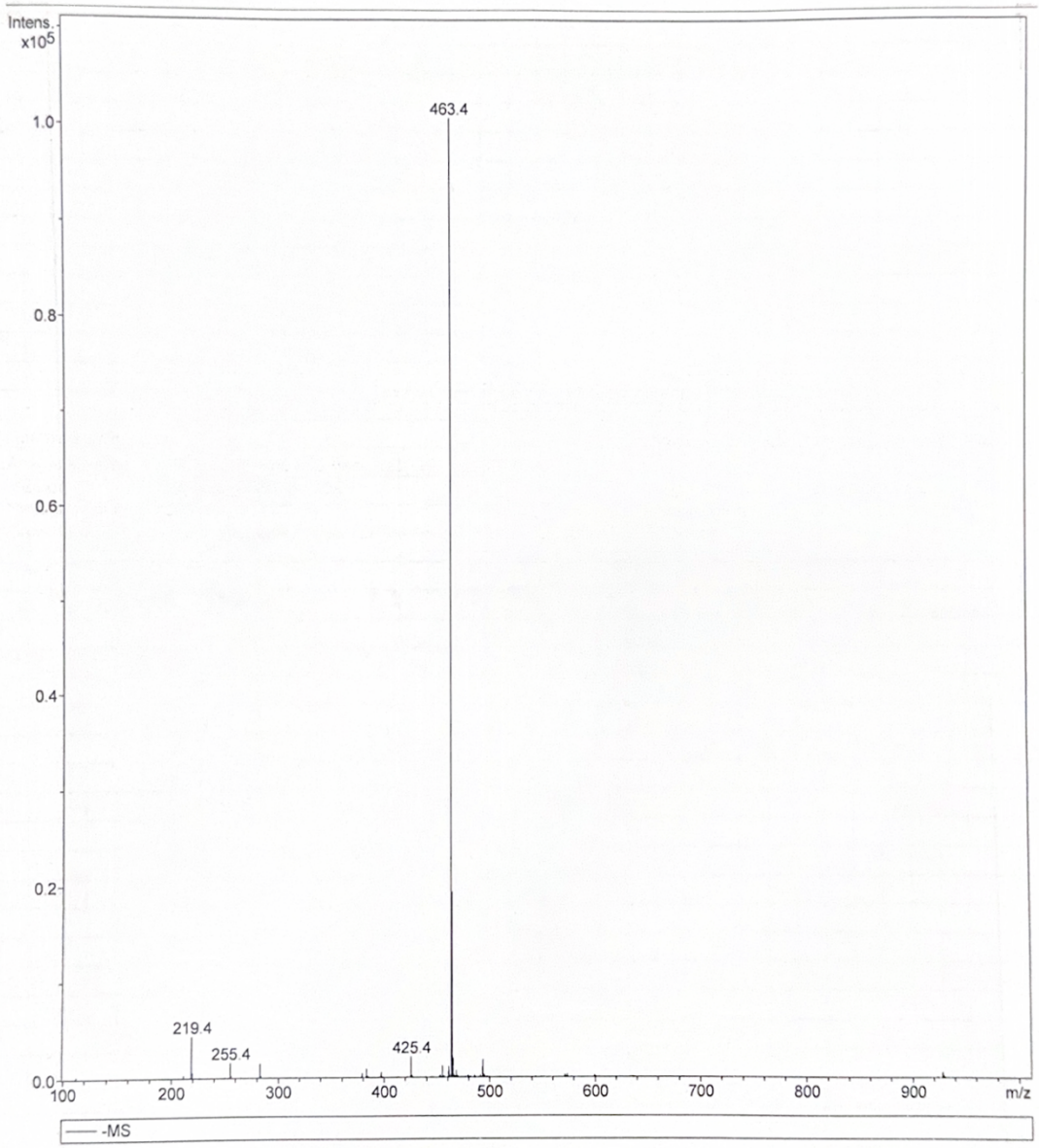

Bruker Daltonics DataAnalysis 3.4 printed: 7/30/2023 3:45:45 PM Page 1 of 1